Alma Mater Studiorum · Università di Bologna

Scuola di Scienze
Corso di Laurea Magistrale in Fisica del Sistema Terra

Sensitivity of forecast skill to the parameterisation of moist convection in the COSMO model

Relatore:
Prof.ssa Silvana Di Sabatino

Correlatori:
Dott. Andrea Montani
Dott.ssa Tiziana Paccagnella

Presentata da:
Matteo Vasconi

Sessione II
Anno Accademico 2016/2017

Sommario

La parametrizzazione della convezione umida nei modelli ad area limitata costituisce un' importante fonte di incertezza nella previsione spazio-temporale della precipitazione. Lo sviluppo e l'implementazione di sistemi di ensemble dove diversi schemi di convezione sono usati fornisce pertanto l'opportunità di migliorare i sistemi probabilistici alle scale in cui la convezione è parametrizzata.

In particolare in questo lavoro è stata studiata la sensibilità del modello COSMO all'uso di diversi schemi, attraverso alcuni esperimenti.

Per un caso di precipitazione intensa su un piccolo bacino idrografico in Toscana, sono state studiate le prestazioni del modello quando è girato rispettivamente con lo schema di Bechtold o quello di Tiedtke, con particolare riguardo ai tipi di errori previsionali riscontrati nella verifica dei campi di precipitazione prevista (localizzazione, timing) nelle due configurazioni.

Inoltre un sistema di ensemble composto da 10 membri, che usano lo schema di Bechtold, è stato girato per un periodo di circa 2 mesi, avvalendosi delle stesse condizioni iniziali e al contorno dei membri 1-10 di COSMO-LEPS (costituito da 20 membri, tutti girati con lo schema di Tiedtke). Le prestazioni di questo sistema nella previsione delle cumulate di precipitazione sono state valutate e confrontate a quelle dei membri 1-10 di COSMO-LEPS durante l'intero periodo.

Come prova finale un nuovo sistema di ensemble sperimentale, composto da 20 membri (i primi 10 girati con lo schema di Bechtold, i restanti con quello di Tiedtke) è stato confrontato con quello operativo (COSMO-LEPS) lungo il medesimo arco temporale. In questo periodo tale sistema ha mostrato migliori performance nella previsione di precipitazione rispetto all'ensemble operativo. In questo approccio l'uso dello schema di Bechtold è proposto come una perturbazione per l'ensemble operativo COSMO-LEPS, in modo da tener conto dell'incertezza legata alla rappresentazione della convezione umida nel modello.

Abstract

The parameterisation of convection in limited-area models is an important source of uncertainty as regards the spatio-temporal forecast of precipitation. The development and implementation of ensemble systems in which different convection schemes are used provides an opportunity to upgrade state-of-the-art probabilistic systems at the convection-parameterised scale. As for the limited-area model COSMO, the sensitivity of the forecast skill to the use of different convection schemes is assessed by performing different sets of experiments.

For one case of heavy precipitation over Italy, the performance of COSMO model run with the Bechtold scheme or with the Tiedtke scheme is investigated in both deterministic and ensemble modes with particular attention to the types of forecast errors (e.g. location, timing, intensity) provided by the different convection schemes in terms of total precipitation.

In addition to this, a 10-member ensemble has been run for approximately 2 months with the Bechtold scheme, using the same initial and boundary conditions as members 1-10 of the operational COSMO-LEPS ensemble system (which has 20 members, all run with the Tiedtke scheme). The performance of these members is assessed and compared to that of the system made of members 1-10 of COSMO-LEPS; in particular the spread/skill relation of the two 10-member ensembles in terms of total precipitation is evaluated.

Finally, the performance of an experimental 20-member ensemble system (which has 10 members run with the Bechtold plus 10 members run with the Tiedtke scheme) is compared to that of operational COSMO-LEPS over the 2-month period. The new system turned out to have higher skill in terms of precipitation forecast with respect to COSMO-LEPS over the period. In this approach the use of the Bechtold scheme is proposed as a perturbation for the COSMO-LEPS ensemble, relatively to how uncertainties in the model representation of the cumulus convection can be described and quantified.

Contents

List of Figures

List of Tables

List of Acronyms

ARPA *Agenzia Regionale Prevenzione Ambiente*

BS *Brier Score*

BSS *Brier Skill Score*

CDF *Cumulative Density Function*

CAPE *Convective Avalaible Potential Energy*

CFL *Courant-Friedrichs-Lewy*

CTL *Cloud Top Level*

COSMO *COnsortium for Small-Scale MOdelling*

COSMO-LEPS *COnsortium for Small-Scale MOdelling Limited-area Ensemble Prediction System*

DWD *Deutscher WetterDienst*

ECMWF *European Centre for Medium range Weather Forecast*

ENS *ENsemble System*

EPS *Ensemble Prediction System*

ERA *ECMWF ReAnalysis*

ETL *Equilibrium Temperature Level*

GCM *General Circulation Model*

GME *Global Model for Europe*

GPH *GeoPotential Height*

GPS *Global Positioning System*

HE-VI *Horizontal Explicit- Vertical Implicit*

HRES *High RESolution*

IFS *Integrated Forecasting System*

LAM *Limited Area Model*

LCL *Lifting Condensation Level*

LM *Lokal Modell*

LFS *Level of Free Sinking*

MAE *Mean Absolute Error*

MPP *Massive Parallel Processing*

MSLP *Mean Sea Level Pressure*

NWP *Numerical Weather Prediction*

PBL *Planetary Boundary Layer*

QPF *Quantitative Precipitation Forecasting*

RADAR *RAdar Detection And Ranging*

RASS *Radar Analysis Support System*

RM *Representative Member*

ROC *Relative Operative Curve*

RPS *Ranked Probability Scores*

RPSS *Ranked Probability Skill Scores*

SIMC Servizio IdroMeteo Clima

SPPT Stochastic Perturbations of Physical Tendencies

SYNOP surface SYNOPtic observations

TVD Total Variation Diminishing

UTC Universal Time Coordinate

VAD Velocity Azimuth Display

WCB Warm Conveyor Belt

Introduction

Numerical Weather Prediction (NWP) models have been developed over the last 50 years in order to quantitatively predict the future states of the atmosphere using the current weather conditions. Despite the constant increase in horizontal and vertical resolutions of these models, some atmospheric processes have typical horizontal dimension too small to be explicitly resolved. Thus the only way to represent the overall effects of these sub-grid physical processes in NWP models is by means of parameterisations.

From an operational point of view, one of the most interesting parameterisation is that relative to moist convection (cumulus convection) because it regards the spatio-temporal forecast of precipitation.

Many methods have been implemented in NWP models over the last 40 years to represent cumulus convection. The different approaches mainly differ in terms of cloud model, closure assumptions and computational efficiency. The progress in this aspect of atmospheric modeling has been especially slow over the past decades (Randall et al., 2003) because, in addition to the basic question of how to pose the problem, there are a number of uncertainties in modeling these processes, as reviewed by Arakawa (2004). This is a signature of both the complexity of the physical processes involved and the uncertainty linked to the use of a particular scheme instead of another.

In order to provide a representation of the model uncertanty, due to the imperfect knowledge of atmospheric initial conditions and the approximate model formulation, ensemble forecasting was introduced at the beginning of the nineties. This approach has now become commonplace in operational weather forecasting by the major meteorological institutes. Instead of running just one forecast with an unknown error, an ensemble of slightly dif-

ferent forecasts are run, in order to integrate the deterministic forecast with an estimate of the "forecast of forecast skill" (Tennekes et al., 1986). The estimation of uncertainty is even more crucial when a high spatio-temporal detail is required as in the case of precipitation.

The aim of this work is to assess the sensitivity of the forecast skill of a limited-area model to the use of different parameterisation of moist convection. In particular, the attention is focussed on the ability to predict the occurrence of precipitation events by the model of the COnsortium for Small-scale MOdelling (COSMO, http://www.cosmo-model.org).

In fact either the Tietdke scheme (Tiedtke et al., 1989), which has been operationally used so far, or the Bechtold scheme (Bechtold et al., 2001; 2014), initially implemented for the ECMWF (European Centre for Medium-range Weather Forecast) global model and recently adapted to COSMO model, are now available for the model applications. However before implementing the Bechtold scheme in any operational suite, it is necessary to assess how the system performs with the newer scheme.

In particular the main issues to be addressed in this thesis can be summarised as follows:

1. *What are the main differences in COSMO precipitation forecasts when it is run with different moist convection schemes?*

2. *How does the model perform in ensemble mode when it is run with different schemes?*

3. *Can the use of either the schemes provide an opportunity to ameliorate the skill of the operational ensemble system of the COSMO consortium?*

In order to answer these questions, different experiments will be performed in this study, which is part of a COSMO Priority Task.

After a brief introduction to the COSMO model and to the convective parameterisation schemes adopted in this system in Chapter 1 and 2, an extensive presentation of the main results follows.

In Chapter 3 a comparison of the COSMO model performance when it is run either with one convection scheme or with the other is presented for a

precipitation event occurred over a small river catchment in Northern Italy.

In Chapter 4 the attention is focussed on the implementation of an experimental 20-member ensemble system, in which either the Tietdke or the Bechtold scheme is used. In particular the forecast skill of the new system in terms of total precipitation is assessed over a 2-month period and compared to that of COSMO-LEPS, the operational ensemble system of the consortium (which uses only the Tiedtke scheme).

Finally, conclusions are drawn in Chapter 5.

Chapter 1

Ensemble prediction systems and COSMO LEPS

1.1 Overview on COSMO-model

The COSMO-Model is a nonhydrostatic limited-area atmospheric prediction model (www.cosmo-model.org). It has been designed for both operational numerical weather prediction (NWP) and various scientific applications on the meso-β (2-20 km) and meso-γ (20-100 km) scale (see Fig. 2.1). The COSMO-Model is based on the primitive thermo-hydrodynamical equations describing compressible flow in a moist atmosphere, with a variety of physical processes taken into account by parameterisation schemes (Doms et al., 2015).

The basic version of the COSMO-Model (formerly known as *Lokal Modell (LM)*) has been developed at the Deutscher Wetterdienst (DWD) and it is run operationally since end of 1999.

The subsequent developments related to the model have been organized within COSMO, the *Consortium for Small-Scale Modeling*. COSMO aims at the improvement, maintenance and operational application of a non-hydrostatic limited-area modeling system, which is now consequently called the COSMO-Model.

For operational aims COSMO model is run at different resolutions of 2.8 and 7 km in both deterministic and ensemble mode.

1.1.1 Basic Model design and Features

The nonhydrostatic fully compressible COSMO-Model has been developed to meet high resolution regional forecast requirements of weather services and to provide a flexible tool for various scientific applications on a broad range of spatial scales. When starting with the development of the COSMO-Model, many NWP-models operated on hydrostatic scales of motion with grid spacings down to about 10 km and thus lacked the spatial resolution required to explicitly capture small-scale severe weather events (Schättler et al., 2016).

The COSMO-Model has been designed for meso-β and meso-γ scales where nonhydrostatic effects begin to play an essential role in the evolution of atmospheric flows.

However only by employing 1 to 3 km grid spacing for operational forecasts over a large domain, it is expected that deep moist convection and the associated feedback mechanisms to the larger scales of motion can be explicitly resolved (Doms et al., 2015).

The requirements for the data assimilation system for the operational COSMO-Model are mainly determined by the very high resolution of the model and by the task to employ it also for nowcasting purposes in the future. Hence, detailed high-resolution analyses have to be able to be produced frequently and quickly, and this requires a thorough use of asynoptic and high-frequency observations such as aircraft data and remote sensing data. Since both 3-dimensional and 4-dimensional variational methods tend to be less appropriate for this purpose, a scheme based on the observation nudging technique has been chosen for data assimilation.

COSMO model is used for a wide range of applications, which imposes a number of requirements for the physical, numerical and technical design of the model.

The main design requirements are (Schättler et al., 2016):

- Use of nonhydrostatic, compressible dynamical equations to avoid restrictions on the spatial scales and the domain size, and application of an efficient numerical method of solution;

- Provision of a comprehensive physics package to cover adequately the spatial scales of application, and provision of high-resolution data sets for all external parameters required by the parameterisation schemes;

- Flexible choice of initial and boundary conditions to accommodate both real data cases and idealized initial states, and use of a mesh-refinement technique to focus on regions of interest and to handle multi-scale phenomena;

- Use of a high-resolution analysis method capable of assimilating high-frequency asynoptic data and remote sensing data;

- Use of pure Fortran constructs (i.e. Fortran90) to render the code portable among a variety of computer systems, and application of the standard MPI-software for message passing on distributed memory machines to accommodate broad classes of parallel computers.

The development of the COSMO-Model was organized along these basic guidelines.

However, not all of the requirements are fully implemented, and development work and further improvement is an ongoing task.

The main features and characteristics of the present release are then summarized.

Dynamics

- *Model Equations*: Non-hydrostatic, full compressible hydro-thermodynamical equations in advection form. Subtraction of a hydrostatic base state at rest.

- *Prognostic Variables*: Horizontal and vertical Cartesian wind components, pressure perturbation, temperature, specific humidity, cloud water content. Optionally: cloud ice content, turbulent kinetic energy, specific water content of rain, snow and graupel.

- *Diagnostic Variables*: Total air density, precipitation fluxes of rain and snow.

- *Coordinate System*: Generalized terrain-following height coordinate with rotated geographical coordinates and user defined grid stretching in the vertical. Options for (i) base-state pressure based height coordinate, (ii) Gal-Chen height coordinate and (iii) exponential height coordinate according to Schaer et al. (2002).

Numerics

- *Grid Structure*: Arakawa C-grid, Lorenz vertical grid staggering.
- *Spatial Discretization*: Second-order finite differences. For the two time-level scheme also 1st and 3rd to 6th order horizontal advection (default: 5th order). Option for explicit higher order vertical advection.
- *Time Integration*: Two time-level 2nd and 3rd order Runge-Kutta split-explicit scheme after Wicker and Skamarock (2002) and a TVD-variant (Total Variation Diminishing) of a 3rd order Runge-Kutta split-explicit scheme. Option for a second-order leapfrog HE-VI (horizontally explicit, vertically implicit) time-split integration scheme, including extensions proposed by Skamarock and Klemp (1992). Option for a three time-level 3-d semi-implicit scheme (Thomaset al. (2000)) based on the leapfrog scheme.
- *Numerical Smoothing*: 4th-order linear horizontal diffusion with option for a monotonic version including an orographic limiter. Rayleigh damping in upper layers. 2-d divergence damping and off-centering in the vertical in split time steps.
- *Initial and Boundary Conditions*: Initial Conditions and Lateral Boundary Conditions interpolated initial data from various coarse-grid driving models (GME, ECMWF, COSMO-Model) or from the continuous data assimilation stream. Option for user-specified idealized initial fields. Options for rigid lid condition and Rayleigh damping layer for Top Boundary condition.

- *Initialization*: Digital-filter initialization of unbalanced initial states (Lynch et al. (1997)) with options for adiabatic and diabatic initialization.

Physical Parameterisations

- *Subgrid-Scale Turbulence*: Prognostic turbulent kinetic energy closure at level 2.5 including effects from subgrid-scale condensation and from thermal circulations.

- *Surface Layer Parameterisation*: A Surface layer scheme (based on turbulent kinetic energy) including a laminar-turbulent roughness layer.

- *Grid-Scale Clouds and Precipitation*: Cloud water condensation and evaporation by saturation adjustment. Precipitation formation by a bulk microphysics parameterisation including water vapour, cloud water, cloud ice, rain and snow with 3D transport for the precipitating phases. Option for a new bulk scheme including graupel. Option for a simpler column equilibrium scheme.

- *Subgrid-Scale Clouds*: Subgrid-scale cloudiness is interpreted by an empirical function depending on relative humidity and height. A corresponding cloud water content is also interpreted. Option for a statistical subgrid-scale cloud diagnostic for turbulence.

- *Moist Convection*: Tiedtke (1989) mass-flux convection scheme with equilibrium closure based on moisture convergence. Option for the Bechtold (Bechtold and al. (2014)) convection scheme with CAPE-type closure.

- *Shallow Convection*: Reduced Tiedtke (or Bechtold) scheme for shallow convection only.

- *Radiation*: δ two-stream radiation scheme after Ritter and Geleyn (1992) short and longwave fluxes (employing eight spectral intervals); full cloud-radiation feedback.

- *Soil Model*: Multi-layer version of the former two-layer soil model based on the direct numerical solution of the heat conduction equation. Snow and interception storage are included. Option for the (old) two-layer soil model employing the extended force-restore method still included.

- *Fresh-Water Lake Parameterisation*: Two-layer bulk model after Mironov (2008) to predict the vertical temperature structure and mixing conditions in fresh-water lakes of various depths.

- *Sea-Ice Scheme*: Parameterisation of thermodynamic processes (without rheology) after Mironov and B. (2004). The scheme basically computes the energy balance at the ices surface, using one layer of sea ice.

- *Terrain and Surface Data*: All external parameters of the model are available at various resolutions for a pre-defined region covering Europe. For other regions or grid-spacings, the external parameter file can be generated by a preprocessor program using high-resolution global data sets.

Data Assimilation

- *Basic Method*: Continuous four-dimensional data assimilation based on observation nudging (Schraff (1996), Schraff (1997)), with lateral spreading of upper-air observation increments along horizontal surfaces. Explicit balancing by a hydrostatic temperature correction for surface pressure updates, a geostrophic wind correction, and a hydrostatic upper-air pressure correction.

- *Assimilated Atmospheric Observations*: Radiosonde (wind, temperature, humidity), aircraft (wind, temperature), wind profiler (wind), and surface-level data (SYNOP, SHIP, BUOY: pressure, wind, humidity). Optionally RASS (temperature), radar VAD wind, and ground-based GPS (integrated water vapour) data. Surface-level temperature is used for the soil moisture analysis only.

- *Radar derived rain rates*: Assimilation of near surface rain rates based on latent heat nudging (Stephan et al. (2008)). It locally adjusts the three-dimensional thermodynamical field of the model in such a way that the modelled precipitation rates should resemble the observed ones.

- *Surface and Soil Fields*: Soil Moisture Analysis, Sea Surface Temperature Analysis, Snow Depth Analysis

Code and Parallelization

- *Code Structure*: Modular code structure using standard Fortran constructs.

- *Parallelization*: The parallelization is done by horizontal domain decomposition using a soft-coded gridline halo (2 lines for Leapfrog, 3 for the Runge-Kutta scheme). The Message Passing Interface software (MPI) is used for message passing on distributed memory machines.

- *Compilation of the Code*: The compilation of all programs is performed by a Unix shell script invoking the Unix make command. All dependencies of the routines are automatically taken into account by the script.

- *Portability*: The model can be easily ported to various platforms; current applications are on conventional scalar machines (UNIX workstations, LINUX and Windows-NT PCs), on vector computers (NEC SX series) and MPP machines (CRAY, IBM, SGI and others).

- *Model Geometry*: 3-d, 2-d and 1-d model configurations. Metrical terms can be adjusted to represent tangential Cartesian geometry with constant or zero Coriolis parameter.

The model equations are formulated with respect to a rotated geographical lat/lon-grid with coordinates (λ,ϕ). The rotated coordinate system results from these coordinates (λ_g, ϕ_g) by tilting the north pole. In the vertical,

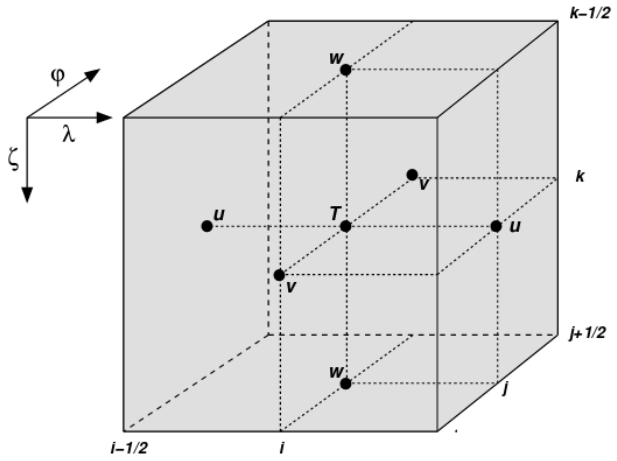

Figure 1.1: A grid box volume $\Delta V = \Delta\zeta\Delta\lambda\Delta\phi$ showing the Arakawa-C/Lorenz (Arakawa et al., 1977) staggering of the dependent model variables. ζ, λ and ϕ refer to the coordinate system.

a generalized terrain-following height coordinate ζ is used, where any unique function of geometrical height can be used for transformation. Since ζ does not depend on time, the (λ,ϕ,ζ) system represents a non-deformable coordinate system, where surfaces of constant ζ are fixed in space - in contrast to the pressure based coordinate system of most hydrostatic models, where the surfaces of constant vertical coordinate move in space with changing surface pressure.

The model variables are staggered on an Arakawa-C/Lorenz (Lorenz, 1960; Arakawa et al., 1977) grid with scalars (temperature, pressure and humidity variables) defined at the centre of a grid box and the normal velocity components defined on the corresponding box faces. For a given grid spacing, this staggering allows for a more accurate representation of differential operators than in the A-grid, where all variables are defined at the same point.

The grid spacing is that relative to the different resolution at which the model is run, while in the vertical there are 40 layers from the surface up to about 24 km above ground.

The set of prognostic model equations for the three components u, v and w of the wind vector, the perturbation pressure p', the temperature T and the humidity variables q is:

$$\begin{aligned}
\frac{\partial u}{\partial t} + V \cdot \nabla u - \frac{uv}{a} tan\phi - fv &= -\frac{1}{\rho a cos\phi}\left(\frac{\partial p'}{\partial \lambda} + \frac{J_\lambda}{\sqrt{G}}\frac{\partial p'}{\partial \zeta}\right) \\
\frac{\partial v}{\partial t} + V \cdot \nabla u - \frac{u^2}{a} tan\phi + fu &= -\frac{1}{\rho a}\left(\frac{\partial p'}{\partial \phi} + \frac{J_\phi}{\sqrt{G}}\frac{\partial p'}{\partial \zeta}\right) \\
\frac{\partial w}{\partial t} + V \cdot \nabla w &= \frac{1}{\rho\sqrt{G}} + B + M_w \\
\frac{\partial p'}{\partial t} + V \cdot \nabla p' - g\rho_0 w &= -(c_{pd}/c_{vd})\rho D \\
\frac{\partial T}{\partial t} + V \cdot \nabla T &= -\frac{p}{\rho c_{vd}} D + Q_T \\
\frac{\partial q^v}{\partial t} + V \cdot \nabla q^v &= -(S^l + S^f) + M_{q^v} \\
\frac{\partial q^{l,f}}{\partial t} + V \cdot \nabla q^{l,f} + \frac{1}{\rho\sqrt{G}}\frac{\partial P_{l.f}}{\partial \zeta} &= S^{l,f} + M_{q^{l,f}}
\end{aligned} \tag{1.1}$$

Here, the continuity equation has been replaced by an equation for p'. In Eqs. (1.1) a is the radius of the earth, c_{pd} and c_{vd} are the specific heat of dry air at constant pressure and constant volume, g is the gravity acceleration, f is the Coriolis parameter, R_v and R_d are the gas constants for water vapour and dry air.

Furthermore $J_\lambda = \left(\frac{\partial z}{\partial \lambda}\right)_{zeta}$, $J_\phi = \left(\frac{\partial z}{\partial \phi}\right)_{zeta}$ are the element of the Jacobian matrix linked to the transformation from the zeta coordinate to the ζ.

$\sqrt{G} = |det(J^z)|\left|\frac{\partial z}{\partial \zeta}\right|$ the Jacobian of the transformation from the z- to the ζ- system.

ρ is the density of moist air which is calculated as a diagnostic variable from the equation of state:

$$\rho = p\left[R_d(1 + (R_v/R_d - 1)q^v - q^l - q^f)T\right]^{-1}$$

q_v is the specific humidity, q^l represents the specific water content of a category of liquid water (cloud or rain water) and q^f represents the specific water

content of a category of frozen water (cloud ice, snow or graupel). The corresponding precipitation fluxes are denoted by P_l and P_f. The terms M denote contributions from subgrid-scale processes as, e.g. turbulence and convection and Q_T summarizes the diabatic heating rate due to this processes. The term B in the equation for the vertical velocity is the buoyant acceleration.

The equations (1.1) are solved numerically in the model using the traditional finite difference method. In this technique, spatial differential operators are simply replaced by suitable finite difference operators.

The time integration is also by discrete stepping using a fixed timestep Δt depending on the horizontal resolution, in order to satisfy the CFL stability condition (that is $\Delta t \leq \frac{\Delta x}{c}$, where Δx is the horizontal grid spacing and c the magnitude of velocity).

More details on COSMO model features can be found in the COSMO User Guide (www.cosmo-model.org).

1.2 The ensemble approach

Despite the constant increase of computer power resources, which has allowed the development of more and more sophisticated and resolved NWP models, accurate forecasts of extreme weather conditions, especially when related to intense and localised precipitation structures, are still difficult beyond day 2 and, in selected cases, even at 24 hours (Mullen and Buizza, 2001a). This limitation is due, among other reasons, to the inherently low degree of predictability typical of the relevant physical phenomena.

In fact the weather is a chaotic system. Small errors in the initial conditions of a forecast grow rapidly, and affect predictability, so that a tiny error in the analysis can become a large error in the forecast (Lorenz, 1963). Even with the best observations it is not possible to make a perfect analysis, so it is not possible to make perfect forecasts.

Furthermore, predictability is limited by model errors due to the approximate simulation of atmospheric processes of the state-of-the-art numerical models (Buizza, 2001).

These two sources of uncertainties limit the skill of single, deterministic forecasts in an unpredictable way, with days of high/poor quality forecasts randomly followed by days of high/poor quality forecasts. To deal with this problem the probabilistic approach has been recently more and more explored: the main goal is to try to come to terms with the chaotic behaviour of the atmosphere and to help forecasting phenomena with low deterministic predictability. Techniques which have evolved to counter it include ensemble weather prediction, where an ensemble of initial conditions, within some tolerance of the analysis (our best guess of the current state), is run forward under the model to get an impression of the likely range of future states (Toth and Kalnay, 1993; Molteni et al., 1996). Therefore instead of running the NWP model once (a deterministic forecast), the model is run many times from different initial conditions. The model physics too can be also slightly perturbed, and even some ensembles can use more than one model within the ensemble (multi-model EPS) or the same model but with different combinations of physical parameterisation schemes (multi-physics EPS).

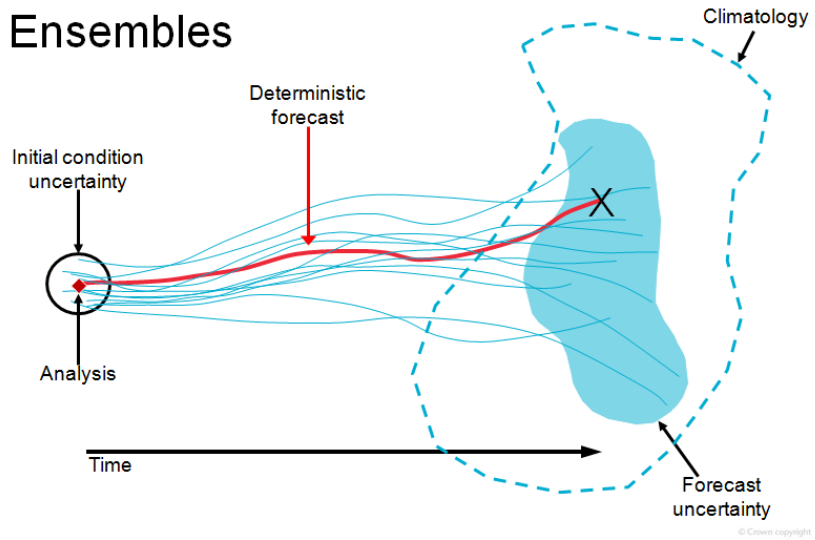

Figure 1.2: Schematic illustration of ensemble forecasting: the main goal is to explore all the possible future states of the atmosphere. A good forecast is the one in which analysis lies inside the ensemble spread (www.metoffice.gov.uk).

Furthermore the uncertainty in a weather forecast can vary widely from day to day according to the synoptic situation, and the EPS approach provides an estimate of this day-to-day uncertainty.

Owing to the cost of running a NWP model many times, the EPS is often run at lower horizontal resolution with respect to the equivalent deterministic NWP model.

The EPS normally includes a control forecast that uses the ensemble resolution model but without any perturbations to the analysis or model. The individual NWP solutions that make up the ensemble are often referred to as the ensemble members.

The range of different solutions in the forecast allows to assess the uncertainty in the forecast, and how confident the user should be in a deterministic forecast. Therefore an ensemble of forecasts produces a range of possible scenarios rather than a single predicted value. The distribution of the ensemble members gives an indication of the likelihood of occurrence of those scenarios. If the different forecasts in the ensemble are all very similar to each other then we can be confident of our forecast, but if they all develop differently,

and for example some develop a major storm while others develop a much weaker depression, then we will be much less confident. However, by looking at the proportion of the ensemble members that predict -for example- a storm, an estimate of how likely the storm is can be made.

Therefore probabilistic forecasting can be seen as "a forecast of the forecast skill" and a feasible method to integrate a deterministic forecast with an estimate of the probability distribution of future atmospheric states (Buizza, 1997), taking into account various sources of possible errors in forecast models.

It is worth pointing out that in a good ensemble forecast the spread of the ensemble members should on average correspond to the error of the ensemble mean. This ensures that the forecast is reliable. It means that, when an ensemble forecast predicts a probability of say 80% for an event to occur, it really will occur in 80% of cases when such a forecast is made. Getting the spread right is thus vital for a successful forecast.

1.2.1 The COSMO-LEPS ensemble system

As far as operational implementations are concerned, the COnsortium for Small-Scale MOdelling Limited-area Ensemble Prediction System (COSMO-LEPS) was the first mesoscale ensemble application running on a daily basis in Europe. This system, initially developed and implemented by the HydroMeteoClimate Regional Service of Emilia-Romagna, in Bologna, Italy (ARPA-SIMC), has been running at ECMWF since November 2002 (Montani et al., 2003a).

Nowadays, COSMO-LEPS is based on 20 integrations of the non-hydrostatic mesoscale model COSMO, formerly known as the Lokal Modell (Steppeler et al., 2003).

The methodology (described more thoroughly in the next section) aims at combining the advantages of the probabilistic approach by global ensemble systems with the high-resolution details gained in the mesoscale integrations. In the construction of COSMO-LEPS, an algorithm selects a number of members (referred to as Representative Members, RMs) from a "driving" global

ensemble system (Marsigli et al., 2001). This intermediate step, referred to as "ensemble-size reduction", is required to keep the computational load operationally affordable, since it is not presently feasible to nest the limited-area model on each individual member of a global ensemble with size larger than 30 members. After the "ensemble-size reduction", the selected RMs are used to provide both initial and boundary conditions to the integrations with the COSMO model, which is run once for each RM.

The impact of the large ensemble-size reduction on the forecast accuracy has been studied for some case studies and it could be concluded that the accuracy of the probabilistic forecast is not noticeably improved by the increase of LEPS size. Since a large amount of computer time is spent to perform many limited-area integrations, the advantages of the clustering-selection methodology are well evident (Montani et al, 2003). The comparison of statistics from different ensemble configurations has shown that the probability distribution obtained from the high-resolution RMs provides a very good approximation to the distribution generated by a an ensemble made of 51 members (Molteni et al., 2001), one for each member of ECMWF EPS.

Therefore, COSMO-LEPS performs a sort of dynamical downscaling of a global-model probabilistic system, limiting to a certain extent the computational cost (Tibaldi et al., 2006).

In the course of its operational activity, the COSMO-LEPS system has undergone a number of changes in order to improve the model performance (Montani et al., 2011). A time series of RPSS (Ranked Probability Skill Score, see Chapter 4) for different forecast ranges in terms of 12-h precipitation prediction is presented for COSMO-LEPS in Fig. 1.3. The higher the score is, the better the forecast skill will be. The increase of the quality of COSMO-LEPS forecasts in the years is evident, although the pace of improvement is different depending on the forecast range.

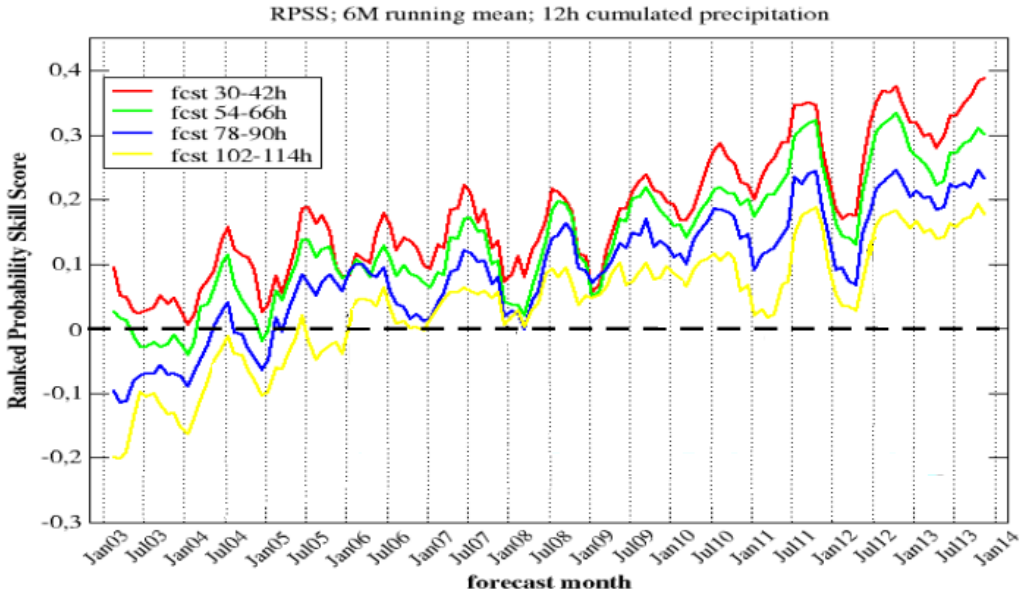

Figure 1.3: Time-series of the Ranked Probability Skill Score in COSMO-LEPS for the 30-42 h (red line), 54-66 h (green line), 78-90 h (blue-line) and 102-114 h (yellow line) forecast ranges. A 6-month running mean is applied to improve the readability of the plot. Verification from January 2003 to January 2014 over the Alpine area.

Description of the COSMO-LEPS methodology

A more detailed description of the LEPS methology is presented in this section. As already pointed out, this methodology, proposed in 2001 by ARPA-SIM, attempts to combine the benefits of the probabilistic approach with the high-resolution capabilities of the LAM integrations, limiting the computational investment.

The method is based on an algorithm to select a number of members out of a global ensemble system (ECMWF ENS in this case). The selected ensemble members (called Representative Members, RMs) provide initial and boundary conditions to integrate a limited-area model (Marsigli et al., 2005).

Therefore the transfer of information from the large-scale to the mesoscale can be viewed as a dynamical downscaling of the forecast provided by the global-model probabilistic system. The "core" of COSMO-LEPS method-

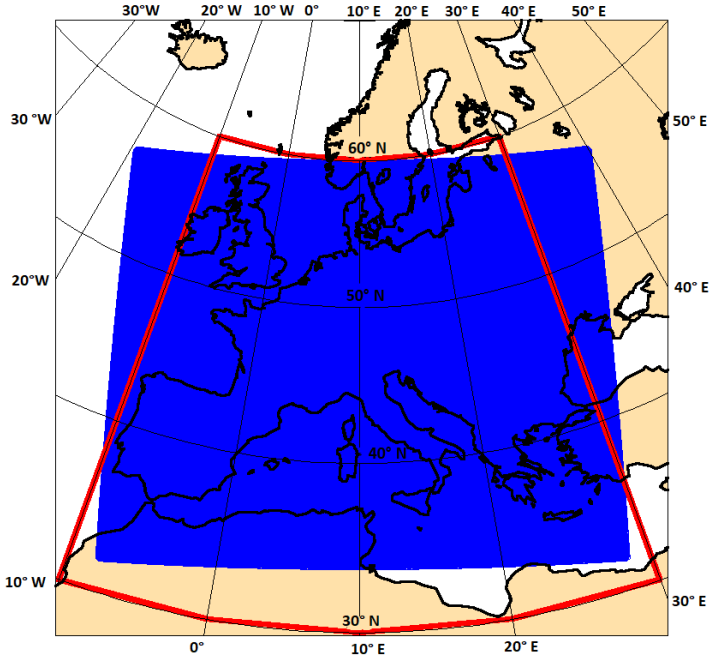

Figure 1.4: COSMO-LEPS integration domain (blue area) and clustering area (inside the red line).

ology lies in the idea of reducing the number of global ensemble elements driving the limited area runs, still retaining a large fraction of the driving-ensemble information.

The operational procedure can be described as follows (Montani et al., 2011):

1. Two successive runs of ECMWF Ensemble Prediction System (EPS) are joined together, thus generating a 102-member lagged-ensemble, since each EPS is made up of one control run plus 50 perturbed members.

2. EPS members are grouped into twenty clusters, the discriminating variable being a combination of four variables at three pressure levels and at two forecast steps: the two horizontal wind components, the geopotential height and the specific humidity at 500, 700 and 850 hPa and at the ranges of 96 and 120 h (the ranges are relative to the "youngest"

ensemble).

3. For each variable at each forecast step, the mean over the clustering area is calculated and, then, subtracted from any gridpoint value. Then, the result is divided by the standard deviation, thus obtaining a non-dimensional field.

4. The quadratic distances among the EPS members are computed for all variables at all levels at all steps and, then, space-averaged.

5. The cluster analysis is performed over the following area: 40N-60N, 10W-30E; the clusters are constructed using the complete-linkage algorithm (Wilks, 1995).

6. Within each cluster (with different populations), one RM is selected, using the same discriminating variables as before; the RM is that cluster element which minimizes the ratio between its distance from the other members of its own cluster and its distance from the members of the other clusters.

7. The so-selected RMs provide both initial and boundary conditions for the integrations with the COSMO model, which is run once for each RM over a domain covering Central and Southern Europe (shaded area in Fig (1.4).

8. The twenty COSMO integrations which generate the COSMO-LEPS system, start at 00 UTC and 12 UTC of day d, with a horizontal resolution of 7 km, 40 vertical levels and a forecast length of 132 h.

From the description above, it is clear that COSMO-LEPS acts like a local zooming of ECMWF EPS for the first 5 days of integration and, as such, is designed from the outset for the "short to early medium range" timescale (namely, 48-132 h). Initial conditions are taken from the driving EPS members and interpolated on COSMO grid.

Despite the reductions in number of the ensemble members, the procedure described above allows to account for most of the variety of the scenarios

represented in ECMWF EPS members, giving informations on uncertanties in initial conditions.

Perturbations entering the model from the lateral boundaries, are still provided by the driving EPS members and play a more and more important role in the behaviour of the limited-area system as the forecast range increases. These are due to the SPPT scheme (Stochastic Perturbations of Physical Tendencies) performed at ECMWF (Buizza et al. 1999).

In general model physics schemes apply adjustments (called "tendencies") to the variables temperature, humidity and wind that are used in the equations describing atmospheric circulation. ECMWF's Integrated Forecasting System (IFS) represents uncertainty in the model physics by perturbing these physics tendencies, introducing different perturbations for each ensemble member. The tendencies are perturbed randomly within certain limits. There is a system to the randomness because the collection of ensemble members has to describe a realistic distribution of possible forecast outcomes. This is achieved by using time- and spatially-varying patterns of random numbers to provide the perturbations.

Therefore the random error in parameterised forcings is assumed to be coherent between the different parameterisation modules, having a certain coherence on the space and time scales associated. Moreover, the scheme assumes that the larger the parameterised tendencies are, the larger the random error component is.

Chapter 2

Parameterisation of Moist Convection

2.1 Introduction

2.1.1 Dry and Moist Convection

A first definition of convection is that provided by the principal of Archimedes (260, b.C.) saying that a body immersed in a fluid is driven upward by a force equal to the difference between its weight and the weight of the fluid displaced. In the atmosphere a necessary (but not sufficient) condition for convection is that the environmental lapse rate (the rate of decrease of temperature with height) is steeper than the lapse rate experienced by a rising parcel of air. When this condition is met, upward-displaced air parcels can become buoyant and thus experience a further upward force as a consequence of convective instability.

Convection is often discriminated between "Dry" and "Moist". Dry convection refers to the vertical exchange of air associated with this instability, without clouds or precipitation.

On the other hand, moist convection is associated with upward and downward motions ("thermals") linked to moist air and water phase changes (clouds). One main difference between the two convection type is the lapse rate, which is typically lower for the moist one. The release of heat associated to condensation of water vapour in the air mass tends to heat the

environment, enhancing in a certain way the vertical instability of the flow.

In this work the attention will be focused especially to the moist convection processes and how they are resolved in mesoscale meteorological models.

2.1.2 Moist Convection in Numerical Weather Prediction Models

Cumulus convection is one of the major processes that affects the dynamics and energetics of atmospheric circulation systems. Convective processes typically operate on horizontal scales which are much smaller than those resolved by large-scale and mesoscale numerical weather-prediction (NWP) models. Neverthless, current and next generation limited area versions of models can use horizontal resolutions of O(1-3 km), and therefore can resolve at least deep convection with reasonable accuracy.

However at coarser resolution the only way to represent the overall effect of moist convection in these type of models is by means of parameterisations. Since 1960 many cumulus parameterisation schemes have been developed for both NWP models and general-circulation models (GCMs), to account for the subgrid-scale release of latent heat and mass transport associated with convective clouds. A non-exhaustive list of these schemes includes, among others, Arakawa and Schubert (1974), Anthes (1977), Kuo and Raymond (1980), Fritsch and Chappell(1980), Bougeault (1985), Betts and Miller (1986), Tiedtke (1989).

The common point of all cumulus parameterisations is that they aim to diagnose the presence of larger-scale conditions that would support the development of convective activity and, under appropriate conditions, to introduce tendencies for temperature and moisture (and possibly momentum) that would be consistent with the effects of convective activity. In particular, most parameterisations are designed to drive the model atmosphere towards a convectively adjusted state when they activate. This adjusted state is either predefined ("adjustment" schemes), or is computed using a bulk or spectral cloud model and adjusting the atmosphere through mass exchange between the cloud and the environment (mass-flux schemes).

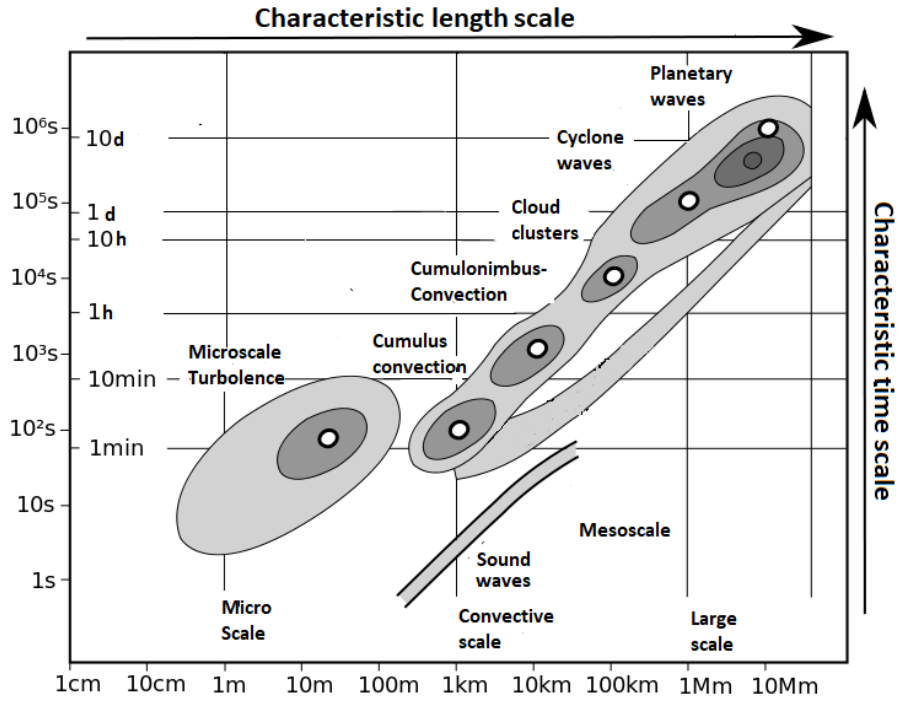

Figure 2.1: Characteristic scales of atmospheric processes. Cumulus convection occurs at typical horizontal scales from some hundreds to several kilometers.

From the practical point of view of a weather forecaster, a convection scheme used in a mesoscale model for a 1-2 day forecast provides valuable information if it has skill in predicting the initiation and evolution of convective events, especially if they involve severe convection. In addition, convective parameterisation plays a critically important role in the accurate quantitative prediction of rainfall, especially heavy rain episodes, which present a major challenge for forecasters (Fritsch et al. 1998). In contrast, for long-range GCM integrations, a convective parameterisation may be judged to be successful if it enhances the ability of the model to accurately represent the mean climate and variability of the tropical atmosphere.

Because of these seemingly disparate expectations, cumulus parameterisations have been developed typically with a particular application in mind and may contain inherent biases towards that application. However, beyond the detection of convective activity a primary purpose of convective parameteri-

sation is to mitigate the effects of inappropriate scale selection in a modelling system's representation of deep convection. It might be possible to develop numerically efficient parameterisations that are useful over a broad range of scales and type of applications, in particular if the parametrized convection nudges the model atmosphere towards a reasonable adjusted state and if it activates in a timely manner.

2.2 General aspects of a moist convection scheme

The task a convection parameterisation scheme has to fulfill is to calculate the collective effects of an ensemble of convective clouds in a model column as a function of grid-scale variables. In particular convection parameterisations include three steps (Bechtold et al., 2017):

1. Determine the occurrence and localisation of convection: this is often named as "Trigger of convection".

2. Determine the vertical distribution of heating, moistening and momentum changes: this task is generally done with the aid of a cloud model.

3. Determine the overall amount of convective precipitation = energy conversion: this is the final step in a convection parameterisations and is called "Closure".

As a consequence some basic effects of moist convection have to be considered by cumulus parameterisations schemes. These are diabatic heating due to the release of latent heat resulting from cloud condensation and from the formation and evaporation of precipitation and the vertical transports of heat, moisture and momentum in cumulus updraughts and downdraughts as well as in the regions with compensating downward motions, which in turn interact with the cumulus clouds by lateral exchange processes (entrainment and detrainment). All these processes tend in general to stabilise the original thermally unstable stratification.

As already mentioned various methods are presently applied for cumulus parameterisations in mesoscale NWP models. This shows both the complex-

ity of the processes to be considered and the uncertainty as to whether moist convection can be correctly represented by means of parameterisations.

For operational applications of COSMO-model to the meso$-\beta$ scale, the mass-flux scheme of Tiedtke (1989) has been used until now. A newer mass-flux sheme (Bechtold 2014), implemented in ECMWF global model, has been recently adapted for COSMO-model. These schemes are briefly presented in the next sections.

2.3 Formulation of Mass-Flux schemes in the COSMO model

The cumulus parameterisations schemes according to Tiedtke (1989) and Bechtold (2014) use a mass-flux approach to represent moist convection in numerical models.

The mass flux approach is a general and quite powerful method to tackle (eddy) transport problems in fluid mechanics, in particular for convective overturning where most of the transport is done by the "large" eddy draughts that carry heat and mass upward and downward over relatively large distances. The feedback of subgrid-scale vertical fluxes of mass, heat, moisture and momentum in up- and downdraughts is then calculated by using a simple bulk cloud model.

The basic features of the schemes, which differ mainly for the *closure assumptions*, are outlined in the following sections (Doms et al., 2011).

2.3.1 Trigger function

The first important task of a convection parameterisations is to decide whether or not convection takes place in a model grid column. This is done in a very simplified "first-guess" updraught computation that implies the determination of the cloud base level, i.e. the Lifting Condensation Level (LCL). The test is done by adding a T and q perturbation to an ideal near surface air parcel. By considering parcel ascending until the CTL is reached (i.e. Cloud Top Level, also defined as the level at which vertical velocity vanishes), if the calculated vertical velocity at LCL is positive, convection is supposed to occur.

The selection of convection type depends on the depth of the computed cloud: if the difference between the pressure of CTL and the pressure of LCL exceeds a fixed threshold (i.e. 200hPa in the ECMWF IFS Bechtold scheme) deep covection occurs, while lower values are associated with shallow convection. If neither deep or shallow convection is found, a midlevel convection can be activated, from any model level several hundreds meters above ground level.

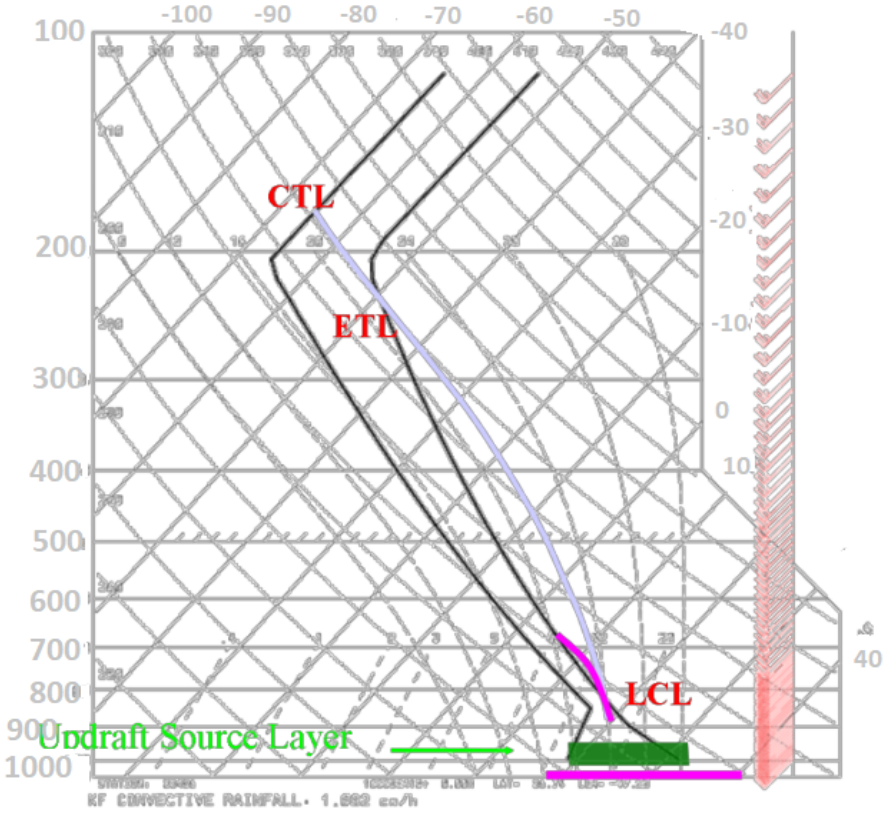

Figure 2.2: Illustration of Trigger procedure on a Skew-T diagram, including environmental profiles of temperature and dewpoint temperature (black), a near surface layer used as departure level for shallow ascent (pink), and a 30 hPa thick source layer (dark green) used for a first guess deep ascent (sky blue). If no deep ascent is found, the procedure is repeated for departure layers in the lowest 300 hPa. Note also that the cloud top level (CTL) might lie above the equilibrium temperature level (ETL), as it is determined by the level where the parcel vertical velocity vanishes, and the parcel might overshoot its ETL.

2.3.2 Large scale convective tendencies

The prognostic equations for the grid-scale equations are obtained by averaging the microturbulent equations for heat, moisture and momentum over the spatial scales which correspond to the model grid spacing.

The thermodynamic forcing due to moist convection can be formulated by the following tendencies:

$$\left(\frac{\partial s}{\partial t}\right) = -\frac{1}{\rho}\frac{\partial}{\partial z}[M_u(s_u - s) + M_d(s_d - s)] + L(c_u - e_d - e_l - e_p) + L_f(Melt - F)$$

$$\left(\frac{\partial q^v}{\partial t}\right) = -\frac{1}{\rho}\frac{\partial}{\partial z}[M_u(q_u^v - q^v) + M_d(q_d^v - q^v)] + (c_u - e_d - e_l - e_p) \quad (2.1)$$

$$\left(\frac{\partial \alpha}{\partial t}\right) = -\frac{1}{\rho}\frac{\partial}{\partial z}[M_u(\alpha_u - \alpha) + M_d(\alpha_d - \alpha)]$$

In Eqs. (2.1) s is the dry static energy, α denotes the horizontal wind components (u or v), q^v specific humidity and the subscripts u and d indicate variables within the updraughts and the downdraughts, respectively. Furthermore:

M_u, updraught mass flux, defined by $M_u = \rho a_u(w_u - w)$;

a_u, area fraction of the updraught;

w_u vertical velocity in the updraught;

M_d downdraught mass flux, defined by $M_d = \rho a_d(w_d - w)$;

a_d area fraction of the downdraught;

w_d vertical velocity in the downdraught;

s_u, s_d dry static energy within the up- and downdraught, resp.;

q_u, q_d specific humidity within the up- and downdraught, resp.;

α_u, α_u horizontal wind components in the up- and downdraught, resp.;

c_u condensation in the updraught (area mean);

e_d evaporation of precipitation inthe downdraught (area mean);

e_l evaporation of cloud water in the environment (area mean);

e_p evaporation of precipitation below cloud base (area mean);

L latent heat $L = L_V$(latent heat of evaporation) for $T \geq 273,15K$ and $L = L_S$ (latent heat of sublimation) for $T < 273,15K$, L_f (latent heat of fusion), $Melt$ (melting rate), F (freezing rate);

The horizontal area at which the turbolent equations are averaged, relative to the grid-spacing area of the model, is assumed to be large enough to contain an ensemble of cumulus clouds, as already pointed out. In particular the convective-scale eddy transports of dry static energy, moisture and momentum from cumulus updraughts, downdraughts and the cumulus-induced subsidence in the environmental air are not described in terms of contributions from the individual ensemble components, but are represented by their average values using a one-dimensional bulk cloud model after Yanai et al. (1973). Therefore this approximates the net effects of an ensemble of clouds as resulting from a representative single cloud.

Column equilibrium is supposed for hydrometeors formed in convective clouds.

The budget equation for the area mean value of the flux of convective precipitation (denoted by P) is:

$$\frac{\partial P}{\partial t} = -\rho(g_p - e_d - e_p) \tag{2.2}$$

where g_p denotes the conversion rate of cloud condensate to form precipitation.

The precipitation rate at the surface results from vertical integration of this equation. The equations in (2.1) are solved at the end of the convection code, after having evaluated the mass fluxes, the values in the up-and downdraughts and the precipitation production/evaporation.

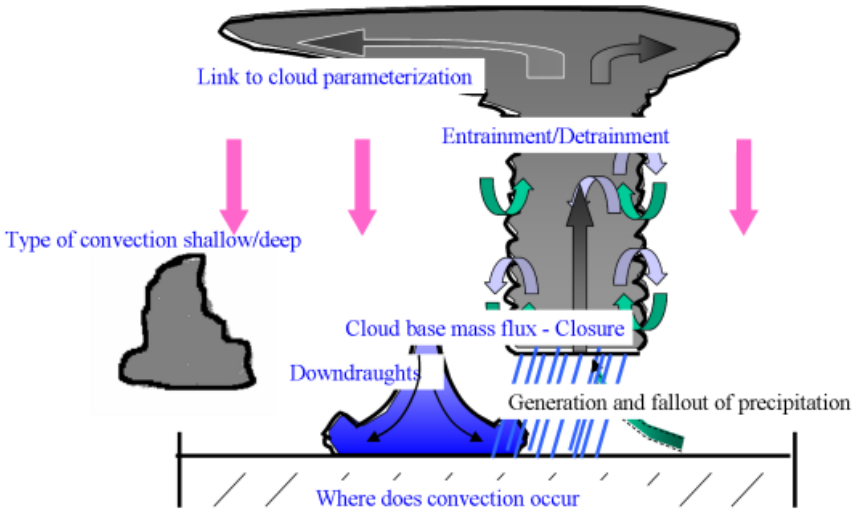

Figure 2.3: Schematic of a bulk convection scheme with a shallow and deep entraining/detraining cloudy ascending plume, and downdraught region. Further represented features are trigger of convection, environmental subsidence, microphysics and precipitation, and detrainment of cloud mass in anvils.

2.3.3 The Cloud Model

Both the Tiedtke and the Bechtold schemes use a simple one-dimensional cloud model to compute the convective tendencies of Eq.(2.1). The updraught of the cloud ensemble is assumed to be in steady state. The budget equations for mass, heat, moisture and momentum for the ascending air are:

$$\frac{\partial M_u}{\partial z} = E_u - D_u$$

$$\begin{aligned}
\frac{\partial}{\partial z}(M_u s_u) &= E_u s - D_u s_u + L\rho c_u \\
\frac{\partial}{\partial z}(M_u q_u^v) &= E_u q^v - D_u q_u^v - \rho c_u \\
\frac{\partial}{\partial z}(M_u q_u^c) &= -D_u q^c + \rho(c_u - g_p) \\
\frac{\partial}{\partial z}(M_u \alpha_u) &= E_u \alpha - D_u \alpha_u
\end{aligned} \tag{2.3}$$

where q_u^c is the cloud water content in the updraughts. A similar system of equations is applied to calculate the variables within the downdraught of the cloud ensemble.

The downdraught region is assumed to be at saturation (being maintained at saturation by evaporation of precipitation) and to contain no cloud water:

$$\begin{aligned}
\frac{\partial M_d}{\partial z} &= E_d - D_d \\
\frac{\partial}{\partial z}(M_d s_d) &= E_d s - D_d s_d - L\rho c_d \\
\frac{\partial}{\partial z}(M_d q_d^v) &= E_u q^v - D_d q_d^v + \rho e_d \\
\frac{\partial}{\partial z}(M_d \alpha_d) &= E_d \alpha - D_d \alpha_d
\end{aligned} \tag{2.4}$$

The vertical integration of (2.3) from cloud base to cloud top and of (2.4) from the top of the downdraughts to the surface yields the values of the variables within the updraught and the downdraught, respectively, which can then be used to calculate the convective tendencies.

To perform the integration, we have to specify:

- the mass flux M_u and the values of the variables s_u, q_u^v, q_u^c and α at the cloud base as lower boundary conditions,
- the mass flux M_d and the values of the variables s_d, q_d^v and α_d at the top of the downdraughts as upper boundary condition,
- the entrainment rates E_u and E_d, and the detrainment rates D_u D_d f the up and downdraughts, respectively, as functions of the available grid-scale model parameters, and
- a parameterisation of the microphysical processes.

All assumptions made in this context can be generally regarded to as "closure conditions". However only those assumptions, which connect the intensity of cumulus convection directly to the grid-scale forcing, are usually referred to as *closure conditions*.

In particular, in these schemes, the rate of horizontal mass exchange has to be specified, and the mass flux at cloud base is determined by the assumption of convective quasi equilibrium. These conditions will be discussed in Section 2.4

The parameterisation of microphysical processes is specific to the cloud model (this can been seen as a parameterisations within a parameterisations) and is briefly summarised below (Doms et al., 2011). Some differences in cloud physics representation are present between the schemes and are reported.

Microphysics and precipitations

- *Condensation/deposition within the updraught*

  The calculation of the condensation rate of water vapour in the ascending updraught air is based on saturation adjustment. Whenever supersaturation occurs, the specific humidity q_u^v is set back to the saturation value and the difference is interpreted as the condensed cloud water.

- *Evaporation of precipitation within the downdraught*

  The computation of e_d is also based on the saturation adjustment technique. Downdraughts are assumed to be at saturation which is maintained by evaporation of precipitation. The associated evaporative cooling is taken into account in the heat equation.

- *Formation of precipitation within the updraught*

  These processes are treated in different ways in the two scheme.

  In the Tiedtke mass-flux a simple parameterisations is used to estimate the conversion of cloud droplets to precipitative drops. Freezing and melting processes are not considered in this representation, so the rate of formation of convective precipitation is simply set to

$$g_p = K_p(z) q_u^c \tag{2.5}$$

depending linearly on the updraught cloud water content and a height dependent conversion function K_p: different values of K_p have been proposed in the literature. Besides, the growth of rainwater due to collection (i.e. the accretion process)is not taken into account explicitly.

For example, in the Tiedke mass-flux scheme implemented in the COSMO-model the conversion function is chosen to be of the form:

$$\begin{cases} 0 & \text{if } z \leq z_b + \Delta z_c \\ \beta_p & \text{if } z > z_b + \Delta z_c \end{cases} \tag{2.6}$$

This functional form suppresses the formation of precipitation in a region Δz_c above cloud base at height z_b. In COSMO-model these parameters are set to $\beta_p = 2.0 \cdot 10^{-3}\ s^{-1}$, $\Delta z_c = 1500$ m over water and $\Delta z_c = 3000$ m over land.

On the other hand, in the Bechtold scheme, the conversion from cloud condensate to precipitation is treated following Sundqvist (1978):

$$g_p = \frac{M_u}{\rho} \frac{c_0}{0.75 w_u} q_u^{li} [1 - exp[-(q_u^{li}/q_{icrit})^2)]] \tag{2.7}$$

with q_u^{li} total cloud condensate (liquid and ice), w_u vertical velocity in the updraught and c_0, q_{icrit} constants depending on the model settings.

- *Evaporation of cloud water in the environment*

  Cloud condensate which has been detrained into the subsaturated environment is assumed to evaporate immediately. Thus,e_l is set to

$$e_l = \frac{\rho}{D_u} q_u^c \tag{2.8}$$

- *Evaporation of precipitation below cloud base* The evaporation rate of precipitation is calculated in the shemes according to Kessler (1969) with slightly modified coefficients. As the evaporation rate depends nonlinearly on the precipitation flux, we have to take into account that convective precipitation covers only a area fraction C_p of a grid cell.

  Thus, the area mean of the evaporation rate is formulated:

$$e_p = C_p \alpha_1 (q_{sw}^v - q^v) \sqrt{\frac{(p/ps)^{0.5}}{\alpha_2} \frac{P}{C_p}}, \tag{2.9}$$

where q^v_{sw} is the saturation specific humudity. α_1, α_2 are two constsnts, set to $\alpha_1 = 5.0 \cdot 10^{-4}$ and $\alpha_2 = 0.011$ repsectively. The correction factor $(p/ps)^{0.5}$ considers approximately the impact of air density on the fall velocity of the particles. C_p depend on the mesh size Δs by using the heuristic relation:

$$C_p = min(1.0, \sqrt{\Delta s_0 / \Delta s}) \tag{2.10}$$

Δs_0 is a limiting horizontal scale which is set to few km.

2.3.4 Forcings to the cloud model

(a) *Downdraught mass flux at the level of free sinking*

In the parameterisation schemes downdraughts are considered to originate from cloud air influenced by the mixing with environmental air at the level of free sinking (LFS).

The LFS is assumed to be the highest model level where a mixture of equal parts of cloud air and saturated environmental air at wet-bulb temperature becomes negative buoyant with respect to the environment. This procedure defines also the boundary values for s_d, q^v_d and α_d at the top of the downdraughts. The downdraught mass flux at z_{LFS} the height of the level of free sinking, is assumed to be directly proportional to the updraught mass flux at cloud base.

That is

$$(M_d)_{z_{LFS}} = \gamma_d (M_u)_{z_b} \tag{2.11}$$

where γ_d (≈ 0.3) is a disposable parameter which determines the intensity of the downdraughts.

(b) *Specification of entrainment and detrainment*

Lateral transports across cloud boundaries is represented by entrainment and detrainment.

For the updraught, entrainment is assumed to occur via turbulent exchange of mass (turbulent entrainment E^T_u) and through organized

inflow associated with large-scale convergence (dynamic entrainment E_u^D).

Detrainment form the updraught is supposed to be made up of contributions from turbulent mixing (D_u^T) and from organized outflow at cloud top (D_u^D). For the downdraught,only turbulent entrainment and detrainment (E_d^T,D_u^T) are considered:

$$\begin{aligned} E_u &= E_u^T + E_u^D \\ E_d &= D_u^T + D_u^D \\ E_d &= E_d^T \\ D_d &= D_d^T \end{aligned} \tag{2.12}$$

The lateral turbulent mixing terms are parameterized according to

$$\begin{aligned} E_u^T &= \epsilon_u M_u \\ D_u^T &= \delta_u M_u \\ E_d^T &= \epsilon_d \left| M_u \right| \\ D_u^T &= \delta_d \left| M_d \right| \end{aligned} \tag{2.13}$$

where $\epsilon_u = \delta_u$ and $\epsilon_d = \delta_d$ is assumed for the entrainment/detrainment parameters to ensure that there is no vertical change of the updraught mass flux due to turbulent mixing processes. In general, these parameters have different values depending on the type of convection.

Dynamic entrainment is parameterised according to the assumption that organized lateral flow into the cloud is directly proportional to the local grid-scale moisture convergence:

$$E_u^D = -\frac{\rho}{q^v} v \cdot \nabla q^v \tag{2.14}$$

Organized entrainment is considered only in the lower part of the convective cloud where large-scale convergence is encountered. It is negleted for shallow convection.

Dynamic detrainment usually occurs in the upper regions of cumulus clouds, where the rising air loses its buoyancy relative to the environment resulting in a deceleration of the updraught vertical velocity and a corresponding organized lateral outflow.

(c) *Temperature and humidity parameters at the cloud base*

In order to integrate the updraught equations (2.3) using the above assumptions, the grid-scalee variables T, q^v, q^c and α at the cloud base level must be specified.

2.4 Closure Assumptions

Both the Tiedtke and Bechtold mass-flux schemes discriminate three types of convection:

- *penetrative convection*
- *shallow convection*
- *midlevel convection*

which are treated by different closure hypotheses. Only one type of convection can be present at a grid point at a time. Thus, layered convection (i.e. midlevel convection above a layer of shallow convection) can not be described by the schemes.

Both shallow and penetrative convection have their roots in the atmospheric boundary layer. They differ, however, in vertical extent, which is predefined by the vertical extend of the unstable thermal stratification where convection is formed. Penetrative convection often occurs in regions with large-scale convergence in the lower troposphere, while shallow convective clouds can also be formed in case of slightly divergent flow. The latter are often driven by evaporation from the ground or water surface.

On the other hand, midlevel convection has its roots not in the boundary layer but originates at levels within the free atmosphere. Convective cells of this type often occur in rainbands at warm fronts or in the warm sector of extratropical cyclones. They are probably formed by dynamically forced lifting of low-level air until it becomes saturated at the level of free convection. Often a low-level temperature inversion exists which inhibits convection to be initiated freely from the surface layer.

Depending on the presence of a specific type of convection, the following closure hypotheses are respectively applied in the two schemes.

2.4.1 Closure assumpions for the Tiedke mass-flux scheme

In case of shallow or penetrative convection, an equilibrium type of closure is applied by imposing a moisture balance for the subcloud layer such that the vertically integrated specific humidity is maintained in the presence of grid-scale, turbulent and convective transports (Kuo-type closure; Kuo et al., 1980).

Using the source term in the budget equation for the specific humidity q_v (second equation in (2.1)), this balance can be formulated as (Tiedtke, 1989):

$$M_u(q_u^v - q^v) + M_d(q_d^v - q^v)_{z_b} = -\int_{z_s}^{z_b} \left(\rho \cdot \nabla q^v + \frac{\partial F^{q^v}}{\partial z}\right) dx \qquad (2.15)$$

where z_s is the terrain height, z_b is the height of the cloud base and F^{q^v} the vertical turbolent flux of specific humudity.

Convection will only occur when the right hand side of Eq.(2.15) is positive, that is when moisture convergence tends to increase the subcloud moisture content.

In case of midlevel convection the updraught mass flux at cloud base is simply set equal to the grid-scale vertical mass transport,

$$(M_u)_{z_b} = (\rho w)_{z_b} \qquad (2.16)$$

This implies that the amount of moisture which is vertically advected through cloud base is made fully available for the formation of convective cells.

2.4.2 Closure assumpions for the Bechtold mass-flux scheme

Following the derivation Bechtold et al.(2014) that included earlier work by Donner and Philips (2003), Nordeng (1994) and Gregory et al. (2000), an equilibrium is assumed between the large-scale and boundary-layer forcing (generating convective available potential energy) and convection (reducing the CAPE).

CAPE (J kg^{-1}), the density-weighted buoyancy integral of an entraining ascending air parcel from the base to the top of the cloud, can be defined as:

$$CAPE = -g \int_{base}^{top} \frac{T_v^u - \bar{T}_v}{\bar{T}_v} \, dz \tag{2.17}$$

where $\bar{T}_v$ is the areal mean of virtual temperature, T_v^u is the temperature of an air parcel lifted pseudoadiabatically (with no entrainment of air), g is gravity.

Taking the time derivative of this equation one can derive a prognostic equation for CAPE and identify the different production/sink terms: the production by lage scale advection (LS), the production by boundary layer processes (surface heat fluxes, BL) and a sink of CAPE due to convective transport and mixing and evaporative cooling:

$$\frac{\partial CAPE}{\partial t} = g \left[\int_{base}^{top} \frac{1}{\bar{T}_v} \frac{\partial T_v}{\partial t} \, dz - \int_{base}^{top} \frac{1}{\bar{T}_v} \frac{\partial T_v^u}{\partial t} \, dz + \frac{T_v^u - \bar{T}_v}{\bar{T}_v}|_{base} \frac{\partial z_{base}}{\partial t} \right] \tag{2.18}$$

which can be rewritten as:

$$\frac{\partial CAPE}{\partial t} = \frac{\partial CAPE}{\partial t}|_{LS} + \frac{\partial CAPE}{\partial t}|_{BL} + \frac{\partial CAPE}{\partial t}|_{CONV=shall+deep} \tag{2.19}$$

The last term is the sum of the contributions from shallow and deep convection. The tendency due to convection can either be approximated assuming that cumulus convection acts to remove CAPE over a convective time scale τ (Frisch and Cappell 1980; Betts and Miller 1986; Nordeng 1994)

$$\frac{\partial CAPE}{\partial t}|_{CONV,1} = -\frac{CAPE - CAPE_{PBL}}{\tau} \tag{2.20}$$

or by assuming that convection counteracts the large-scale forcing by stabilization through environmental compensating subsidence: this latter expression then brings in the convective mass flux which is the required quantity in a mass flux convection scheme.

$$\frac{\partial CAPE}{\partial t}|_{CONV,2} = -\int_{base}^{top} \frac{g}{\bar{T}_v} M \left(\frac{\partial \bar{T}_v}{\partial z} + \frac{g}{c_p} \right) \, dz \tag{2.21}$$

Combining the two equations with:

$$M = M_u + M_d = \frac{(M_u)_{z_b}}{(M_{u*})_{z_b}} M^*$$

the ratio between the actual (final) cloud base mass flux and the unit (initial) cloud base mass flux $\frac{(M_u)_{z_b}}{(M_{u*})_{z_b}}$ is the convective scaling or closure factor. The initial mass flux profile M^* is known from the updraught and downdraught computation starting at cloud base.

The "final" expression for the cloud base mass flux is given by (Bechtold et al., 2014):

$$(M_u)_{z_b} = (M_{u*})_{z_b} \frac{CAPE - CAPE_{PBL}}{\tau} \frac{1}{-\int_{base}^{top} \frac{g}{\bar{T}_v} M^* \left(\frac{\partial \bar{T}_v}{\partial z} + \frac{g}{c_p} \right) dz} \tag{2.22}$$

τ, the convective adjustment time, is given by $\tau = \alpha_{res} \tau_c H / w_H^u$ where τ_c is the convective turnover time scale α_{res} is a factor depending on the horizontal model resolution, H the cloud depth and w_H^u the cloud averaged updraught velocity.

For shallow convection, the mass flux in the PBL is parameterised as:

$$(M_u)_{z_b} = \frac{-g \int_{surf}^{base} \left[\left(\frac{\partial \bar{h}}{\partial t} \right)_{turb} + \left(\frac{\partial \bar{h}}{\partial t} \right)_{dyn} + \left(\frac{\partial \bar{h}}{\partial t} \right)_{rad} \right] dz}{(h_u - \bar{h})_{base}} \tag{2.23}$$

here h is the moist static energy due to contribution from different processes, taking into account the tendencies of the model produced by other parameterisations.

It is worth pointing out is that while the Tiedtke scheme treats shallow non-precipitation convection only, the Bechtold scheme allows "shallow convection" to produce precipitation.

Finally, the closure for midlevel convection is simply set to

$$(M_u)_{z_b} = (\rho w)_{z_b} \tag{2.24}$$

as in the Tiedtke scheme.

Chapter 3

Sensitivity to the moist convection scheme: one case study

3.1 Description of the experiments

In order to study the sensitivity of COSMO-model precipitation forecast to the different moist convection parameterisation scheme, namely the Tiedtke and the Bechtold scheme, an evaluation of the model performance with the two schemes was done for a case study. In particular this investigation was carried out for a precipitation event occured over the catchment of the Serchio river (wich has a size of approximately 2000 km^2, located in the North of Tuscany region, see Fig. 3.1) during the first week of February 2017. This area experienced heavy precipitation amounts over this period, with cumulated peaks up to 300 mm/week, due to the development of intense and stationary precipitation bands.

In fact the investigation of the model performance at high resolution and how it depends on the two different convection schemes which can be used provides useful information about the strength and the weakeness of each scheme in simulating the sub-grid convective contribution to the total cumulated precipitation. In particular in this section this impact is studied when the large-scale forcing played an important role in the total precipitation budget.

The main purpose of Limited Area Models is in fact to represent as well as possible the physical phenomena occuring over high resolution scales, by providing an accurate description of the interaction of large scale fluxes with complex topography.

Therefore this study provides an opportunity to isolate in a quite simple way which errors occured in the model runs with either the Tiedtke or the Bechtold scheme, by considering high resolution precipitation prediction. This is of particular concern also for hydrological applications, because it involves the quantitative precipitation forecasting (QPF) over a small river catchment. In this context the Serchio basin can be seen as a good benchmark as it presents peculiar morphological features: the proximity of the sea to the mountains and their interaction with the synoptic flow makes the forecast of quantitative precipitation amounts particularly challenging, also for energy applications (the area is characterized by the presence of several hydroelectric power plants). This dependence has been investigated in a sistematic way by performing some experiments. The attention has been focussed in precipitation prediction at small horizontal scales.

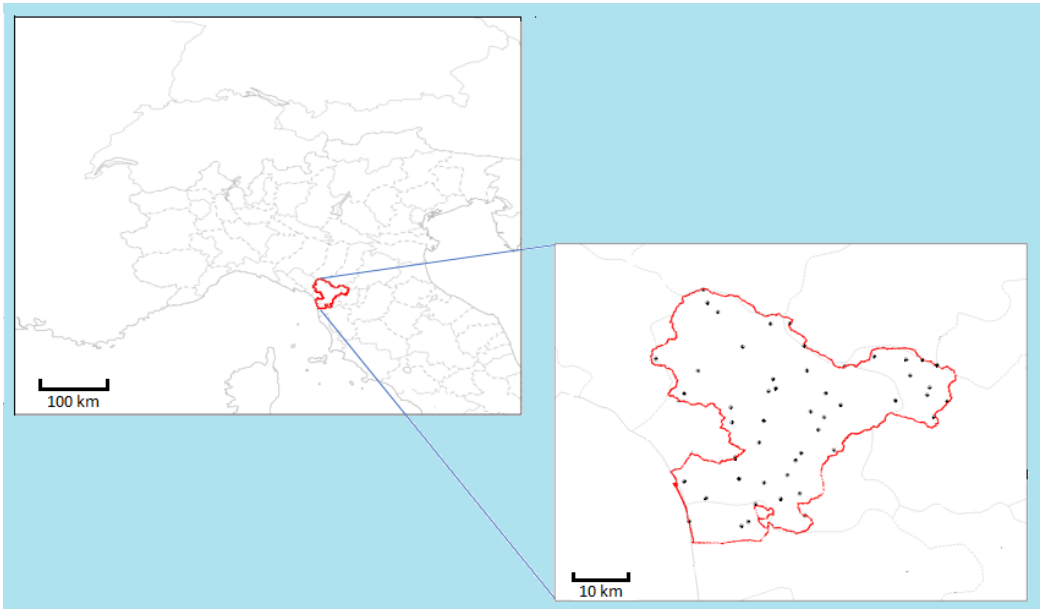

Figure 3.1: Geographical location of the Serchio river catchment's boundaries (red line) and illustration of the stations (black circles) lying in the basin.

Firstly runs of the COSMO model at 7 km horizontal resolution and 40 vertical layers were performed in determistic mode using the Bechtold scheme: these runs used the same initial and boundary conditions as the operational deterministic suite (which is run with the Tiedtke scheme, initial and 3-hourly boundary conditions from ECMWF HRES model). The experimental suite has been run from 00 UTC of 28th January to 7th February 2017, with a 72-hours forecast length. The performance of this model setup in terms of total precipitation forecast are evaluated and compared with that of the operational suite over the period.

Secondly a 10-member ensemble (Cleps-B) suite has been run from 00 UTC of the 29th January to the 5th February 2017, with a 132-hours forecast length. This suite still uses the Bechtold scheme and the same initial and boundary conditions as ensemble members 1-10 of COSMO-LEPS. The performance of this 10-member ensemble system has been quantitatively evaluated and compared to that of the 10-member ensemble made of 1-10 members of COSMO-LEPS, which are all run with the Tiedtke scheme.

3.2 Synoptic description of the case

The meteorological situation over Central and Southern Europe on 2 February 2017 at 00 UTC is that presented in Fig. 3.2. This map is relative to the analysis of ERA-Interim (ECMWF): here the different colours refers to different values of 500 hpa geopotential height[1], as reported in the legend below the figure; white isolines link locations with the same values of mean sea level pressure. The medium troposphere flow was characterized by a trough ranging from the Atlantic ocean to the Iberia while a ridge, associated with an anticyclonic wave, was located over the south-east part of Europe.

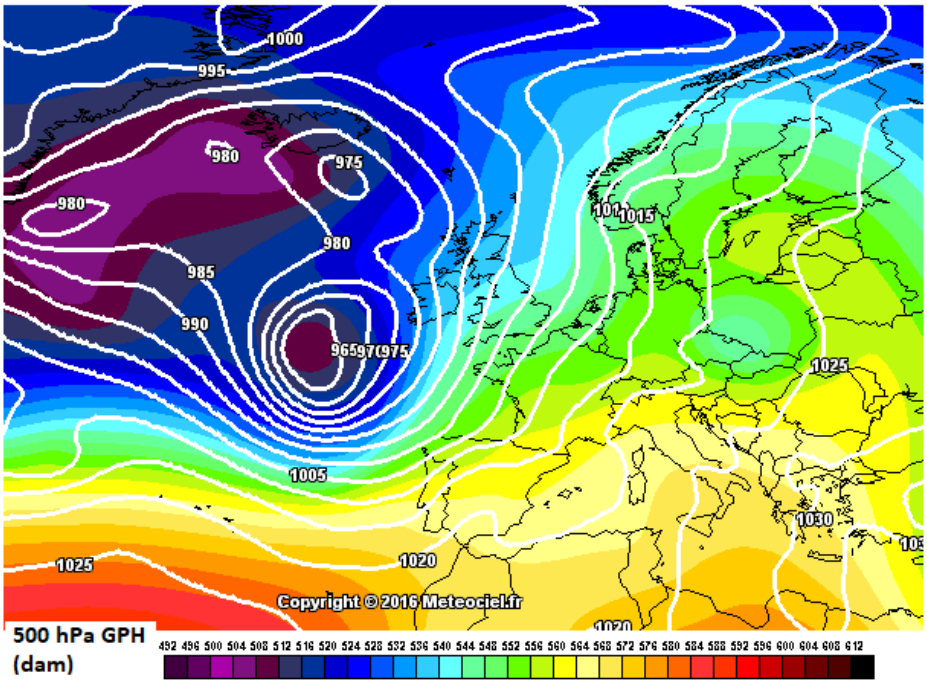

Figure 3.2: Reanalysis from ERA-Interim (ECMWF) valid at 00 UTC of 2$^{\text{th}}$ February: colours distriminate different value of 500 hPa height (in dam); solid white line link point with same MSLP (interpolated by Meteociel (www.meteociel.fr)).

[1]The geopotential Φ at a certain p-level (isobaric coordinates) is defined as $\Phi = \int_0^p g dp$; the geopotential height is computed as $GPH = \frac{\Phi}{g_0}$ considering g_0 (gravity at ground level) constant along the vertical direction.

A deep cyclone at all the vertical levels developed over the Atlantic ocean, with a mean sea level pressure minimum lower then 970 hPa at 00 UTC of 2 February; on the other hand the high pressure system over eastern Europe reached a maximum value of about 1030 hPa at the ground. As a consequence a south westerly flow at all levels blew across Italy, associated with warm and moist air transport from the south-west region of the Mediterranean region to the North of Italy.

The development of organised precipitation bands due to high levels flow divergence was observed over these areas, along the so called Warm Conveyor Belt (WCB).[2]

In the next days (see Fig. 3.3) the deep cyclone over the Atlantic ocean moved towards the British Isles while other baroclinic waves developed west of Iberic peninsula. Mesoscale circulation pattern over the Northern Mediterranean region remained similar with the persistance of a south westerly divergent flow at mid-high tropospheric levels. In Fig. 3.4 the synoptic situation at 00 UTC of 5^{th} February is shown. A deep trough was located over the Atlantic with a westerly flow over most of Europe.

The persistence of the aforementioned mesoscale situation over Northern Italy for some days was favoured by the slow translation of the deep Atlantic trough towards the east due to the presence of the blocking high over the Balcanic Peninsula.

[2]WCB is typically associated to large scale ascending air masses in the warm sector of an extratropical cyclone (Browning, 1971; Harrold, 1973). The horizontal component of the trajectories is almost parallel to the cold front, either running on the warm side of the surface cold front or riding up the frontal surface in the case of ana-cold fronts

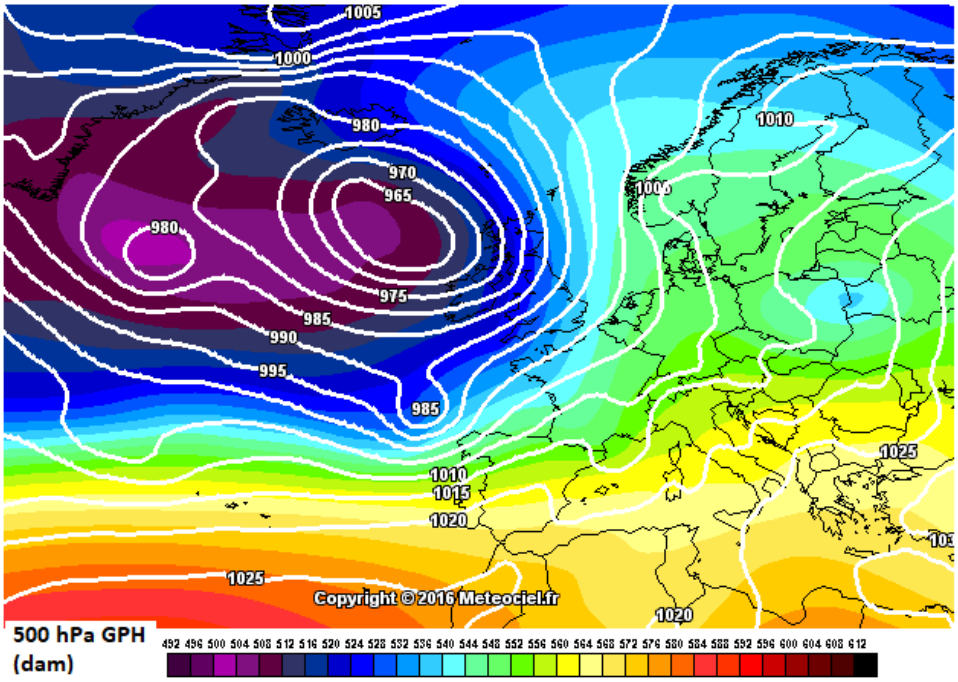

Figure 3.3: The same as Fig. 3.2, but valid at 00 UTC of 3th February.

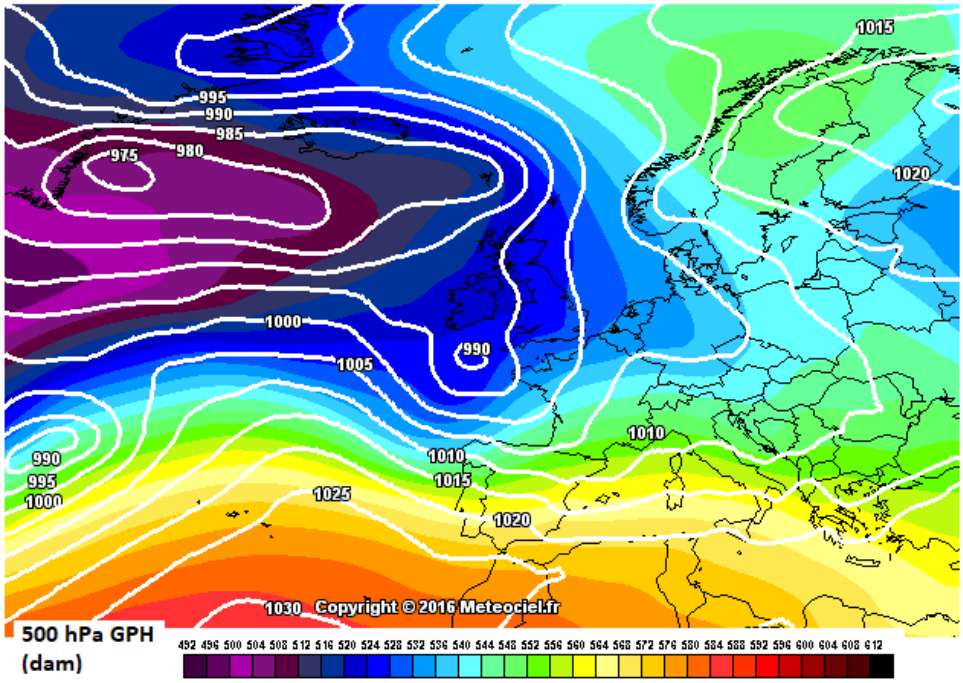

Figure 3.4: The same as Figs. 3.2 and 3.3, but valid at 00 UTC of 5th February.

As a consequence heavy precipitation amounts were observed during 3^{th}, 4^{th}, 5^{th} February over the western regions of Italy, more exposed to strong condensation with this synoptic flow: some stations located in the North-west of Italy recordered cumulated values locally up to 300mm/week in this period. Figs. 3.5 and 3.6 show the maps of 24-h cumulated precipitation as measured by the rain gauge observation network over North-West Italy, where intense precipitation were observed, during 4^{th} and 5^{th} February 2017, respectively.

It is worth underlining that peaks in cumulated precipitation were located over the western slope of Apennines and the southern slope of the Alps -upstream of the main synoptic flow- in which orographic lifting renforced precipitation systems, facilitating there condensation processes. On the other hand, lower precipitation amounts were measured over the downstream areas (i.e. over the Adriatic coastal regions, Emilia Romagna region) because of the combination of two simultaneous effects which typically occur in the atmospheric interaction with orography: the loss of columnar water content due to intense condensation and precipitation over the upstream slope and the evaporation processes encouraged by the flow descent down from the Apennines.

The most rainy day of the period was the 5^{th} February when 24-h cumulated precipitation up to 100 mm/24-h was observed over some areas in Liguria and Tuscany regions; secundary maxima up to 50 mm/24-h were measured over the southern slope of the Alps (see map in Fig 3.6).

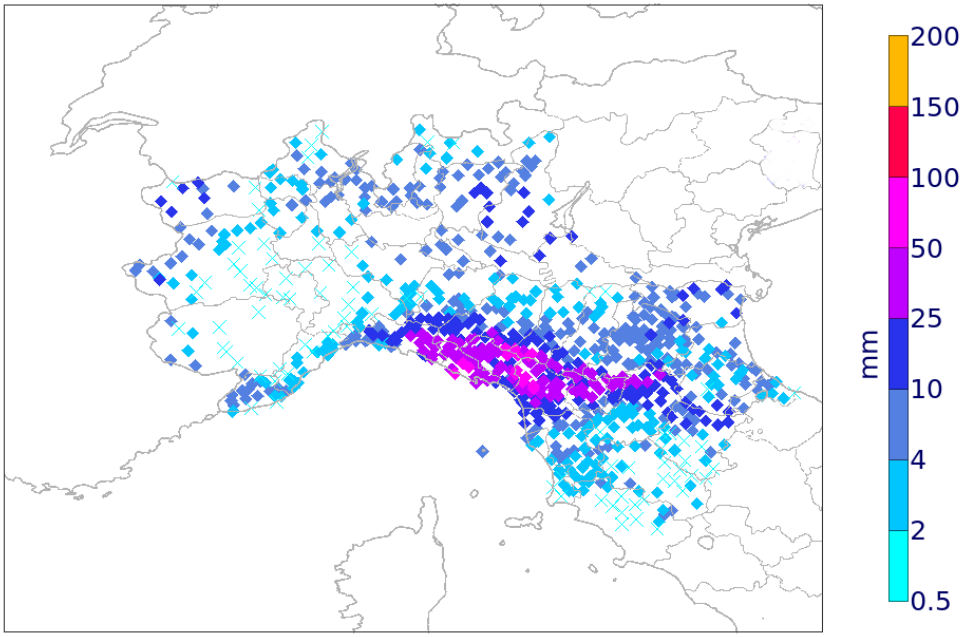

Figure 3.5: Observed 24-h rain-gauge cumulated precipitation in mm on 4$^{\text{th}}$ February 2017.

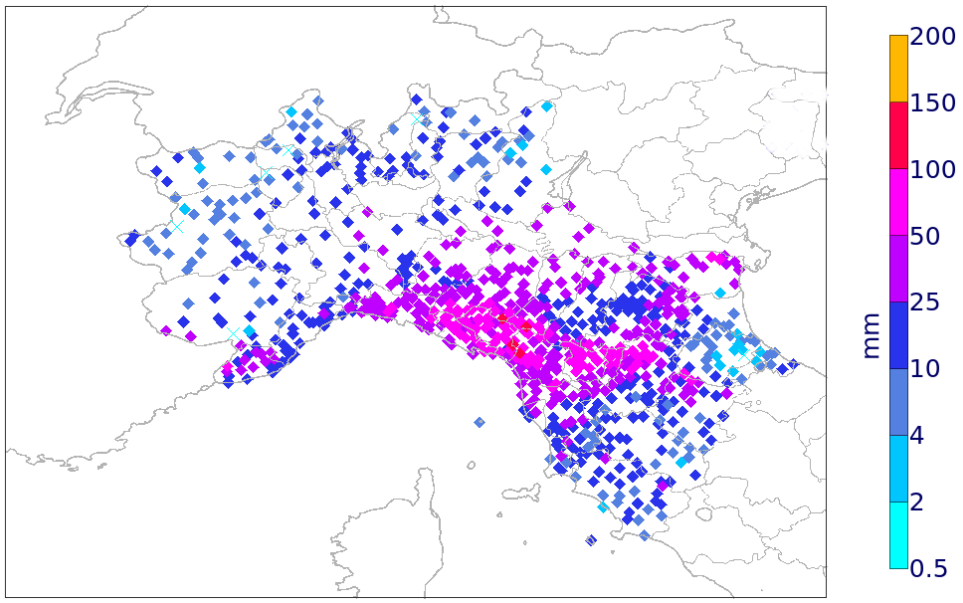

Figure 3.6: The same as Fig. 3.5, but on 5$^{\text{th}}$ February 2017.

In a second phase (between 5th and 6th February 2017) the interaction of the incoming baroclinic disturbance from the west with the Alps caused orographic cyclogenesis in the lee of the Alps (Genoa Low). This can be seen as the result of a baroclinic instability process triggered by the deformation of thermal fiels in the low troposphere produced by the Alps when a cold-front impinges on them coming from the north west (Buzzi and Tibaldi, 1987).

In addition to the medium troposphere analysis (top panel of Fig. 3.7), synoptic chart at 00 UTC of 6 February is presented in the lower panel of Fig. 3.7. This is a synoptic picture at the ground which allows to detect the main mesoscale figures, including fronts. Grey isolines refers to points with the same value of MSLP (Mean Sea Level Pressure). A cut-off low formed from the "primary" cyclone, reaching the pressure value at the ground of approximately 997 hPa at 00 UTC. A very strong cyclone was located over northern Atlantic (with surface pressure minimum below 930 hPa). In this phase precipitation over most of Northern Italy occured in association with the passage of frontal bands, linked to the depression in the gulf of Genoa.

Map of cumulated precipitation as observed by the rain gauge network over Northern Italy shows amounts up to 50 mm/24h over the eastern slope of the Apennines for 6th February (Fig. 3.8).

In the following hours, the cyclone weakened as it moved to the South. Residual precipitation were observed during 7th February over most of Southern Italy mainly in association with the occluded front (not shown here).

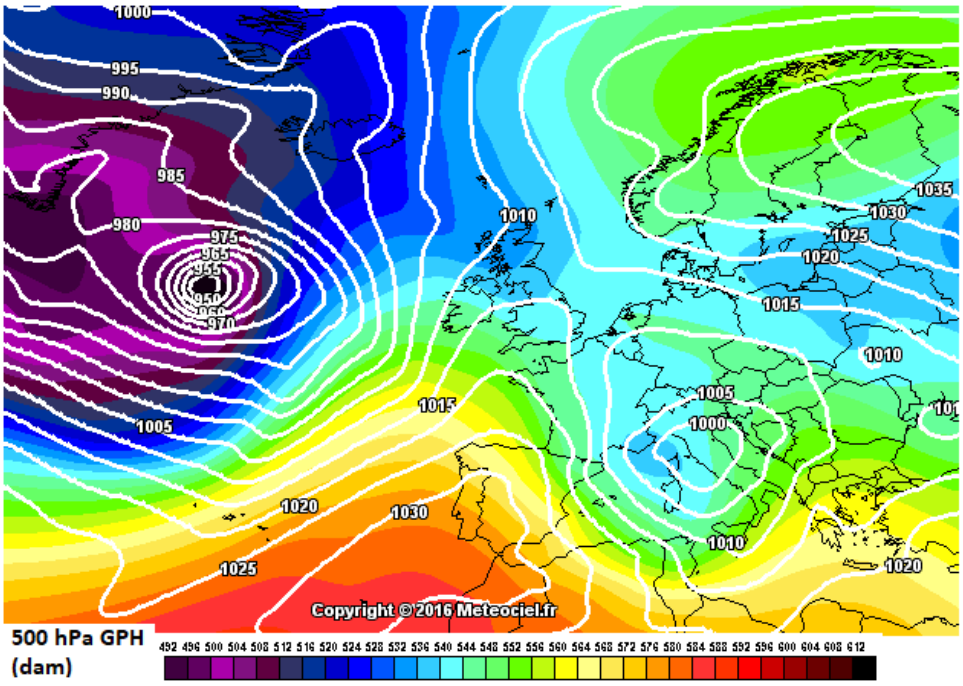

(a)

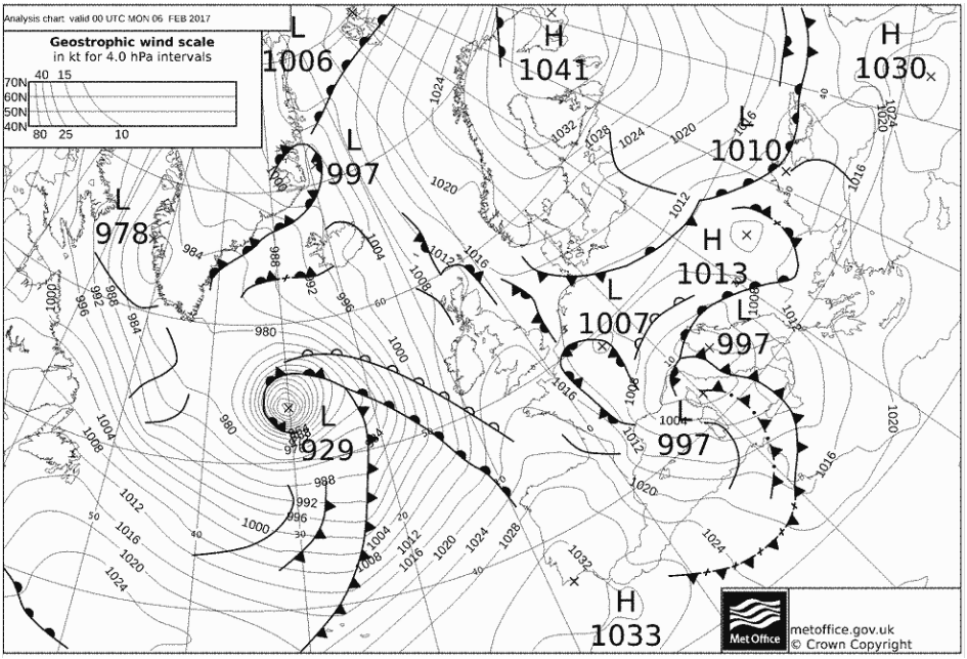

(b)

Figure 3.7: Mid tropospheric (top panel (a)) and surface level (pressure values in hPa; lower panel (b), by UK Met Office) synoptic charts valid at 00 UTC of 6th February 2017.

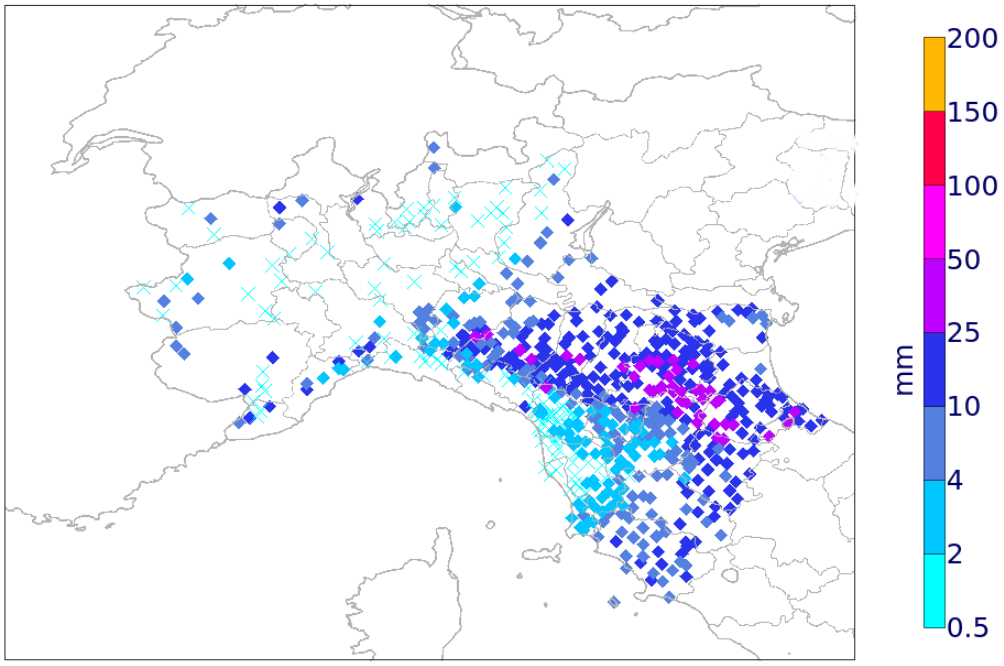

Figure 3.8: Observed 24-h cumulated precipitation in mm from rain-gauge observation on 6th February 2017

3.3 Quantitative evaluation of the experiments

Deterministic scores

In order to objectively evaluate the performance of the model, a number of quality scores has been computed.

For the quantitative evaluation of the deterministic runs, we use the MAE and Bias error:

$$MAE = \frac{1}{M}\sum_{m=1}^{M} |f_m - o_m|$$

$$BIAS = \frac{1}{M}\sum_{m=1}^{M} (f_m - o_m)$$

where M is the total number of points selected, f_m the forecast values and o_m the observed ones.

The MAE for a perfectly forecast field is zero, with larger MAE indicating decreasing accuracy of the forecast.

Positive BIAS values indicate that the forecast is on average greater than the observation, called overestimation. On the other hand, negative BIAS indicates that the forecast is on average smaller than the observation, which is called underestimation (Wilks, 1995).

Probabilistic scores

Conversely for ensemble forecast we compute some traditional probabilistic scores applied in verification tasks like the Brier Scores (BS), which is defined as the mean-square error of the probability forecasts (Brier, 1950), and or the RPS (Ranked Probability Score).

$$BS = \frac{1}{N}\sum_{i=1}^{n} (p_i - o_i)^2$$

where the observation is $o_i = 1$ (o $i = 0$) if the event occurs (does not occur), while p_i is the fraction of ensemble members which forecast the event and the index i denotes a numbering over the whole domain (N is the number of points selected, for which the score is computed). BS can take on values in the range [0,1], the perfect forecast having BS = 0 (Stanski et al., 1989;

Wilks, 1995). The BS averages the squared differences between pairs of forecast probabilities and the corresponding binary observations, representing the occurrence (or non-occurrence) of the event. In this study, the forecast probability (i.e. probability of eccendence) is evaluated for some rainfall thresholds: in this study we use 4 thresholds (1, 5, 10 and 25 mm/24h).

The RPS (Epstein 1969; Murphy 1969, 1971) is a squared measure that compares the cumulative density function (CDF) of a probabilistic forecast with the CDF of the corresponding observation over a given number of discrete probability categories.

Therefore it can be considered as a cumulative BS over the different thresholds studied:

$$RPS = \sum_{k=1}^{K} (p_k - o_k)^2$$

where $p_k = \sum_{i=1}^{M} p_i$ with, again, p_i being the probabilistic forecast for the event to happen in category i and with $o_i = 1$ if the observation is in category i or $o_i = 0$ otherwise. Note that the RPS is zero for a perfect forecast and positive otherwise.

3.4 Test in deterministic mode

Previously we were investigating the sensitivity of COSMO forecast skill in deterministic mode to the two parameterisation schemes for the precipitation event occured in February 2017.

This study can be seen as a sort of preliminary test which attempts to isolate the impact of the use of a different physical formulation on the model total precipitation forecast over the Serchio river catchment area. In fact the runs of the model compared here differs only for the treatment of the moist sub-grid convection processes, using the same initial and boundary conditions; hereafter COSMO-B refers to COSMO-model run with the Bechtold scheme and COSMO-T to model run with the Tiedtke scheme. Figs. 3.9, 3.10 and 3.11 show the 24-h total precipitation predicted by COSMO-B (lower panels) and COSMO-T (upper panels) for the run starting at 00 UTC of 3^{th}, 4^{th} and 5^{th} February 2017, respectively. In all cases, the attention is focussed on the performance of the model for +24-48h forecast range.

Considering 4^{th} and 5^{th} February 2017 (fig 3.9 and 3.10) the two forecasts show a good qualitative agreement in terms of precipitation spatial distribution over the western coast in the North of Italy, while a stronger divergence is present between the cumulated precipitation predicted over these areas by the runs of 5 February (Fig. 3.11).

Nevertheless, there are some relevant differences between the two model runs in describing quantitatively the precipitation field for all the days analysed.

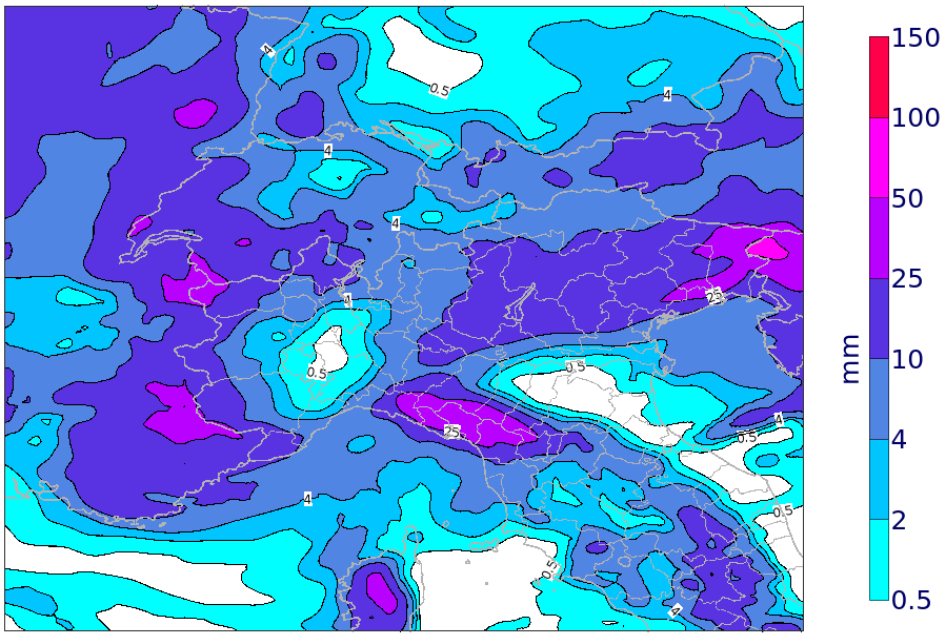

(a)

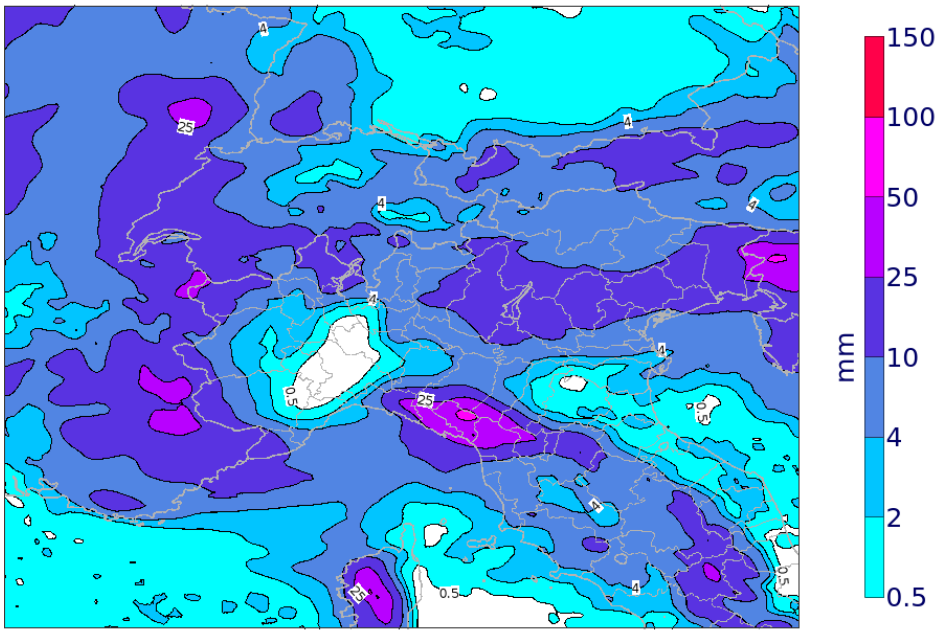

(b)

Figure 3.9: 24-h Total precipitation in mm for 4th February 2017 as predicted by COSMO-T (a) and COSMO-B (b): runs starting at 00 UTC of 3th February 2017 (forecast range +24-48)

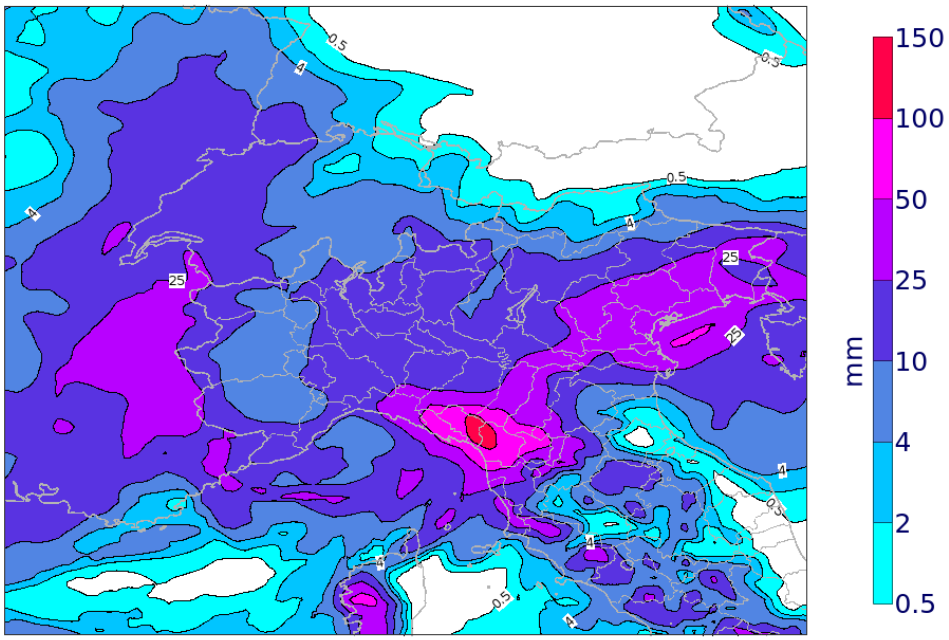

(a)

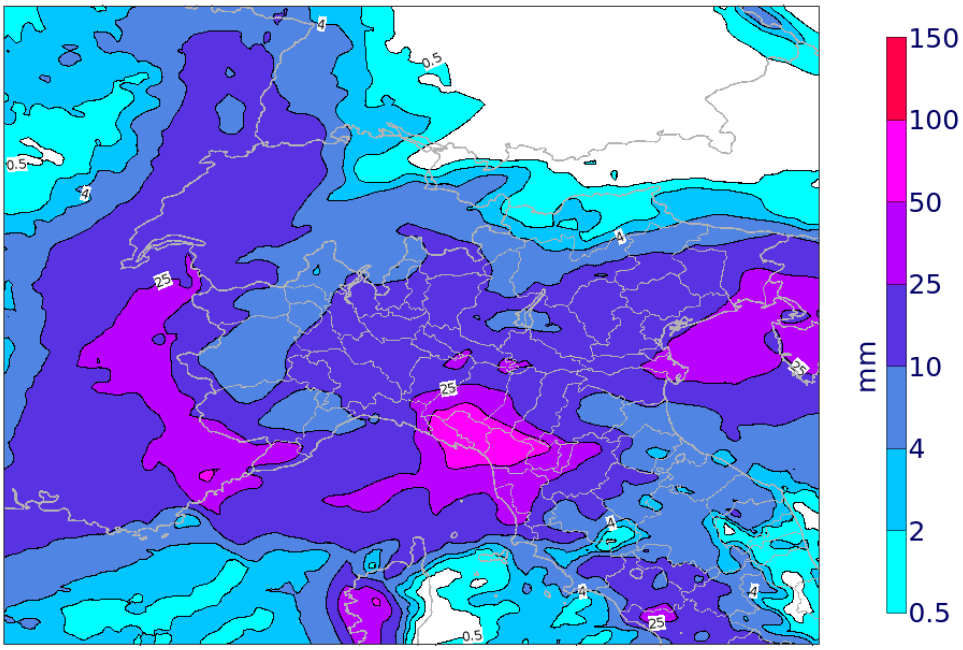

(b)

Figure 3.10: 24-h Total precipitation in mm for 5th February 2017 as predicted by COSMO-T (a) and COSMO-B (b): runs starting at 00 UTC of 4th February 2017 (forecast range +24-48).

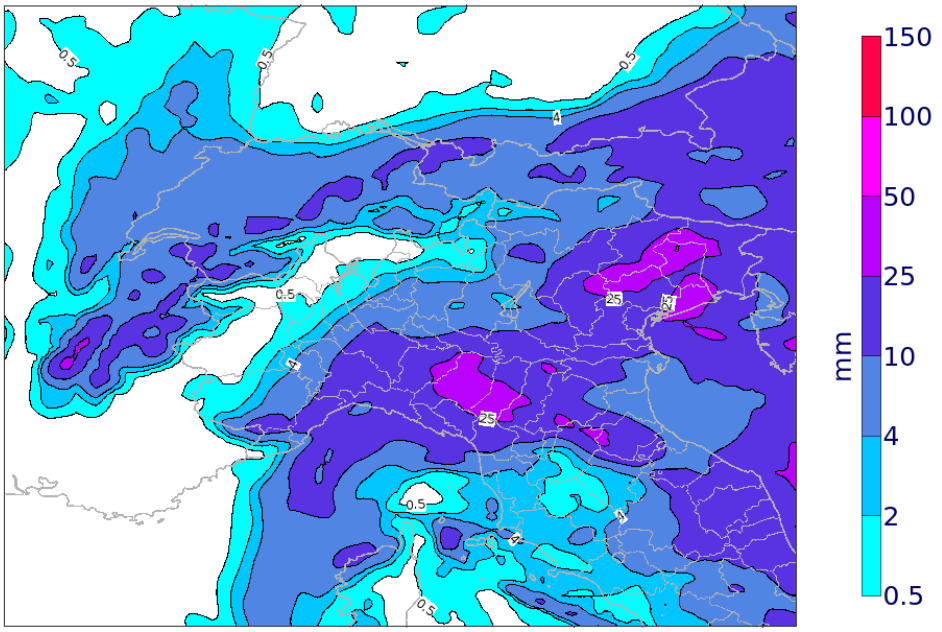

(a)

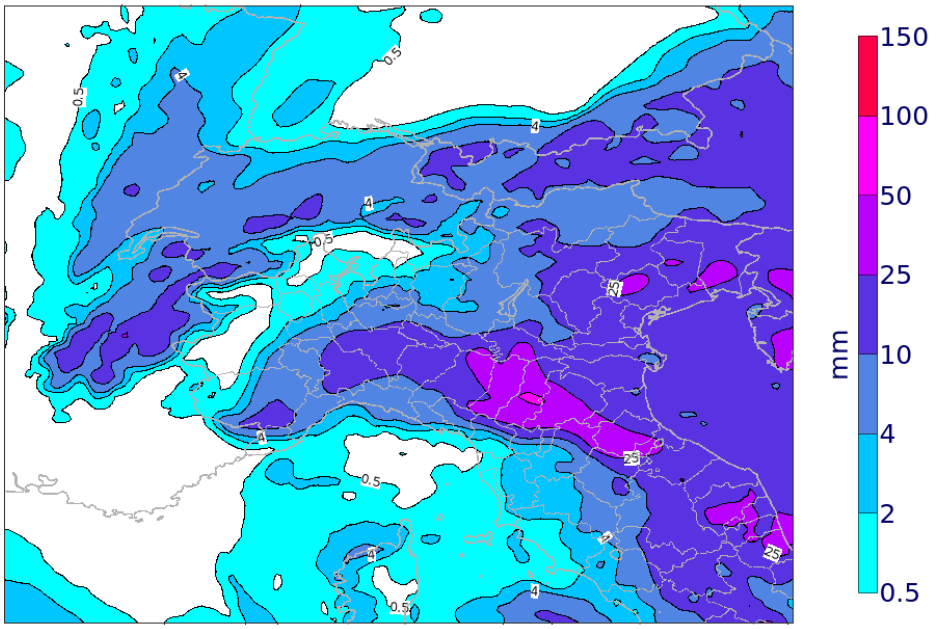

(b)

Figure 3.11: 24-h Total precipitation in mm for 6th February 2017 as predicted by COSMO-T (a) and COSMO-B (b): runs starting at 00 UTC of 4th February 2017 (forecast range +24-48).

This concept is emphasised in Figs. 3.12 and 3.13, which show the forecast differences between the COSMO-B and COSMO-T 24-h cumulated precipitation forecasts for the runs starting at 00 UTC of 4^{th} and 5^{th} February respectively, with a +24-48h forecast range (relative to the maps of Figs. 3.9 and 3.10).

It can be noticed that, for the runs of 4^{th} February (Fig. 3.12), forecast differences are likely to be especially in locating precipitation spots: maxima and minima in precipitation are spatially shifted between the two model runs, the strongest discrepancy being more evident over the northern part of Tuscany region. The difference between predicted fields shows a "dipole pattern" with alternating maxima and minima patterns at short distances.

Converserly the comparison between the runs for 6^{th} February (initialized at 00 UTC of 5^{th} February, Fig.3.13) shows a different behaviour in forecast differences. In this case the predicted fieldsby COSMO-B and COSMO-T show higher spatial coherence (correlation). This result can be interpreted as a footprint of the modification of a larger scale circulation pattern. In fact the run with the Bechtold scheme is associated to lower amounts of precipitation over all the Tyrrenic coast, while higher amounts are predicted over the Adriatic one. This problem will be discussed in the next sections.

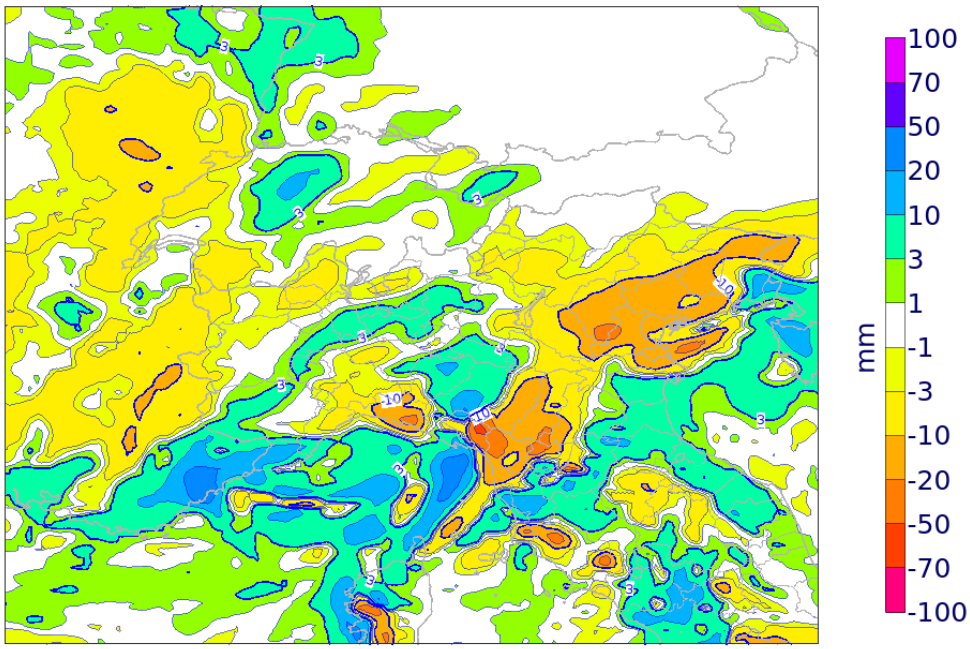

Figure 3.12: Difference in predicted 24h cumulated precipitation (in mm) between COSMO-B and COSMO-T for 5thFebruary 2017. Run initialized at 00 UTC of 4thFebruary.

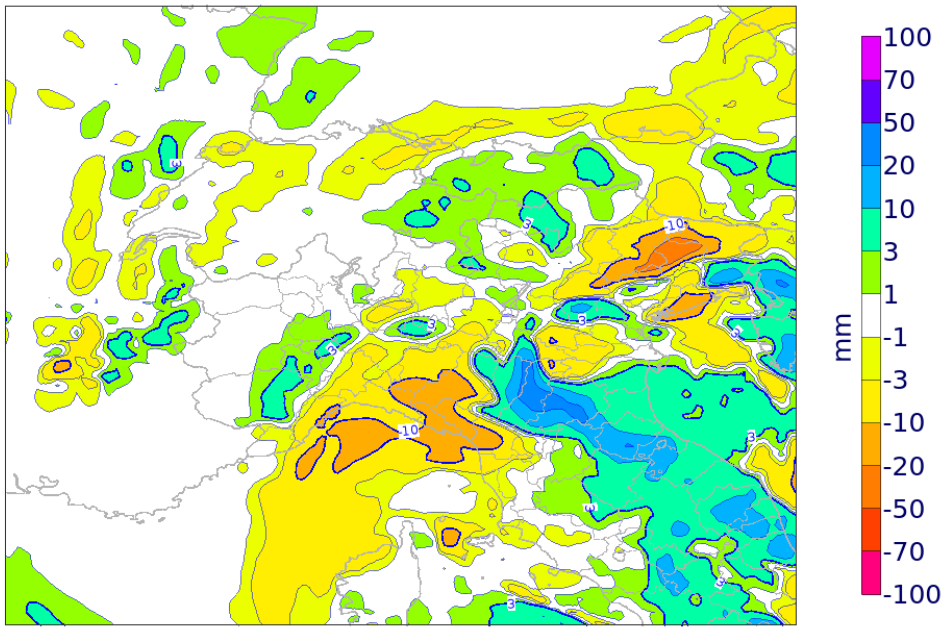

Figure 3.13: Difference in predicted 24-h cumulated precipitation (in mm) between COSMO-B and COSMO-T for 6th February 2017. Run initialized at 00 UTC of 5th February.

3.4.1 Sensitivity of model forecast on convection scheme for the Serchio area

After the qualitative evaluation of COSMO forecasts with the two schemes, a more quantitative comparison between the predicted and observed precipitation values has been carried out for a longer period, from 28th January to the 7th February 2017. In particular verification has been done for precipitations over the Serchio river catchment area.

In this case quantitative precipitations (both observed and predicted) are treated in terms of area mean instead of the points values, in order to have a quite solid statistical (and syntethic) result. This enables a more solid representation of the system performance.

Of course this approach is possible thanks to the dense coverage of regional stations over the river catchment, which allow a detailed representation of the precipitation field in this basin.

Thus predicted precipitations are obtained by averaging the model QPF (Quantitative Precipitation Forecast) in the grid-points (about 50 points) in the Serchio area (that of Fig. 3.1).

A similar procedure is repeated for the observed values, which are relative to the station points in the same geographical area (47 stations, Fig.3.1).

The comparison between the predicted and observed values of 24-h area mean cumulated precipitation over the Serchio area is presented in the figures 3.14, 3.15 and 3.16, relative to three different forecast ranges (0-+24h, +24-48h and +48-72h, respectively).

In the bar plots, red columns refer to COSMO-T, blue columns to COSMO-B and the green ones to the observed values.

COSMO-B area-averaged precipitation forecasts are clearly closer to observations than operational COSMO-T, for cases of both under- and over-estimation. This positive impact of the newly implemented Bechtold convective scheme in precipitation forecast is detectable over all the forecast ranges studied.

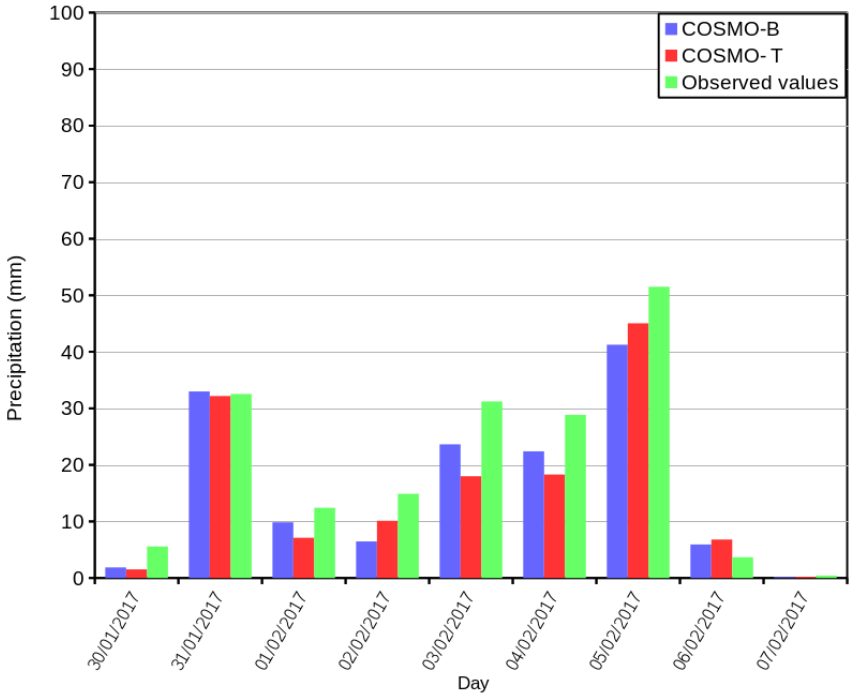

Figure 3.14: Daily predicted and observed area mean cumulated precipitation (in mm) over the Serchio area for runs from 28th January to 7th February with a 0- +24 forecast range.

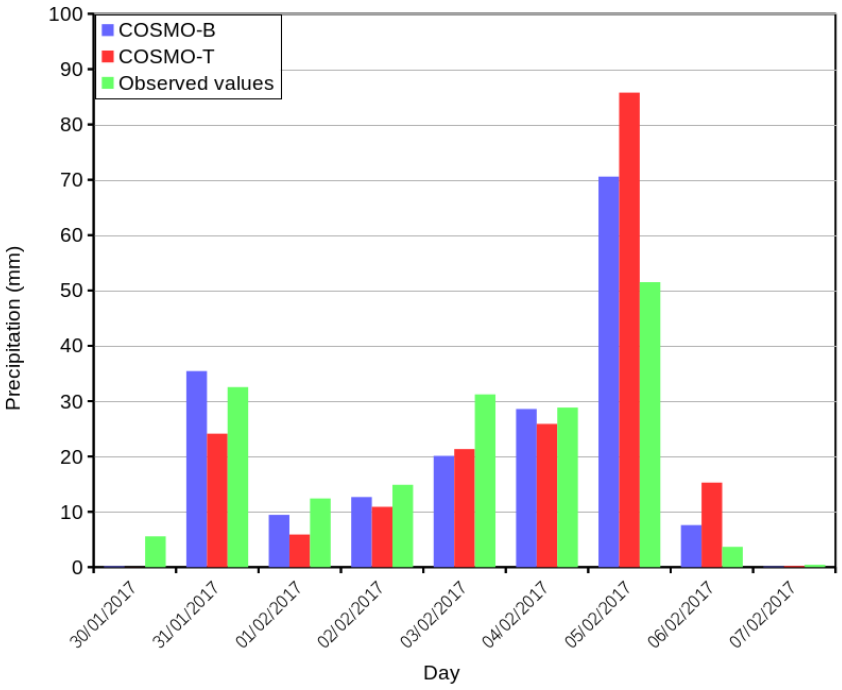

Figure 3.15: The same as Fig. 3.14 but for +24-48 forecast range.

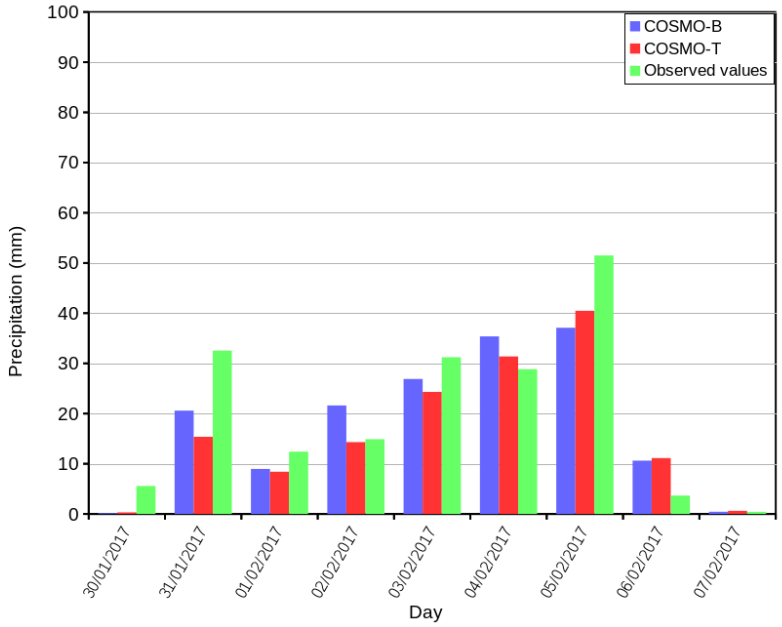

Figure 3.16: The same as Fig. 3.14 and 3.15 but for +48-72 forecast range.

Focussing the attention on the +24-48 forecast range, probably the most interesting from an operational point of view, MAE and Bias error are presented respectively in Fig. 3.17 and in Fig. 3.18 for different runs of the model at 00 UTC from 29th January 2017 to 7th February 2017 (one per day). A general improvement of the model performance can be noted in the runs using the Bechtold scheme (blue lines in the figures). In particular results show a reduction of MAE and BIAS errors for most of days. However it is interesting to underline that both schemes tend to underestimate the predicted area mean total precipitation during the first days under investigation (characterized by a weak large scale south-westerly flow, in which large part of precipitation was forced by the orographic lifting, see Maps 3.2, 3.3) and tend to overestimate in predicted values for the days of more intense events (in which precipiations were observed mainly in association with organized mesoscale frontal bands, with typically larger horizontal dimensions compared to the orographic case, see Maps in Figs. 3.4 and in 3.7).

This implies that model deficiencies are probably responsible for the lack of accurate precipitation forecasts in this case study.

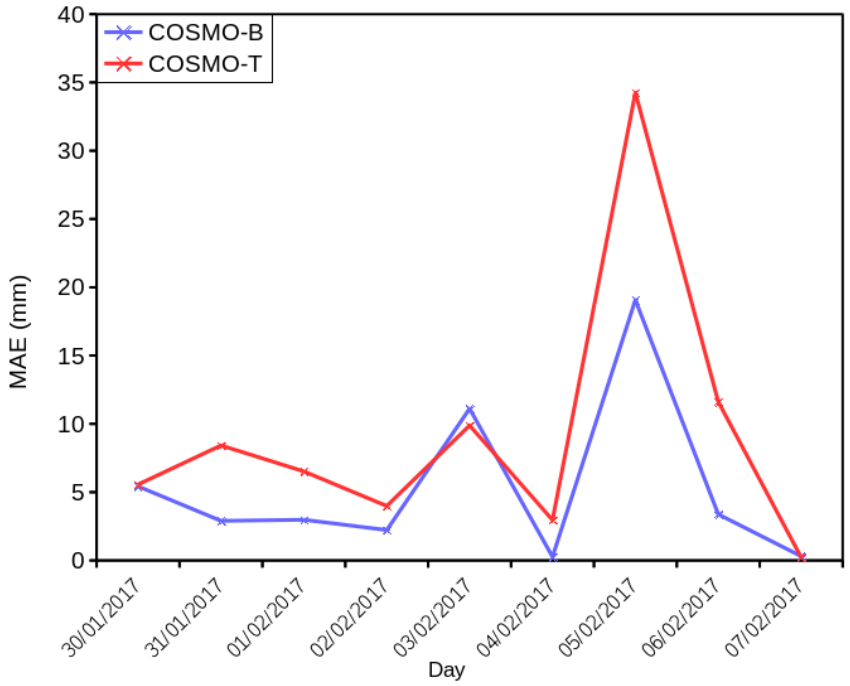

Figure 3.17: MAE (in mm) for predicted 24-h area mean cumulated precipitation over the Serchio area. The model runs are relative to those from 00 UTC of 29th January 2017 to 6th February 2017 (one per day at 00UTC) with a +24-48h forecast range.

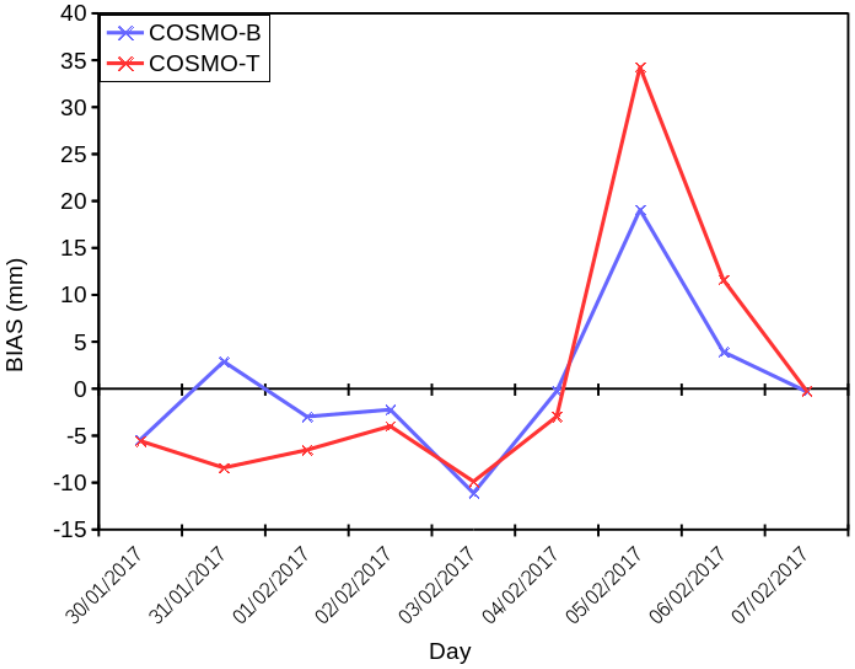

Figure 3.18: The same as Fig. 3.17, but for BIAS error (in mm).

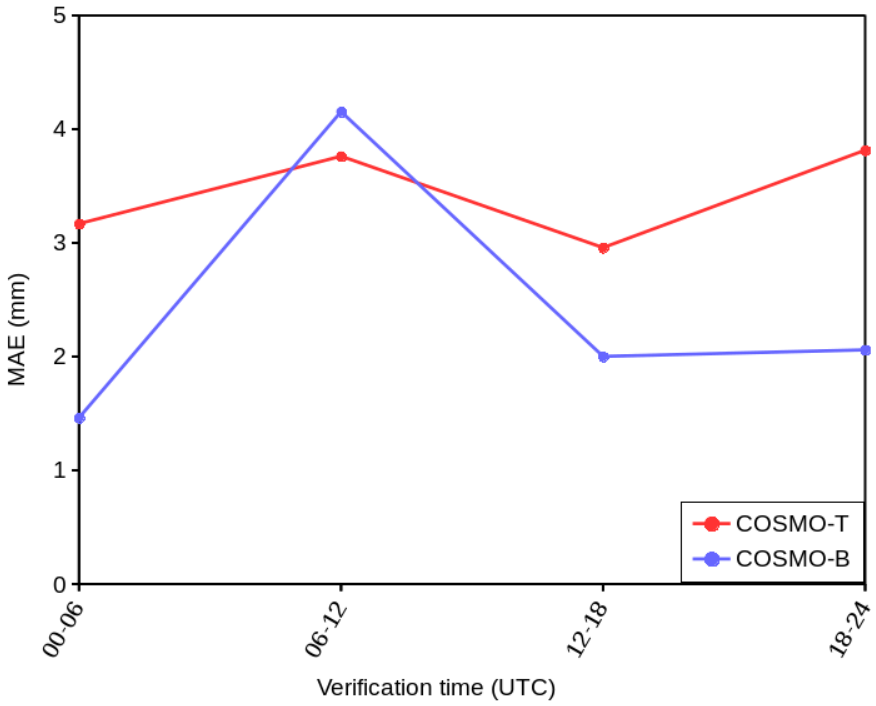

Figure 3.19: Daily distribution of MAE (in mm) for predicted 6-h area mean cumulated precipitation over the Serchio area. The model runs are relative to those from 00 UTC of 29th January 2017 to 6th February 2017 (one per day at 00UTC) for the following day.

In order to provide a more thorough investigation of the model performance during night-time and day-time, the 6-hourly distribution of the errors is studied.

In Fig. 3.19 and Fig. 3.20 the same scores are computed by considering the 6-h area mean cumulated precipitation over the Serchio area in different daily time intervals (00-06, 06-12, 12-18, 18-24; UTC time). A good impact of the newly implemented Bechtold scheme is evident expecially in the nocturnal hours when the MAE decrease, while COSMO-T performed slightly better for cumulated precipitation in the time interval 6-12 UTC. In particular, BIAS error plot (Fig 3.20) shows that the runs with the Tiedtke scheme are associated with an overestimation during the nocturnal hours and an underestimation during the central hours of the day. On the other hand, COSMO-B runs tend to reduce BIAS error, with values of the score

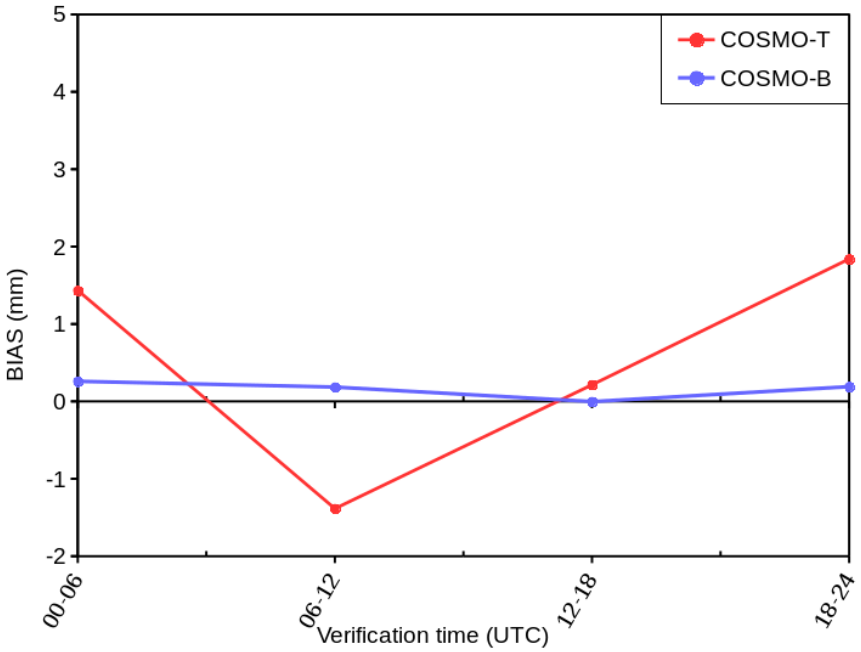

Figure 3.20: Daily distribution of Bias error (in mm) for predicted 6-h area mean cumulated precipitation over the Serchio area. The model runs are relative to those from 00 UTC of 29th January 2017 to 6th February 2017 (one per day at 00UTC) for the following day.

close to zero: COSMO-B shows diminishing systematic errors with respect to COSMO-T for almost all the verification times.

Furthermore, in order to have a picture of the model forecast skill with increasing forecast length, MAE was calculated also for 3-h area mean cumulated precipitation over the Serchio area (Fig. 3.21). Here a 24-h running mean is computed in order to have an overall "smoother" representation of model performance through the time with no day or night time effects.

A positive impact of the new implemented convective scheme is evident over most of the ranges studied, expecially for forecast ranges up to 60-h.

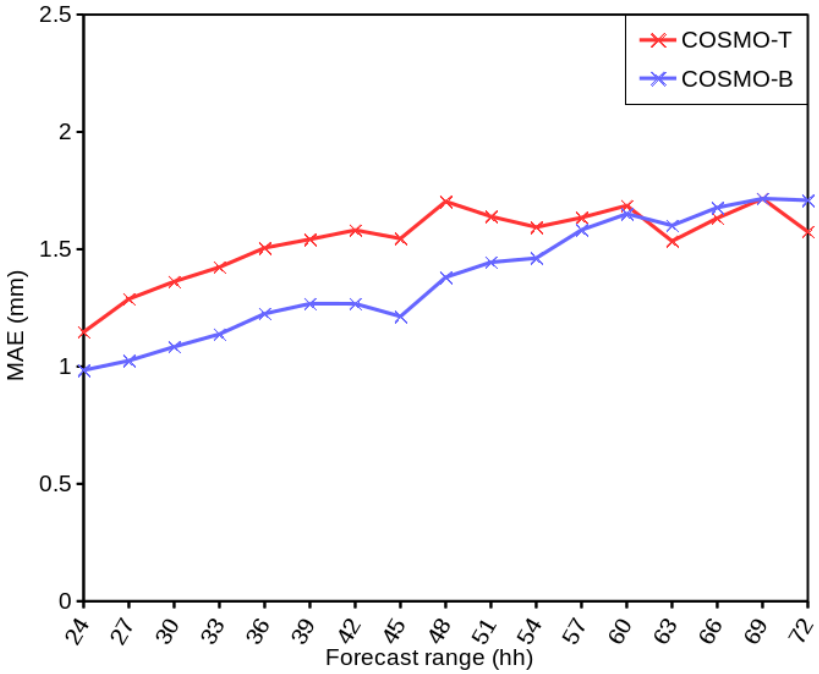

Figure 3.21: 24-h running mean of MAE (in mm) for 3-h cumulated precipitation averaged over the Serchio area.

Finally, in order to study the statistical distribution of the 24-h predicted precipitation values in the gridpoints over the Serchio area and to assess the extent to which it is sensitive to the different moist convection scheme, box-plots are costructed.

For a particular data set, the box plots presented here show the range of data falling between the 25th and 75th percentiles, and the median value (i.e. the value for which half of the total number of values is higher/lower than it, the horizontal line inside the box). The whiskers define all the values inside 1.5 times the interquartile range above the upper quartile and below the lower quartile (supposed to be the complete range of the data). Black circles refer to external values, commonly called "outliers".

A detailed comparison between the predicted (relative to the grid-points in the basin) and observed (relative to the station points lying in the Serchio area) distribution of precipitation values for the Serchio area is then presented, showing the forecast values by the model runs at 00 UTC from 3th to

5th February in the +24-48 forecast range (Figs. 3.22, 3.23, 3.24 respectively).

The boxplots again show a better performance in precipitation values distribution forecasting by COSMO-B than COSMO-T along the three days exhaminated, especially for the runs of 5th February (Fig 3.24).

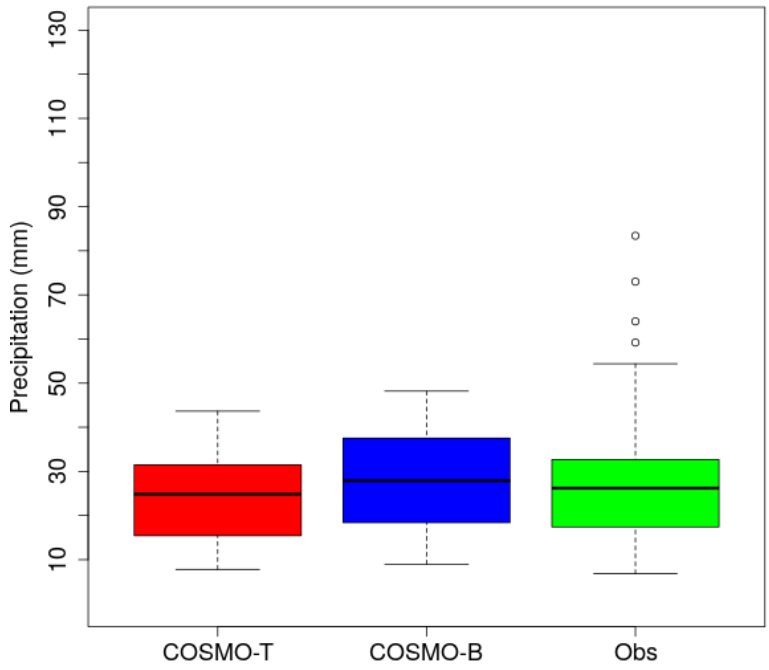

Figure 3.22: Boxplots for 24-h cumulated precipitation (in mm) over the Serchio area. The model runs starts at 00 UTC of 3th February 2017 for +24-48h forecast range. Red, blue and green boxes refer to COSMO-B, COSMO-T and observations, respectively.

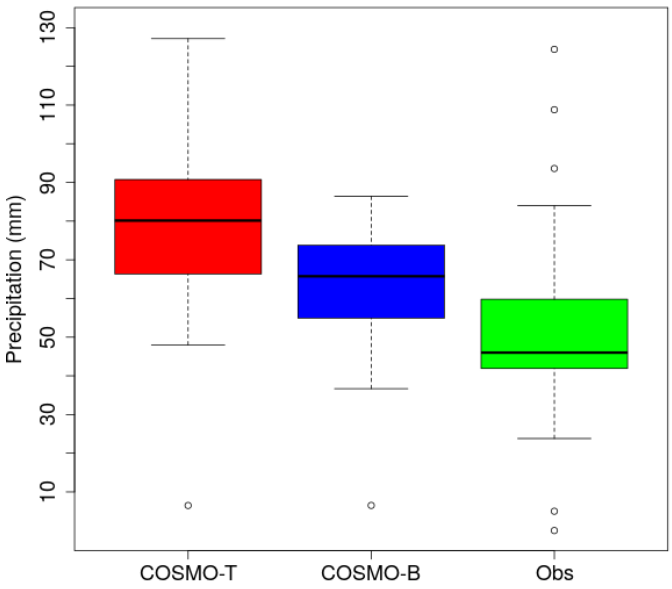

Figure 3.23: The same as Fig. 3.22, but for the runs starting at 00 UTC of 4th February 2017 for +24-48h forecast range.

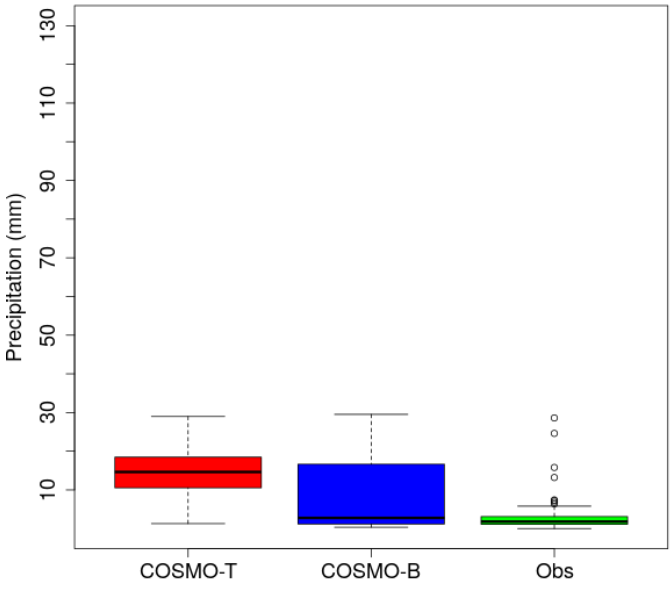

Figure 3.24: The same as Figs. 3.22 and 3.23, but for the runs starting at 00 UTC of 5th February 2017 for +24-48h forecast range.

3.4.2 Sensitivity of large-scale model forecast to the convective scheme

The last test performed in deterministic mode regards a more extensive comparison between the predicted and observed precipitation values for all the station points in the regional network over the North-west of Italy (about 800 stations, shown in Fig 3.25). Also in this case the predicted distributions were assessed by constructing boxplot for each day considered.

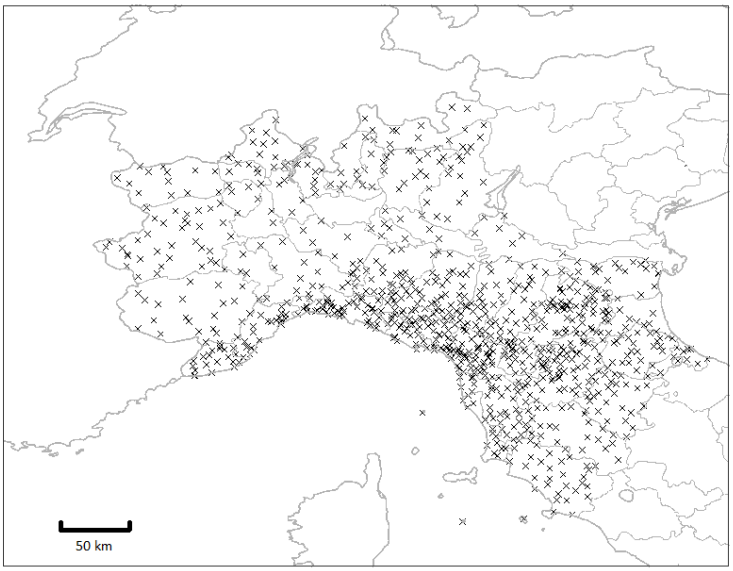

Figure 3.25: Station points adopted for precipitation boxplots over the North-west of Italy.

The principal aim of this work was to study the overall performance of the system in predicting the distribution of 24-h cumulated precipitation over a larger area than that of a small river basin. Figs. 3.26, 3.27, 3.28 show the boxplot distribution of predicted and observed precipitation values valid at 4^{th}(first figure), 5^{th} (second figure) and 6^{th} February (last figure, respectively), relative respectively to runs of the model at 00 UTC from 3^{th} February to 5^{th} February 2017 (with a +24-48 forecast range).

In this case the predicted distributions show in general to be less sensitive to the different model moist convection treatment for the runs from 3^{th} to 5^{th} February compared to the case of the Serchio area.

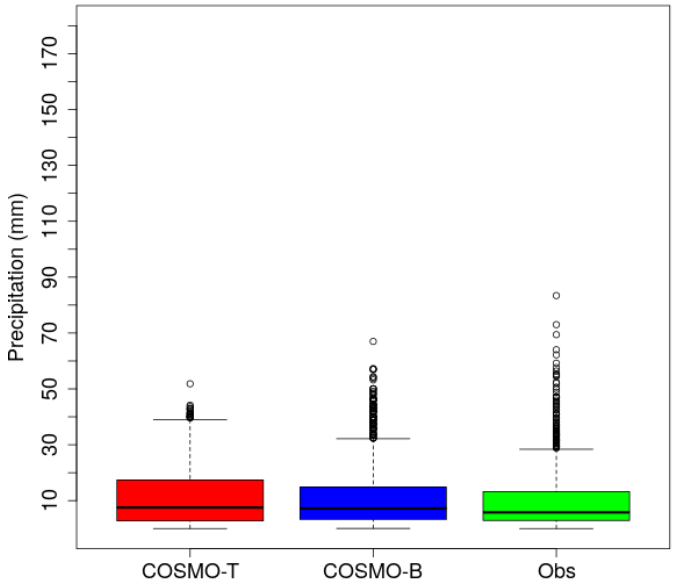

Figure 3.26: Boxplots for +24-48h cumulated precipitation (in mm) over Northern Italy. The runs are relative to 00 UTC of 3th February 2017. Red, blue and gree bars refer to COSMO-T, COSMO-B and observations, resp.

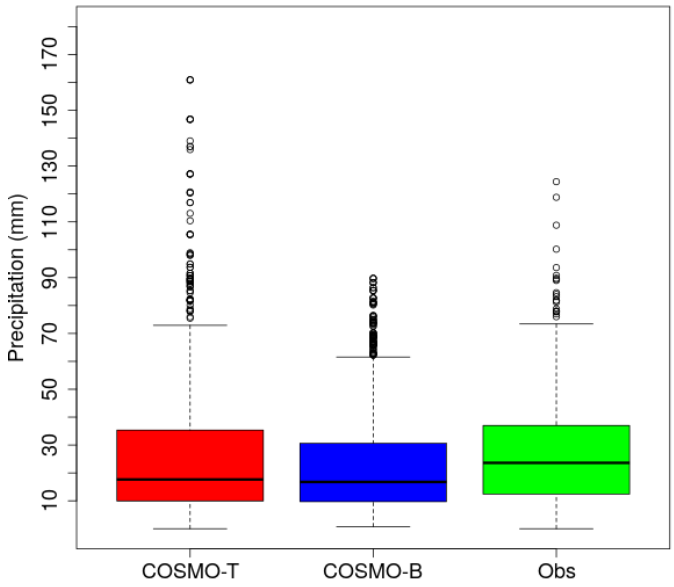

Figure 3.27: The same as Fig. 3.26, but for the runs starting at 00 UTC of 4th February 2017.

It can be noticed that COSMO-T runs predicted higher precipitation peaks for all the days reported than COSMO-B. However a more significant relative diffence in precipitation distribution as predicted by the model runs with the different schemes is noticeable in the boxplot comparison of Fig. 3.28, relative to 00 UTC 5th February runs. In fact focussing on the median values, which identify the 50-percentile, COSMO-B is quite closer to the observed one than COSMO-T.

In this case, as already pointed out, large scale precipitation patterns over all Northern Italy appear to be more sensitive to the use of a different moist convection parameterisation compared to the days before.

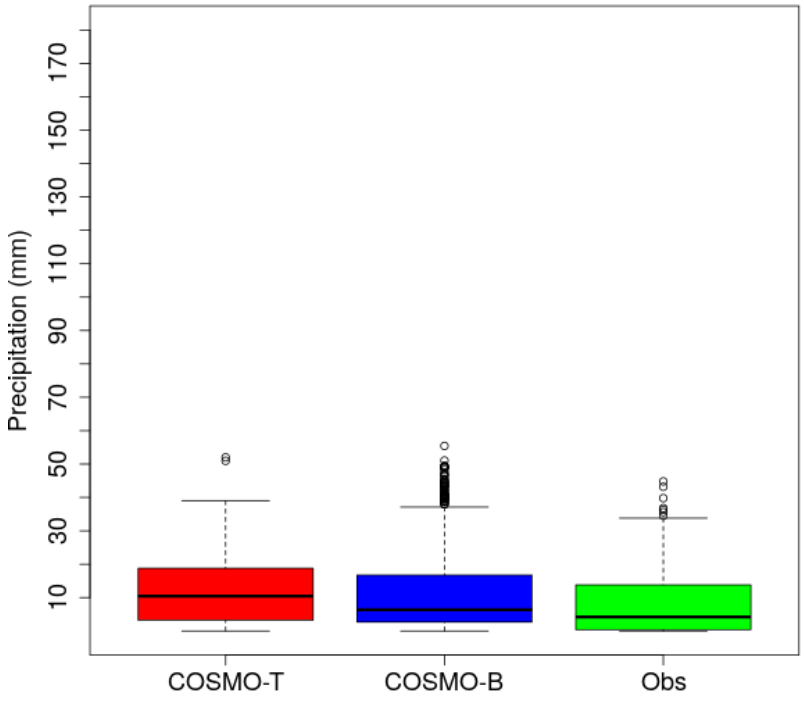

Figure 3.28: The same as Figs. 3.26 and 3.27, but for the runs starting at 00 UTC of 5th February 2017.

This is probably a conseguence of a large scale modification pattern induced by the different model physics. In order to study this effect, atten-

tion was focused also on Mean Sea Level Pressure field, which varies more smoothly than precipitation.

In Fig. 3.29 differences in mean sea level pressure field as predicted by COSMO-B and COSMO-T runs are presented. All runs start at 00 UTC of 5th February and a +36-hours forecast, valid at 12 UTC of 6th February, is considered. An appreaciable difference of some hPas can be detectable between the two runs: in particular over Central Italy, where the surface low pressure system was located. COSMO-B predicts a more "cyclonic" circulation over this area than COSMO-T. ECMWF IFS analysis at 12 UTC of that day shows a better performance of COSMO-B in predicting mean sea level pressure (not shown here).

Thus this result can be seen as an evidence that even the only difference in a "small scale" model parameterisation -i.e. a different sub-grid processes treatment- can produce, for a particular case, a quite significant change in the large-scale pattern.

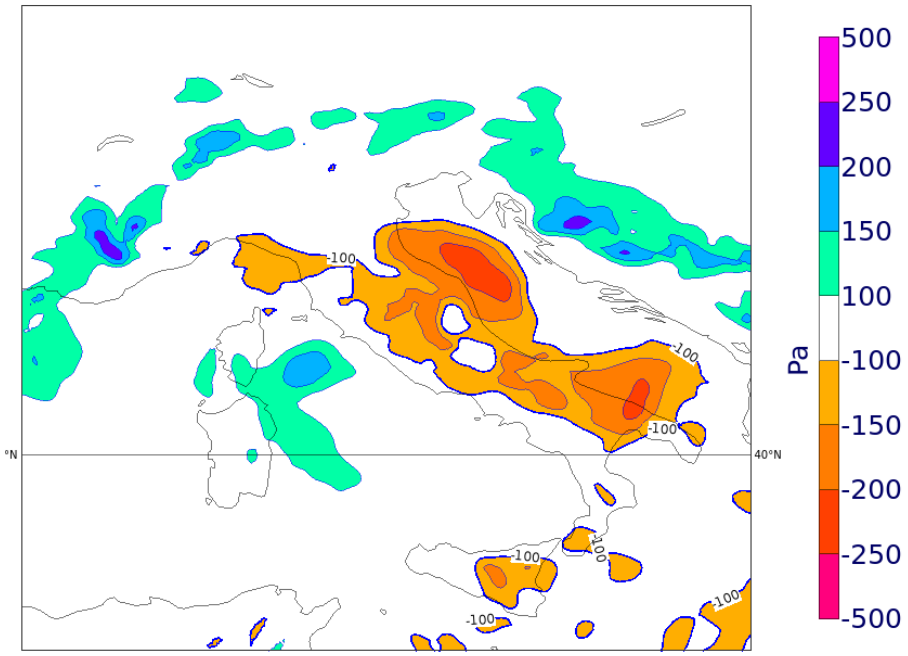

Figure 3.29: Differences in +36-h predicted Mean Sea Level Pressure (in Pa) between COSMO-B and COSMO-T for runs initialised at 00 UTC of 5th February 2017.

3.5 Test in ensemble mode

The last experiment presented in this chapter regards the sensitivity of the COSMO ensemble prediction system for the case study.

In particular an experimental ensemble suite made of 10 members, in which only the Bechtold scheme is used (referred to as Cleps-10B), has been run for the same verification period. This suite, as already mentioned, use the same initial and boundary conditions as members 1-10 of COSMO-LEPS (hereafter Cleps-10T). Therefore the two ensemble systems differ only for the moist convection treatment. This is done in order to have a quantitative evaluation of the COSMO performance in ensemble mode when it is run either with the Tiedtke or the Bechtold scheme. Forecast skills of the systems are evaluated in terms of BS (Brier Score, Fig. 3.30) and RPS (Ranked Probability Score, Fig. 3.31). It is worth pointing out that in this case, diffently from the deterministic test in which QPF was studied, the verification is done by considering the forecast probability that cumulated precipitation exceeds fixed thresholds over 24 hours (i.e. 1, 5, 10, 15, 25, 50 mm over 24 hours) in the gridpoint nearest to each station point of the observation network lying inside the Serchio basin (Fig.3.1).

Fig. 3.30 shows a better performance of Cleps-10B for higher thresholds (here results for 25 mm/24 h is reported, dashed lines) while Cleps10T is better for lower thresholds (10 mm/24h is reported, continue lines).

In Fig 3.31 the comparison between the forecast skill of the two systems is reported in terms of RPS, which is calculated here by considering all the 6 different thresholds. Cleps-10T and Cleps-10B show similar performance up to +72 forecast ranges, while Cleps-10B performs slightly better from this range onwards.

These results seem to indicate that there are no systematic errors between the two ensemble systems generated using the different convection schemes. Therefore the implementation of an ensemble system whose members use either the Tiedtke or the Bechtold scheme, seems a promising approach to improve the operational COSMO-LEPS, which uses only one convection scheme. This topic will be discussed in the next chapter.

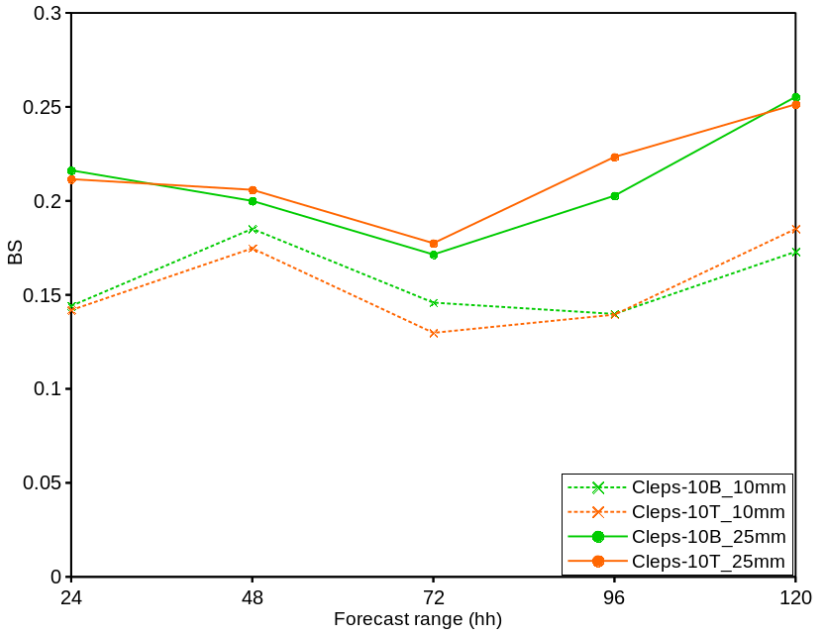

Figure 3.30: BS for 24-h cumulated precipitation averaged over the Serchio area and forecast range up to 120h. Continue lines refer to verification for 10 mm/24h threshold events, dashed ones to verification for 25 mm/24h thresholds events. Runs are relative to those performed from 00 UTC of 29th January 2017 to 00 UTC of 5th February 2017

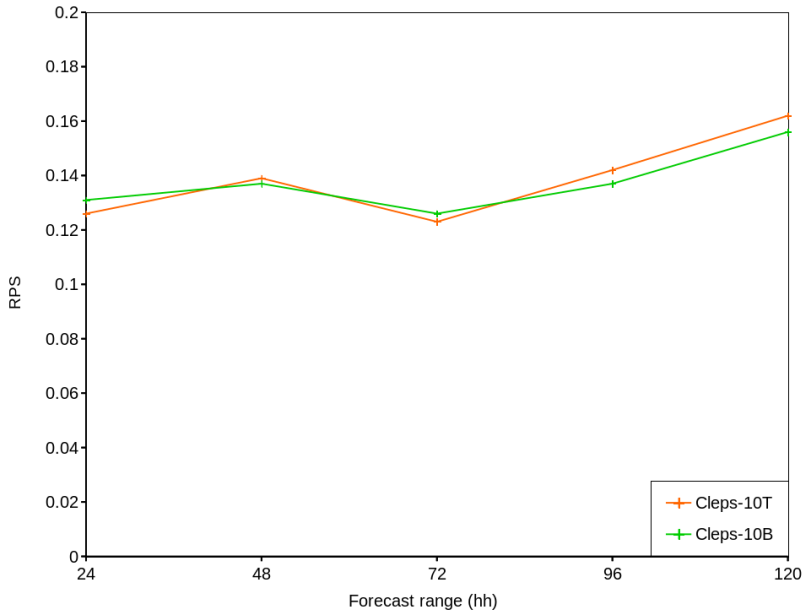

Figure 3.31: RPS for 24-h cumulated precipitation averaged over the Serchio area and forecast range up to 120h. Runs are relative to those performed from 00 UTC of 29th January 2017 to 00 of 5th February 2017

Chapter 4

Statistical dependence of COSMO-LEPS forecast skill on the moist convection scheme

4.1 Description of the experiments

A more systematic and objective evaluation of the COSMO model performance in ensemble mode when it is run with the two schemes is presented in this chapter, so as to assess overall abilities and shortcomings of the system.

The development and implementation of ensemble systems where either the Tiedtke or the Bechtold scheme can be used by the ensemble members, provides an opportunity to upgrade state-of-the-art probabilistic systems at the convection-parameterised scale. In fact the parameterisation of convection in limited-area models is an important source of uncertainty as regards expecially the spatio-temporal forecast of precipitation.

However, before this implementation, it is necessary to assess how the COSMO model runs in ensemble mode performed with the Bechtold scheme (hereafter, Cleps-10B) relate to those using the operational Tiedtke scheme (hereafter, Cleps-10T).

In this study the attention has been focused on how the system performs in terms of total precipitation prediction over a quite large number of events, in order to have an as solid as possible statistical insight on the model forecast skill. Therefore our present interest is not to investigate the performance of

the system on a case by case basis, as done previously in Chapter 3, but on a continous period.

Hence several experiments have been performed.

Firstly, we have built a test suite to run a 10-member ensemble with the Bechtold scheme (referred to as Cleps-10B), which uses the same initial and boundary conditions as members 1-10 of the operational COSMO-LEPS (which has 20 members, all run with the Tiedtke scheme). This suite has been run from 28$^{\text{th}}$ March to 31$^{\text{th}}$ May 2017 with an integration domain covering Central-Southern Europe and Italy (shown in 1.4), at the horizontal resolution of about 7 km and 40 vertical layers, and with a 132-hours forecast range, always starting at 00 UTC. Therefore the sensitivity of the ensemble system to the different parameterisation schemes has been assessed by comparing performance of Cleps-10B to that of Cleps-10T, which is the 10-member ensemble provided by members 1-10 of COSMO-LEPS, the operational ensemble system of the COSMO consortium, over the verification period.

Finally, a new 20-member ensemble system (referred to as Cleps20bt), in which members from Cleps-10B were added to 11-20 members of COSMO-LEPS, was implemented. In this approach, the use of the Bechtold scheme is proposed as a perturbation for the COSMO ensemble system, relatively to how uncertainties in the model representation of the cumulus convection can be described and quantified in meso-beta scale COSMO applications. This may have a good impact on the ensemble forecasts because it introduces some uncertainty into the treatment of a process that, of course, is not fully described in state-of-the-art NWP systems (Houtekamer et al., 1996).

4.2 Methodology of verification

The performance of the ensemble systems was analysed by considering the probabilistic prediction of 6-h cumulated precipitation exceeding a number of thresholds for forecast up to 132 hours. Only the performance of 00 UTC runs has been examined.

In this case it was decided to focus the attention on 6-h accumulated precipitation (accumulated from 0 to 6 UTC, from 6 to 12 UTC, from 12 to 18 UTC and from 18 to 00 UTC) in order to investigate and compare the performance of the systems for both day-time and night-time precipitation forecasts. This should allow the possibility to isolate possible biases and/or systematic errors in the diurnal cycle of the model integrations, which would be otherwise masked if verification were performed over a longer (typically 24-h) window.

Since precipitation has a high-spatial variability, a high-density network, made of about 1000 stations over Northern Italy (Fig 4.1), has been adopted in order to assess the predictive skill of mesoscale ensemble systems.

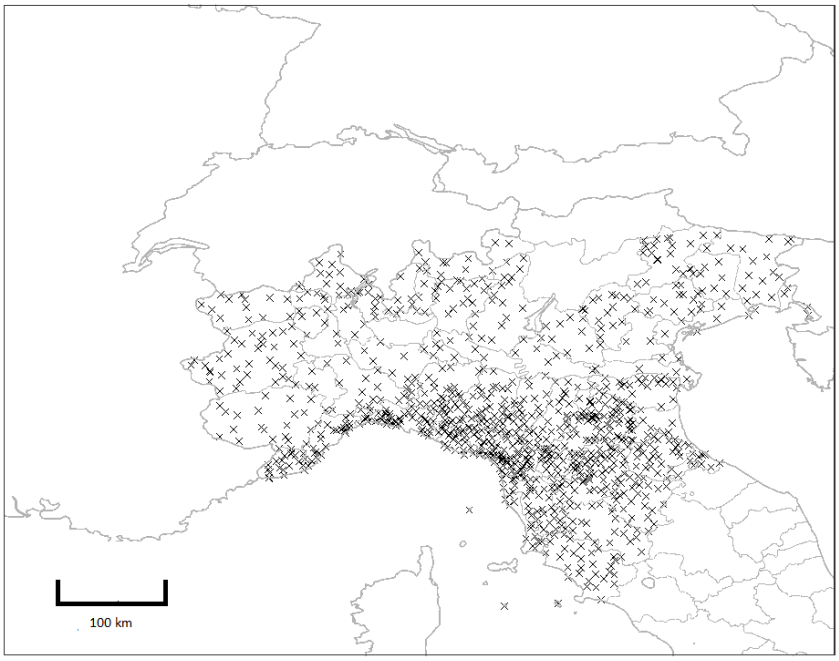

Figure 4.1: Verification network

As already mentioned, the study has the main goal to assess the quality of probabilistic forecasts over a quite large number of events. Figure 4.2 shows the overall number of occurrences for the 1-mm threshold, which is representative of the event rain/no rain, over the verification period for each forecast range studied, according to the reports of the stations of Fig. 4.1. Several thousands of events have been reported over the verification period. It is interesting to notice that a systematic diurnal cycle is detectable in

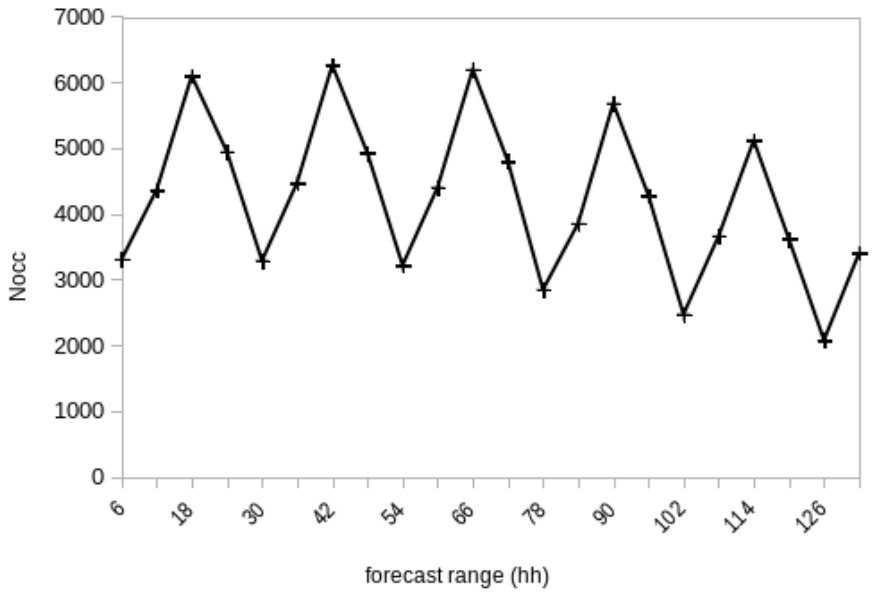

Figure 4.2: Number of occurences for 1-mm accumulated precipitation for different forecast ranges during the verification period (from 28th March to 31th May 2017)

the station reports, with a higher number of occurences reported during the forecast ranges relative to the diurnal hours of the day (those whitch lie from 6-12 to 12-18 UTC) compared to those during nocturnal hours. This is likely due to fact that over spring months, such as April and May, in which verification has been carried out, total precipitation budget starts to be heavily influenced by the convective forcing. In fact the strong solar heating of the ground hours tends to make the lower atmospheric layers more unstable during the day-time, especially over continental areas. This contributes to renforce convective cells and the vertical motions associated,

enhancing the probability of occurence of clouds (and so precipitation) during the afternoon.

For the comparison of the model forecasts against station reports the grid point closest to the observation one is selected. In particular the performance of COSMO-LEPS is examined for six different 6-h cumulated precipitation thresholds: 1, 5, 10, 15, 25, 50 mm/6-h. Several thousands of events were reported for the first two thresholds, and several hundreds for 15mm/6 h threshold. On the other hand it is immediately worth pointing out that, when considering the highest thresholds (25, 50 mm/6-h), a low number of occurrences, even below 10 for the 50 mm/6h, was found over the verification period. As a conseguence this does not allow any solid statistical conclusion on the effective performance of the system for these events over the period.

For each forecast range, the model performance has been evaluated by computing the following "traditional" probabilistic scores: the Brier Skill Score (BSS), the Ranked Probability Skill Score (RPSS), the Relative Operating Characteristic Curve (ROC) Area and the Percentage of Outliers (OUTL).

The Brier Skill Score (BSS) is defined as the BS (Brier Score) percentage improvement of the forecast system with respect to climatology and it is computed as:

$$BSS = \frac{BS_{CLI} - BS}{BS_{CLI}}$$

In general a positive BSS indicates that a system has more predictive power than a model climatology during that period. The higher this value is, the better the forecast will be.

Similarly the Ranked Probability Skill Score (RPSS) is defined as:

$$RPSS = \frac{RPS_{CLI} - RPS}{RPS_{CLI}}$$

The ranked probability skill score relates RPS (Ranked Probability Score) of the forecasting system and RPS_{CLI} relative to climatalogy such that, again, a positive value of RPSS indicates forecast benefit with respect to the climatological forecast (Wilks 1995).

Finally the Relative Operating Characteristic Curve Area (ROC Area) is defined as the area under the curve generated by plotting of the cumulative

Hit Rate (H) against the False Alarm Rate (F). Hit Rate and the False Alarm Rate for each probability class (threshold) are defined as:

$$H_k = \frac{a_k}{a_k + c_k}$$

$$F_k = \frac{b_k}{b_k + d_k}$$

following the contingency table:

	Observed Y	Observed N
Forecast Y	a	b
Forecast N	c	d

Table 4.1: Contingency table

The two scores indicate, respectively, the proportion of events which were predicted by k ensemble members and actually happened, and the proportion of events forecast by k members and did not occur. It is commonly used as a probabilistic score, its maximum value being 1, and a value of 0.5 indicating a no-skill forecast system (Mason and Graham, 1999).

The Percentage of Outliers of a probabilistic forecast system is defined as the probability of the analysis (or observation) lying outside the forecast range (Buizza, 1997). Therefore this can be seen as the percentage of times the "truth" falls out of the range spanned by the forecast values. Here, it is computed as the fraction of points of the domain where the observed value lies outside the minimum or maximum forecast values.

4.3 Results

4.3.1 Comparison of 10-member ensemble system run with different schemes

As already mentioned, firstly a comparison between the 10-member ensemble system run with the Bechtold scheme (Cleps-10B) and the 10-member ensemble run with the Tiedtke scheme (Cleps-10T, made of members 1-10 of COSMO-LEPS) has been undertaken over the full 2-month period. It is important to underline again that each member of one ensemble system Cleps-10B differs from Cleps-10T (the first ten members of the operational ensemble) only for the way the moist convection processes are treated: in fact the two systems use the same initial and boundary conditions.

Similarly to what done in the previous chapter, some verification scores have been computed over the verification period, as reported in Table 4.2.

Figure 4.3 shows the comparison of BS (Brier Score) of the two ensemble systems for 6-h accumulated precipitation forecast exceeding three different thresholds. On the x-axis forecast ranges are reported.

Verification features	
variable:	6-h cumulated precipitation (00-06, 06-12,..UTC);
Period:	from 28th March to 31th May 2017 (about 60 days);
region:	Northern Italy;
method:	nearest grid-point; no-weighted fcst;
obs:	non-GTS network, no obs error;
fcst ranges:	0-6h, 6-12h,..., 126-132;
thresholds:	1, 5, 10, 15, 25, 50 mm/6h;
systems:	Cleps-10B vs Cleps-10T;
scores:	RPS, BS, BSS, Outliers,..

Table 4.2: Main features of the verification configuration for the 10-member ensembles

It is evident that, for the events under investigation, both the systems has a sort of "diurnal cycle" with higher scores for forecast ranges relative to "night-time" verification, and lower for those relative to the time interval between 6 UTC to 18 UTC ("day-time"). As already discussed this is probably

a consequence that, during the verification period, day-time precipitation is likely to be strongly driven by convection sub-grid processes, which are parameterised and not explicitly resolved when the model is run at horizontal resolution coarser than 2-3 km.

However Cleps-10B and Cleps-10T have similar BS score for all the forecast ranges, especially from 48 hours onward.

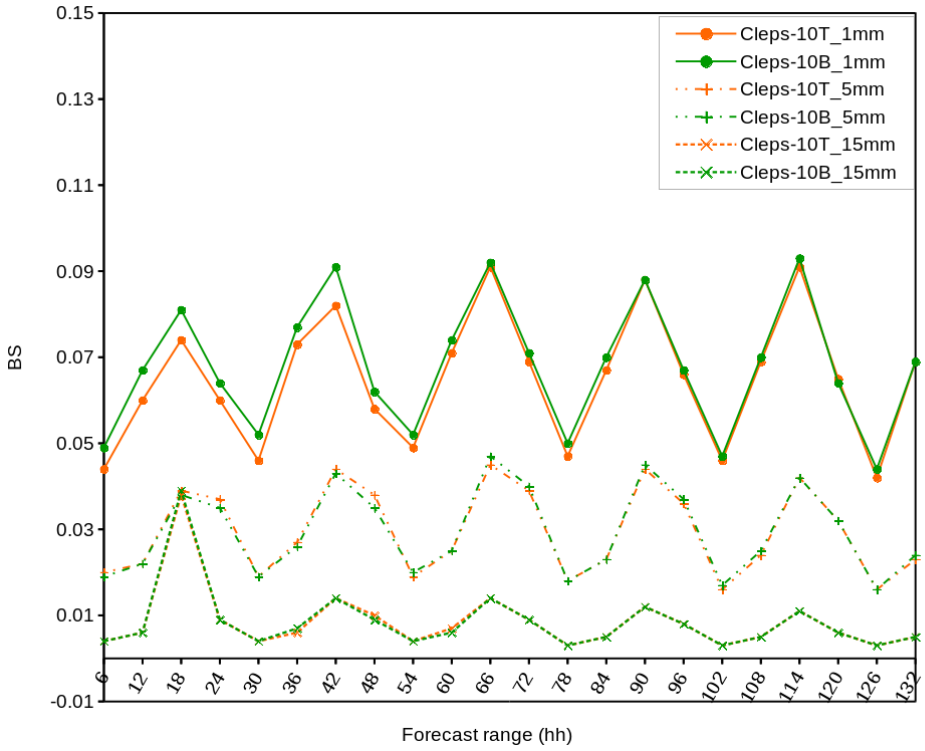

Figure 4.3: BS values for precipitation exceeding different thresholds (1, 5, 15 mm in 6 h in solid, dashed dotted and dashed lines, respectively) over different forecast ranges for Cleps-10T (orange line) and Cleps-10B (green line).

This behaviour can be detectable also in the RPS (Ranked Probability Score) which is presented in Fig. 4.4.

This is consistent with the hypothesis that the average skill of the Cleps-10B runs should be indistinguishable, from a statistical point of view, from that provided by the Cleps-10T ones, even if Cleps-10B forecasts are likely to be different from Cleps-10T on a case-by-case basis. In other words, over

the large number of cases considered in this survey, one parameterisation scheme appears to be almost statistically equivalent to the other in terms of precipitation forecast skill. Over a large number of cases errors in Cleps-10B equal to a certain extent those in Cleps-10T.

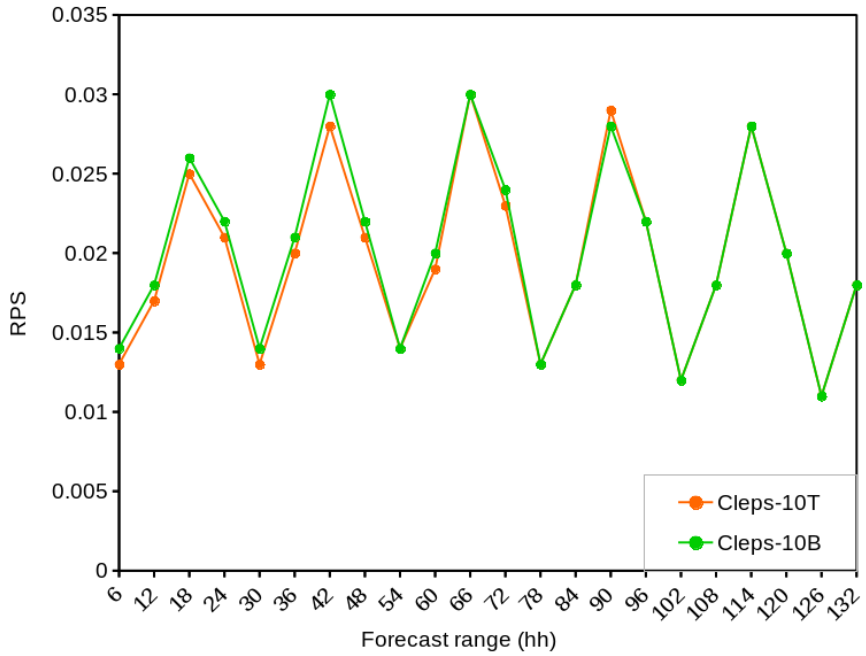

Figure 4.4: RPS values for 6-h accumulated precipitation over different forecast ranges for Cleps-10T (orange line) and Cleps-10B (green line).

In addition to this, BSS (Brier Skill Score) for the Cleps-10T and Cleps-10B is presented in Fig. 4.5. A 24-h running mean is here applied to "smooth" the diurnal cycle in model performance. This score, as already pointed out, tries to represent a quantitative estimate of the added value detectable in precipitation prediction by using the model forecast rather than a reference one (climatology). The attention has been focused on some thresholds (1mm/6-h and 15 mm/6-h), which have a quite large number of occurences (higher than 1000 for the former, some hundreds for the latter) over the verification period. It is worth noticing that the BSS shows clearly the loss of predictability with increasing forecast range for both systems. Anyway the model forecast has added value compared to climatology up to +120 hours.

However the plot shows a different skill of the 2 systems when different thresholds and forecast ranges are considered. Over the verification period, Cleps-10T performs generally better than Cleps-10B for the lower threshold (1mm/6-h) while the opposite is true in high precipitation rates prediction for forecast ranges from 3 days onwards. This can be seen as a result consistent with the theory according to which the ensemble systems which are run using either convection schemes can describe a larger variety of uncertainty and errors in precipitation prediction.

Thus the implementation of ensemble systems in which the two schemes are "mixed" is a reasonable issue to deal with uncertanties due to the ambiguity linked to the use of a scheme or the other.

This argument will be discussed also in the next section.

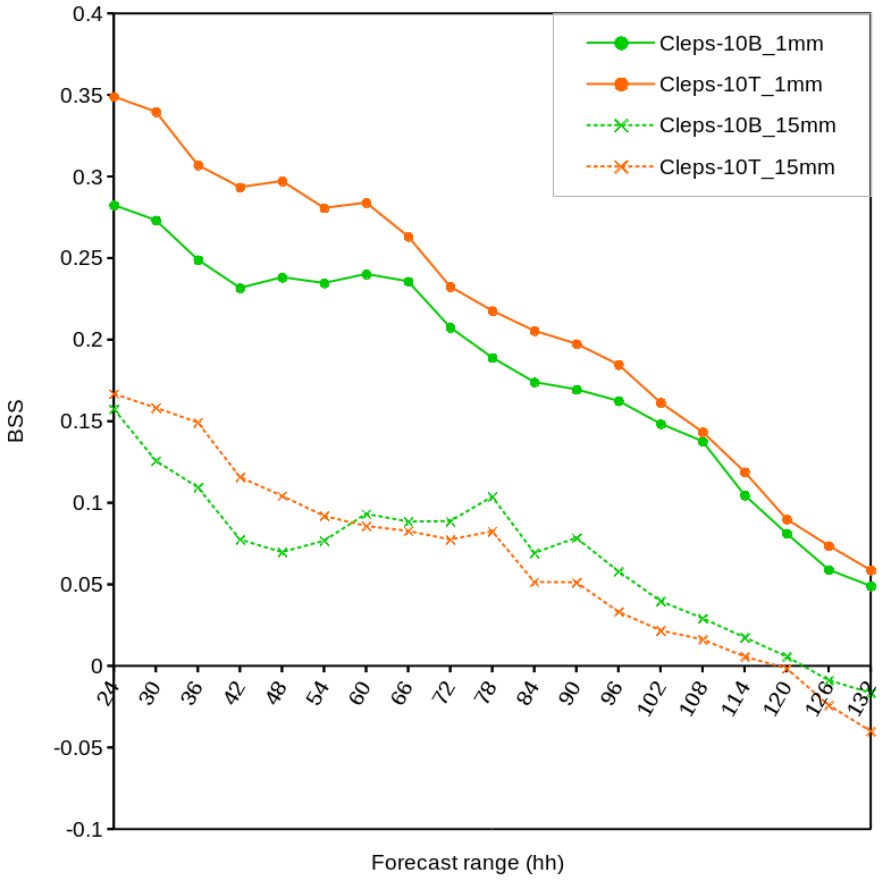

Figure 4.5: 24-h running mean of BSS in Cleps-10T (orange line) and Cleps-10B (green line) for 1 mm/6h (continous line) and 15 mm/6h (dashed line) thresholds.

Finally, the skill of the two systems has been assessed in terms of Percentage of Outliers in Fig. 4.6. Firstly it is worth pointing out that the percentage of outliers for both systems tends to decrease with increasing forecast range because of the increasing spread with time between the ensemble members. Fig. 4.6 indicates a better performance of Cleps-10T, which has a lower number of outliers than Cleps-10B, in particular for the first forecast ranges studied.

Fig. 4.7 represents respectively the fraction of points in which observations lie above/below the range of predicted values by the ensemble system. A large amount of $outl_{min}$, indicative of an overestimation of minima of precipitation amount by Cleps-10B runs, can be seen. In particular the percentage of outliers lying below the minimum predicted values is higher for Cleps-10B than for Cleps-10T for all the forecast ranges studied. This seems to indicate that members with the Bechtold scheme tend to produce some light prepitation also when it is not observed. On the other hand fraction of analysis point above the maximum tends to be similar or slightly lower for Cleps-10B.

This excessive drizzle effect could be due to the shallow convection treatment adopted by the Bechtold scheme. This scheme in fact allows "shallow convection" to produce precipitation, whereas the Tiedtke scheme does not.

It is possible that further tuning of the Bechtold scheme, when adopted at high resolution, is still necessary.

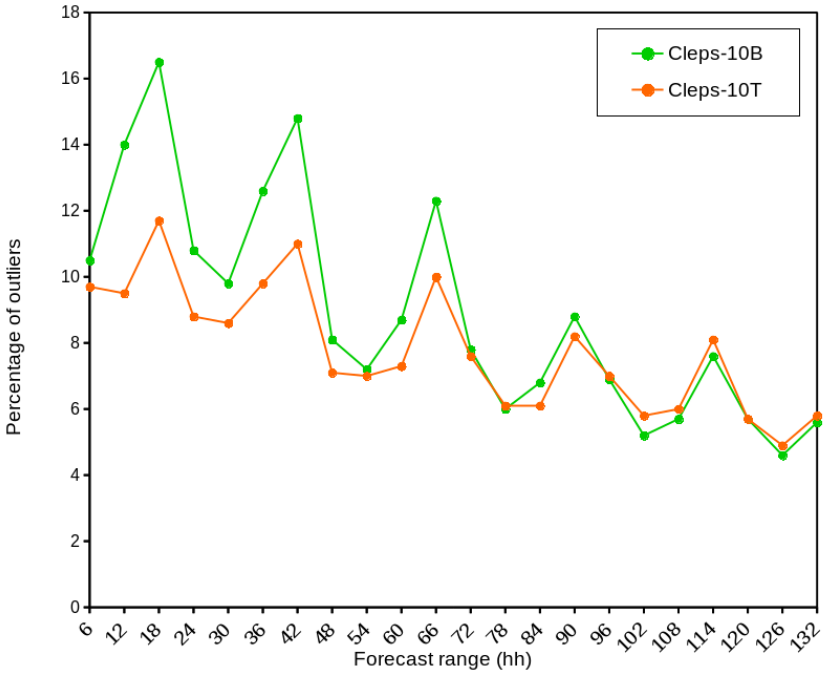

Figure 4.6: Percentage of Outliers in Cleps-10T (orange line) and Cleps-10B (green line) for different forecast ranges.

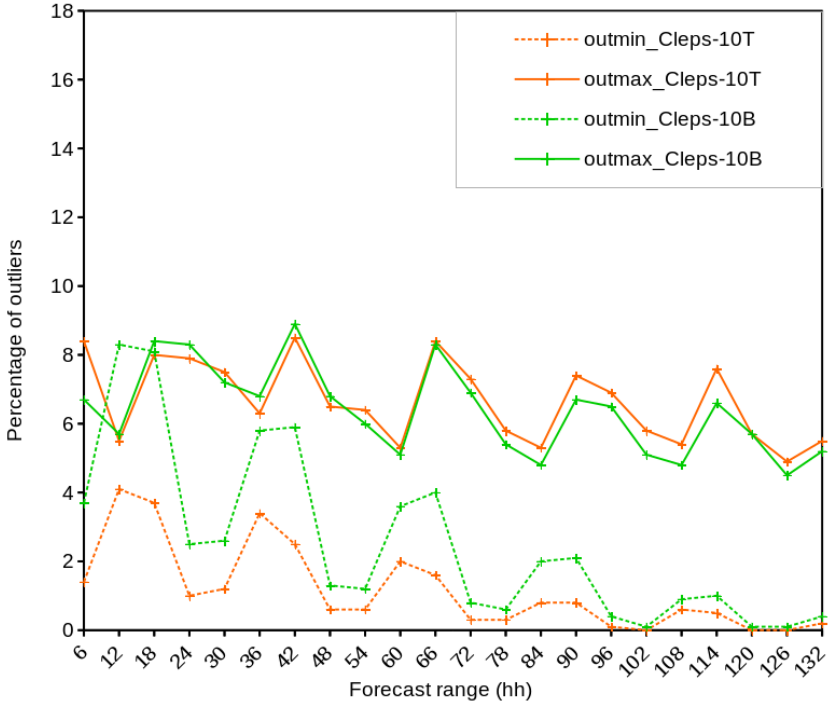

Figure 4.7: Percentage of analysis points lying below (dashed lines) and above (continous line) the forecast in Cleps-10B and Cleps-10T for different forecast ranges.

4.3.2 Implementation of Cleps20bt

A further step in the study of COSMO ensemble system sensivity to the different paramerisations of moist convection is the implementation of a new probabilistic system, hereafter Cleps20bt, in which the Bechtold scheme is treated as a perturbation for the operational ensemble COSMO-LEPS.

As previously mentioned this system is generated by adding the members of Cleps-10B to members 11-20 of COSMO-LEPS. Therefore, Cleps20bt has 10 members run with the Bechtold scheme plus 10 members run with the Tiedtke scheme and no duplication of initial and boundary conditions.

It is worth pointing out that this procedure is consistent only because the average skill of the model when it is run in ensemble mode with the Bechtold scheme turned out to be indistinguishable, from a statistical point of view, from that provided by running the model with the Tiedtke scheme, as shown in Section 4.3.1. In fact, in a well-constructed ensemble, the skill of each individual member, averaged over a large number of events, should be approximately identical not to introduced biases and/or systematic errors in the ensemble members distribution.

The basic idea of the Cleps20bt implementation is that certain closure parameters used in model formulation (as for the moist convective processes) may be based on approximate physical knowledge. As a conseguence their values may be somewhat arbitrary, or they may have been tuned to give optimal results for test cases that are not necessarily representative of more general applications and/or for applications at high resolution.

In general, ensembles using multiple model formulations can provide better estimate of uncertanty in the model physics, facilitating the reduction of forecast errors, helping to take into account all the possible future states of the atmosphere and providing a more reliable estimate ot the day-to-day "forecast skill".

4.3.3 Performance of Cleps20bt and comparison with that of COSMO-LEPS

Verification of Cleps20bt performance has been carried out for the same verification period, from 28th March to 31th May 2017, and over the same geographical domain (Fig. 4.1) adopted for the evaluation of 10 member-ensembles examined in section 4.3.1 (see Table 4.3).

The forecast skill of Cleps20bt and COSMO-LEPS has been assessed, once again, by computing some traditional skill scores described in Section 4.2 (ROCA, BSS, RPSS..).

The main results of this study are presented in the following plots. It is worth undelining that, again, the attention is primarly focused only on the probabilistic prediction of those precipitaion events (thresholds) for which it was possible to provide an acceptable statistical information.

Figs. 4.8 and 4.9 show the ROC (Relative Operating Curve) area respectively for 1 mm/6-h (interesting for discriminating between rain/no rain events) and the 5 mm/6-h thresholds considering forecast ranges up to 132 hours. In both figures a linear tendency line is added in order to help in understanding the evolution of the score with increasing forecast range in the two cases.

Verification features	
variable:	6-h cumulated precipitation (00-06, 06-12,..UTC);
Period:	from 28th March to 31th May 2017 (about 60 days);
region:	Northern Italy;
method:	nearest grid-point; no-weighted fcst;
obs:	non-GTS network, no obs error;
fcst ranges:	0-6h, 6-12h,..., 126-132;
thresholds:	1, 5, 10, 15, 25, 50 mm/6h;
systems:	Cleps20bt vs COSMO-LEPS;
scores:	ROC area, BSS, RPSS, Outliers,..

Table 4.3: Main features of the verification configuration for the 20-member ensembles

Some common features can be detectable in the plots. In general ROCA decreases with time: this is an evidence of the loss of predictability of the atmospheric system with increasing forecast range. In addition to this the diurnal cycle in forecast skill is evident also in the ROCA behaviour, with the lower values (the worse skill) observed during the central part of the day.

Cleps20bt turns out to perform better especially for the 1 mm threshold (Fig. 4.8), indicating a more enhanced capability of the system in discriminating between rain/no rain event prediction.

For the higher threshold (Fig. 4.9), results are less clear, with approximately the same performance between Cleps20bt and COSMO-LEPS.

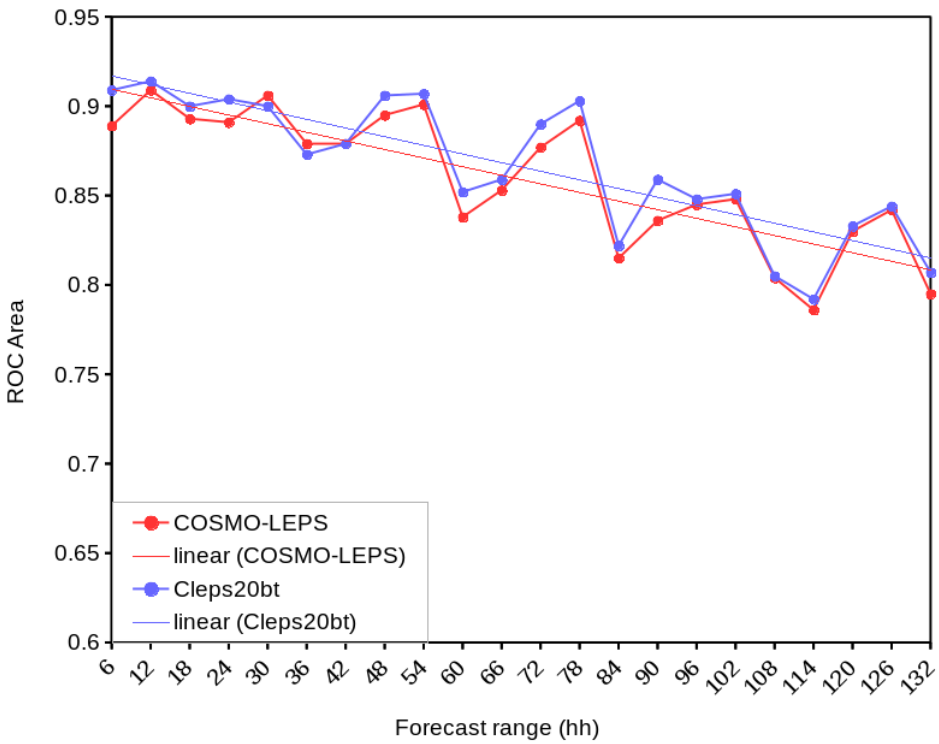

Figure 4.8: ROC area values for the event "6-h accumulated precipitation exceeding 1 mm" over different forecast ranges in COSMO-LEPS (red line) and Cleps20bt (blue line): linear tendencies are added. Results are averaged over the verification period.

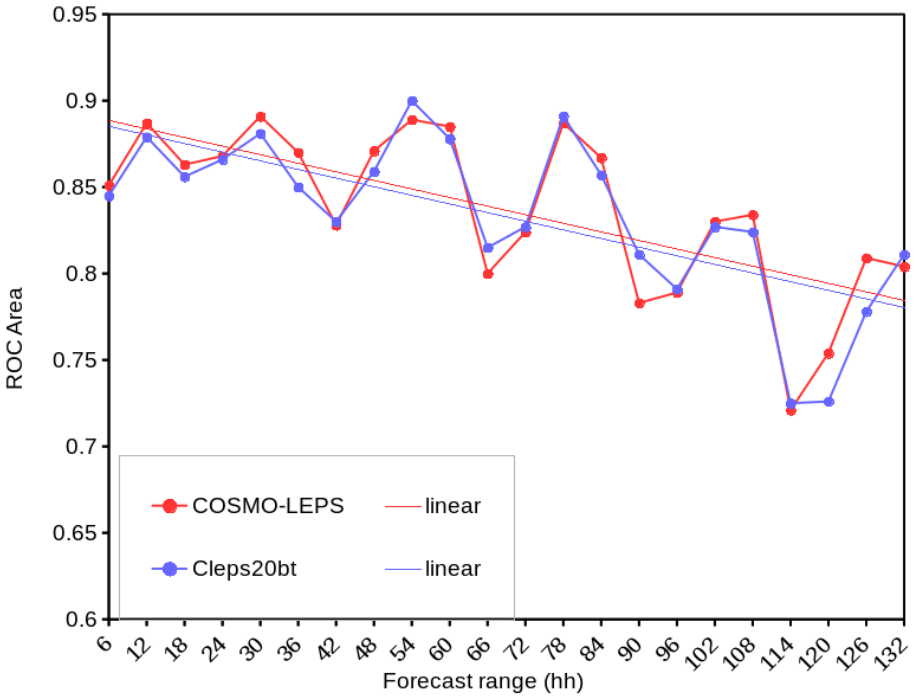

Figure 4.9: The same as Fig. 4.8, but for the event "6-h accumulated precipitation exceeding 5 mm".

In fig 4.10 BSS (Brier Skill Score) is presented for different forecast ranges by considering several thresholds. In particular the focus is on the highest ones for which a relative large number of events has been reported, in addition to the 1 mm/6-h (1, 10, 15 mm/6h). As already mentioned this score provides an estimate of the added value of the model precipitation prediction with respect to a reference one (climatology). In order to filter the diurnal cycle and to provide an overall description of the model system performance for different precipitation thresholds, the values reported in the plot are obtained by computing the running mean of the 6-h precipitation forecast skill over 24 hours. In fact the diurnal cycle in the model performance is evident also in this score trend, with better skill for nocturnal events.

The plot shows that Cleps20bt has higher values of BSS than COSMO-LEPS for all the thresholds reported, especially for forecast ranges from 42 hours onwards.

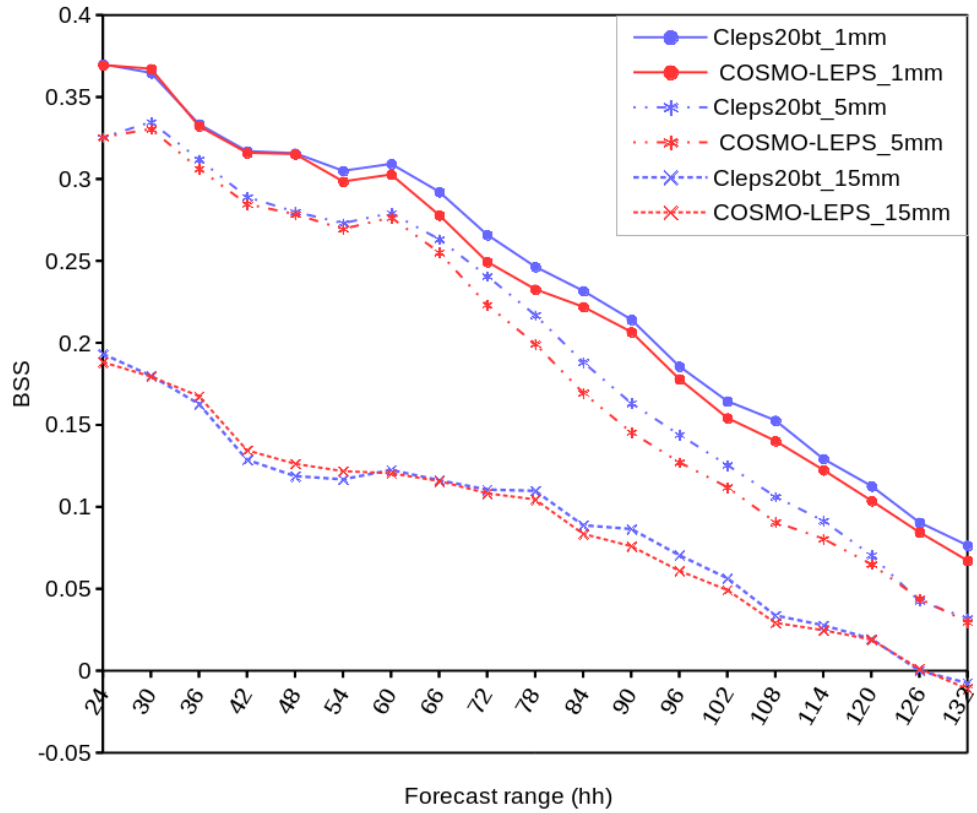

Figure 4.10: 24-h running mean of BSS values for 6-h accumulated precipitation exceeding 1 mm (continous line), 5 mm (point dashed line), 15 mm (dashed line) for different forecast ranges in COSMO-LEPS (red line) and Cleps20bt (blue line).

In addition to this, the RPSS (Ranked Probability Skill Score) of this system has been computed for different forecast ranges and compared to that of COSMO-LEPS during the same period. The RPSS can be seen as a cumulative BSS, obtained by considering all the six precipitation thresholds studied over the verification period (see Table 4.3).

The comparison between the two system is presented in Fig. 4.11. As for the other scores, RPSS too shows a dependence of model performance on the diurnal cycle and tends to decrease with increasing forecast range: however Cleps20bt shows higher RPSS values than COSMO-LEPS skill for most of the forecast ranges, especially during day-time.

Similarly to what was done for the BSS, the 24-h running mean of the

RPSS is reported in Fig. 4.12 in order to help the interpretation of the results. Also in this case a better performance of Cleps20bt than that of COSMO-LEPS is evident for forecast ranges from 2 days onwards: for example RPSS in the forecast range +60-66 hours is about 5% higher in Cleps20bt than in COSMO-LEPS; it is about 10% higher in the new system for +90-96, +96-102 ranges.

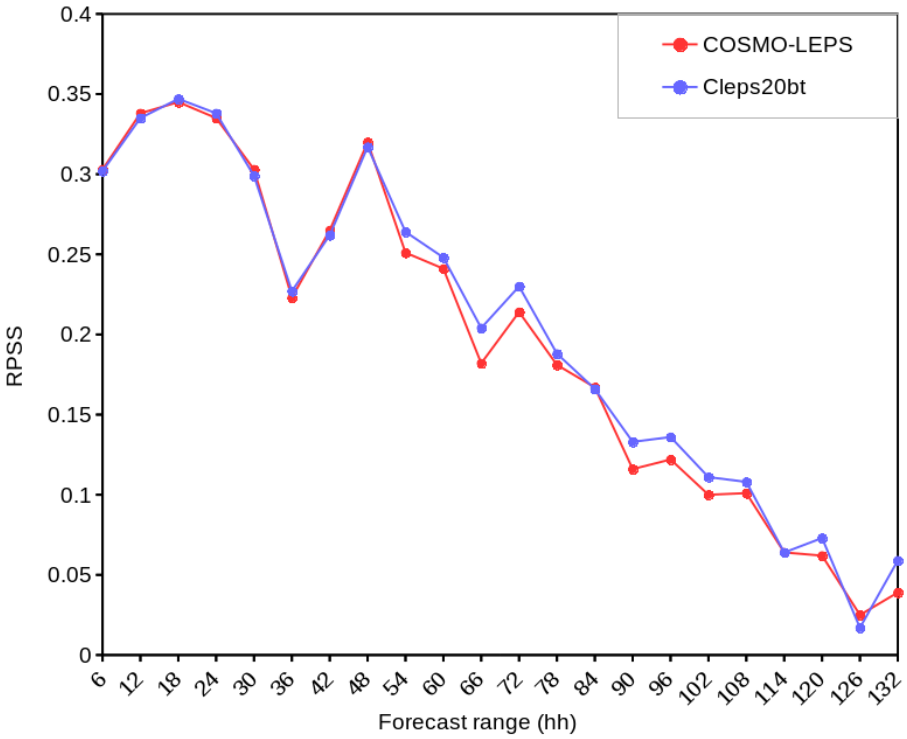

Figure 4.11: RPSS for 6-h accumulated precipitation for different forecast ranges in COSMO-LEPS (red line) and Cleps20bt (blue line).

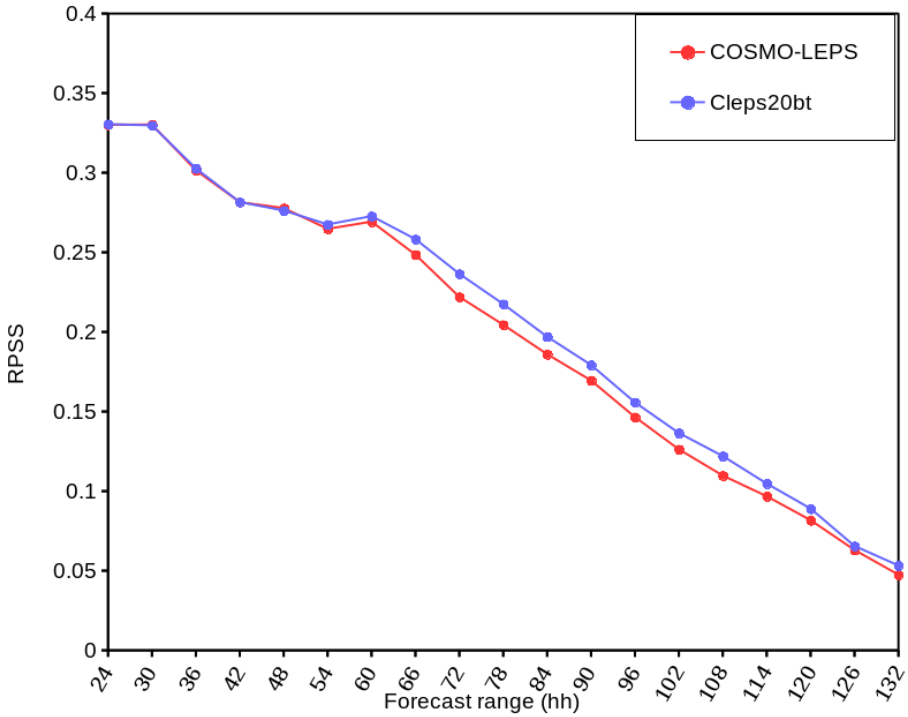

Figure 4.12: 24-h running mean of RPSS for 6-h accumulated precipitation over different forecast ranges in COSMO-LEPS (red line) and Cleps20bt (blue line).

Finally the performance of the systems is evaluated in terms of the percentage of outliers (i.e. the cases in which observed rainfall value is not inside the ranges of possible values predicted by the ensemble members). Fig. 4.13 shows the comparison between Cleps20bt and COSMO-LEPS in terms of this score for forecast ranges up to 132 hours.

It is interesting to underline two features in this plot. First of all, the total percentage of outliers in both the systems is lower compared to the 10-member ensemble case (Fig. 4.6) for all the forecast ranges. Therefore the increasing size of the ensemble has an effect in limiting outliers over the verification period. Secondly, outliers decrease with the increasing forecast range in this plot, similarly to what noticed for the 10-member ensembles.

Neverthless percentage of outliers is reduced in Cleps20bt over most of the forecast ranges with respect to COSMO-LEPS, especially from 3 days (+72 hours) onwards.

Similarly to the 10-member ensembles case, the percentage of outliers in Fig. 4.13 are discriminated between the fractions of points in which observed values lay outside the forecast range over the full verification period (Fig. 4.14). As already pointed out the "total" percentage of outliers results as a sum of these two ratios.

Fig. 4.14 shows that the total percentage of outliers is reduced in Cleps20bt as a consequence of a limitation in number of spatial points in which the total precipitation maxima are underestimated compared to COSMO-LEPS. In fact the fraction of observations found above the maximum forecast value is lower in Cleps20bt than in COSMO-LEPS, for most of forecast ranges, especially in the medium range (from +72 hours onwards).

This is a quite encouraging result because Cleps-20bt turns out to perform better than the operational COSMO-LEPS in forecasting the possible peaks in cumulated precipitation over the 2-month period. It is worth underlining that the probabilistic forecast of these values is one of the most important issue of operational systems, because it regards the correct prediction of heavy rainfalls, which have a great impact on the society.

This result, together with those presented in this section, substantially agrees with the idea that, by adding a physical perturbation to the system (like what we have done in this work using an ensemble system in which two different moist convective schemes are used), we can obtain a more appropriate description of the phase-space of all possible future atmospheric states which are compatible with the uncertain model formulation of the moist convection sub-grid processes.

Thus, according to this experimentation, the generation of a multi-physics ensemble system provides a positive impact on the forecast capability at high resolution. This is especially true in early-medium range, when model errors start playing an important role and it is crucial for an ensemble system to provide an accurate description of the different sources of forecast deficiency.

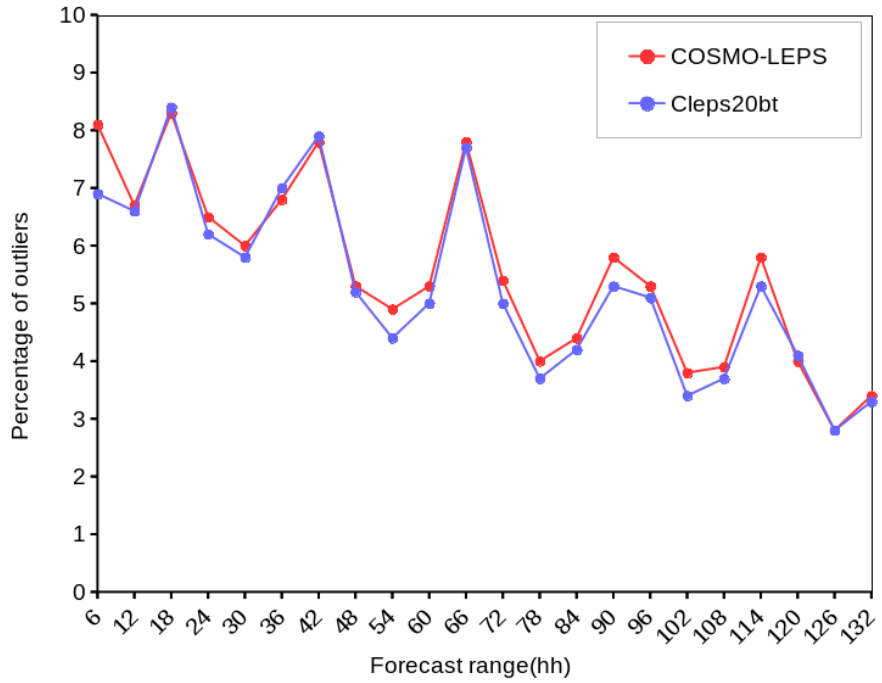

Figure 4.13: Percentage of outliers for different forecast ranges in COSMO-LEPS (red line) and Cleps20bt (blue line).

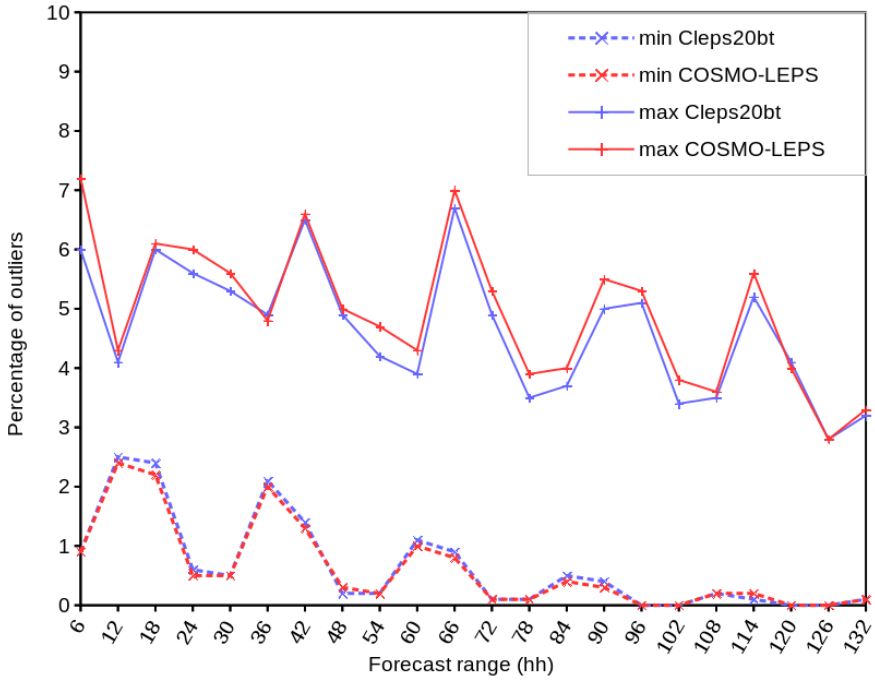

Figure 4.14: Percentage of outliers above/below maximum/minimum predicted values for different forecast ranges in COSMO-LEPS (red line) and Cleps20bt (blue line).

Chapter 5

Conclusions

The present work has the purpose to assess the sensitivity of COSMO model forecast skill to different representation of moist convection. Two schemes can be used in COSMO model to represent the sub grid process linked to moist convection, when it is run at convection-parameterised scales: the Tiedtke scheme, which has been used in operational suites until now, and the Bechtold scheme, implemented at ECMWF, and recently adapted for COSMO model applications. The study of the impact of a parameterisation of convection in limited-area models is of particular concern because it is an important source of uncertainty as regards the spatio-temporal forecast of precipitation.

This impact has been studied in both deterministic and ensemble modes. In particular for one case of heavy precipitation, occurred during the first week of February 2017 over a small river cacthment in Northern Italy (Serchio river basin), the performance of COSMO-B (deterministic COSMO model run with the Bechtold scheme) and COSMO-T (deterministic COSMO model run with the Tiedtke scheme) has been investigated. Verification has been carried out by computing some traditional skill scores like MAE, BIAS error for the cumulated precipitation forecast averaged over the river basin because this variable has important hydrological applications and provides a useful measure of precipitation intensity over a broad region. In addition to this, averaged values at high resolution scales provide a more solid statistical information of the overall performance of the system than considering grid-point

values. In this study particular attention was paid to the types of forecast errors (e.g. location, timing, intensity) provided by the runs with the different convection schemes. Results show a better performance of COSMO-B than COSMO-T for most of the days considered in the case study.

Furthermore a 10-member ensemble using only the Bechtold scheme (Cleps-10B) and the same initial and boundary conditions as members 1-10 of the operational COSMO-LEPS (which has 20 members, all run with Tiedtke scheme), has been run. The probabilistic prediction of 24-h rainfall provided by Cleps-10B in the grid points lying in the Serchio basin was assessed and compared to that of Cleps-10T, the 10-member ensemble made of members 1-10 of COSMO-LEPS. In this case Cleps-10B has been shown to have higher skill than to Cleps-10T for higher cumulated precipitation thresholds; on the other hand Cleps-T performed better than the other for the 1mm/24h precipitation threshold.

In order to study in a more statistical way the dependence of forecast skill on the use of the different convective schemes in ensemble mode, the 10-member ensemble with the Becthtold scheme (Cleps-10B) has been run for approximately 2 months. The performance of these members has been assessed and compared again to that of Cleps-10T; in particular the spread/skill relation of the two 10-member ensemble in terms of total precipitation is evaluated. Verification has been performed for precipitation events occurred over Northern Italy (using the forecast at the gridpoints nearest to about 1000 stations) from 28$^{\text{th}}$ March to 31$^{\text{th}}$ May 2017. The average skill of the Cleps-10B runs turned out to be substantially indistinguishable, from a statistical point of view, from that provided by the Cleps-10T ones. However a deeper analysis suggests that the two ensemble systems are characterised by different types of forecast errors.

Therefore a new 20-member ensemble system (which has 10 members run with Bechtold plus 10 members run with Tiedtke and no duplication of boundary conditions) has been implemented. In this system the Bechtold scheme is used as a perturbation for the COSMO-LEPS ensemble, so as to provide a quantitative description of uncertainties linked to the model representation of the cumulus convection.

Cleps20bt has been shown to have higher skill (ROCA, BSS, RPSS) than COSMO-LEPS over the verification period. In addition to this the comparison of the Percentage of Outliers in the two systems shows a reduction in the fraction of observed points lying outside the maximum or minimum forecast value in Cleps20bt.

These results suggest that the use of a probabilistic system in which a multiple moist convection formulation is used, provides the opportunity to have a more comprehensive description of the uncertainties in total precipitation forecast linked to sub-grid cumulus representation. In other words, by adding an adeguate physical perturbation to the ensemble (like what we have done in this work using an ensemble system with the Bechtold scheme), we can obtain a more adequate "exploration" of the phase-space of the future atmospheric states which are compatible with uncertain model formulation of the sub-grid covective process, in addition to our imperfect knowledge of the atmospheric initial conditions.

However, further work is necessary on this topic. Firstly the sensitivity of model forecast skill in terms of other variables (2-m temperature, humidity, 10m- wind speed) has to be assessed. In fact the use of different schemes is expected to have a great impact also on these variables at high resolution scales.

In addition to this it is worth pointing out that this work has regarded mainly precipitation events occurred during spring season, apart from the case study. Therefore verification over a longer period including other seasons has to be performed. In particular it can be interesting to evaluate the system performance over a number of winter deep convection cases, in which large scale dynamic forcing is typically predominant.

Furthermore it can be useful to study in a systematic way the sensitivity of large scale variables prediction to the use of different sub-grid convective parameterisation schemes. In fact a better representation of the uncertainties linked to the sub-grid convection in the ensemble systems may have a good impact also in the large scale predictability, especially in those case in which the convective forcing plays an important role in the mesoscale dynamics. Most of these tests are planned for the next months and, in case of satisfactory

results, the operational implementation of Cleps20bt should be envisaged.

The main outcomes of this work have been presented to the scientific community at the Annual Meeting of the European Meteorological Society, which took place in Dublin from 4 to 8 September 2017, and at the COSMO General Meeting, held in Jerusalem from 11 to 14 September 2017.

References

[1] Arakawa, 2004. The cumulus parameterization problem: Past, present, and future. *J. Cli.*, **17**, 2493-2525.

[2] Arakawa and Lamb, 1977. Computational design of the basic dynamical processes of the UCLA general circulation model. Chapter 17, Methods of Computational Physics. New York Academic Press, 173-265.

[3] Arakawa and Schubert, 1974. Interaction of a Cumulus Cloud Ensemble with the Large-Scale Environment, Part I. *J. Atmosph. Sc.*, **31**, 674-701.

[4] Anthes, 1977. A Cumulus Parameterization Scheme Utilizing a One-Dimensional cloud Model. *Mon. Wea. Rev.*, **105**, 270-286.

[5] Bechtold, Bazile, Guichard, Mascart and Richard, 2001. A mass-flux convection scheme for regional and global models. *Quart. J. Roy. Meteor. Soc.*, **127**, 869-886.

[6] Bechtold, Semane, Lopez, Chaboureau, Beljaars and Bormann, 2014. Representing Equilibrium and Nonequilibrium Convection in Large-Scale Models. *J. Atmosph. Sc.*, **71**, 734-753.

[7] Bechtold, 2009-2017. Atmospheric moist convection. Meteorological Training Course Lecture Series, ECMWF.

[8] Betts and Miller, 1986. A new convective adjustment scheme. Part I: Observational and theoretical basis. *Quart. J. Roy. Meteor. Soc.*, **112**, 677-691.

[9] Bougeault, 1985. A Simple Parameterization of the Large-Scale Effects of Cumulus Convection. *Mon. Wea. Rev.*, **113**, 2108-2121.

[10] Brier, 1950. Verification of Forecast Expressed in Terms of Probability. *Mon. Wea. Rev.*, **78**, 1-3.

[11] Browning, 1971. Structure of the atmosphere in the vicinity of large-amplitude Kelvin-Helmholtz billows. *Quart. J. Roy. Meteor. Soc.*, **97**, 283-299.

[12] Buizza, 1997. Potential Forecast Skill of Ensemble Prediction and Spread and Skill Distributions of the ECMWF Ensemble Prediction System. *Mon. Wea. Rev.*, **125**, 99-119.

[13] Buizza, Milleer and Palmer, 1999. Stochastic Representation of model uncertanties in the ECMWF Ensemble Prediction System. *Quart. J. Roy. Meteor. Soc.* **125**, 2887-2908.

[14] Buizza, 2001. Chaos and weather prediction - A review of recent advances in Numerical Weather Prediction: Ensemble forecasting and adaptive observation targeting. *Il Nuovo Cimento*, **24C**, 273-301.

[15] Buizza, 2005. The ECMWF Ensemble Prediction System. In Palmer and Hagedorn editors, *Predictability of Weather and Climate*. Cambridge University Press

[16] Buzzi and Tibaldi, 1978. Cyclogenesis in the lee of the Alps: a case study. *Quart. J. Roy. Meteor. Soc.*, **104**, 271-287.

[17] Doms, Förstner, Heise, Herzog, Mironov, Raschendorfer, Reinhardt, Ritter, Schrodin, Schulz and Vogel, 2001. A Description of the Nonhydrostatic Regional COSMO Model. Part II: Physical Parameterization. (www.cosmo-model.org)

[18] Doms and Baldauf, 2015. A Description of the Nonhydrostatic Regional COSMO-Model. Part I: Dynamics and Numerics. (www.cosmo-model.org)

[19] Donner and Philips, 2003. Boundary layer control on convective available potential energy: Implications for cumulus parameterization. *J. Geophys. Res.*, **108**, 1-12.

[20] Epstein, 1969. Stochastic dynamic prediction. *Tellus*, **21**, 739-759.

[21] Fritsch and Chappell, 1980. Numerical Prediction of Convectively Driven Mesoscale Pressure Systems. Part II. Mesoscale Model. *J. Atmosph. Sc.*, **37**, 1734-1762.

[22] Gregory, Tett and Hibling, 2000. Camelot - a database for climate model output. *Meteor. Appl.*, **7**, 83-90.

[23] Harrold, 1973. Mechanisms influencing the distribution of precipitation within baroclinic disturbances. *Quart. J. Roy. Meteor. Soc.*, **99**, 232-251.

[24] Holton and Hakim, 2012. An introduction to dynamic meteorology, Vol 88. Academic press.

[25] Hautekamer, Lefaivre, Derome, Ritchie and Herschel, 1996. A system simulation approach to Ensemble Prediction. *Mon. Wea. Rev.*, **124**, 1224-1241.

[26] Kalnay, 2003. Atmospheric modeling, data assimilation and predictability. Cambridge University Press.

[27] Kessler, 1969. On the distribution and continuity of water substance in atmospheric circulation. *Meteorological Monographs*, **10**, 1-81.

[28] Kuo and Raymond, 1980. A Quasi-one-Dimensional Cumulus Cloud Model and Parameterization of Cumulus Heating and Mixing Effects. *Mon. Wea. Rev.*, **108**, 991-1009.

[29] Lorenz, 1960. Energy and Numerical Weather Prediction. *Tellus*, **12**, 364-373.

[30] Lorenz, 1963. Deterministic Nonperiodic flow. *J. Atmosph. Sc.*, **20**, 130-141.

[31] Lynch, Giard and Ivanovici, 1997. Improving the Efficiency of a Digital Filtering Scheme for Diabatic Initialization. *Mon. Wea. Rev.*, **125**, 1976-1982.

[32] Marsigli, Montani, Nerozzi, Paccagnella, Tibaldi and co-authors. 2001. A strategy for high-resolution ensemble prediction. Part II: limited-area experiments in four Alpine flood events. *Quart. J. Roy. Meteor. Soc.*, **127**, 2095-2115.

[33] Marsigli, Boccanera, Montani and Paccagnella, 2005a. The COSMO-LEPS ensemble system: validation of the methodology and verification. *Nonlin. Proc. in Geophys.*, **12**, 527-536.

[34] Mason and Graham, 1999. Conditional Probabilities, Relative Operating Characteristics, and Relative Operating Levels. *Wea. For.*, **14**, 713-725.

[35] Mironov and Ritter, 2004. A New Sea Ice Model for GME. Technical Note, Deutscher Wetterdienst, Offenbach am Main, Germany

[36] Molteni, Buizza, Palmer and Petroliagis, 1996. The ECMWF Ensemble Prediction System: Methodology and validation. *Quart. J. Roy. Meteor. Soc.*, **122**, 73-119.

[37] Molteni, Buizza, Marsigli, Montani, Nerozzi and co-authors. 2001. A strategy for high-resolution ensemble prediction. Part I: definition of representative members and global-model experiments. *Quart. J. Roy. Meteor. Soc.*, **127**, 2069-2094.

[38] Montani, Capaldo, Cesari, Marsigli, Modigliani and co-authors. 2003a. Operational limited-area ensemble forecasts based on the Lokal Modell. ECMWF Newsletter 98, 2-7. Available at: http://www.ecmwf.int/publications/.

[39] Montani, Marsigli, Nerozzi, Paccagnella, Tibaldi and Buizza, 2003b. The Soverato flood in Southern Italy: performance of global and limited-area ensemble forecasts. *Nonlin. Proc. Geophys.*, **10**, 261-274.

[40] Montani, Cesari, Marsigli and Paccagnella, 2011. Seven years of activity in the field of mesoscale ensemble forecasting by the COSMO-LEPS system: main achievements and open challenges. *Tellus*, **63**, 605-624.

[41] Mullen and Buizza, 2001. Quantitative Precipitation Forecasts over the United States by the ECMWF Ensemble Prediction System. *Mon. Wea. Rev.*, **129**, 638-663.

[42] Murphy, 1969. On the "Ranked Probability Score" *J. Appl. Meteor.*, **8**, 988-989.

[43] Murphy, 1971. A note on the ranked probability score. *J. Appl. Meteor.*, **10**, 155-156.

[44] Nordeng, 1994. Extended versions of the convective parameterization scheme at ECMWF and their impact on the mean and transient activity of the model in the tropics European Centre for Medium-Range Weather Forecasts. *Tech. Memo.*, **206**, 41.

[45] Randall, Arakawa and Grabowski, 2003. Breaking the Cloud Parameterization Deadlock. *Bull. Amer. Met. Soc.*, **115**, 1547-1564.

[46] Ritter and Geleyn, 1992. A comprehensive radiation scheme for numerical weather prediction models with potential applications in climate simulations. *Mon. Wea. Rev.*, **120**, 303-325.

[47] Schaer, Leuenberger, Fuhrer, L$\acute{}$uthi and Girard, 2002. A New Terrain-Following Vertical Coordinate Formulation for Atmospheric Prediction Models. *Mon. Wea. Rev.*, **130**, 2459-2480.

[48] Schättler, Doms and Schraff, 2016. A Description of the Nonhydrostatic Regional COSMO-Model. Part VII: User Guide. (www.cosmo-model.org)

[49] Schraff, 1996. Data assimilation and mesoscale weather prediction: A study with a forecast model for the Alpine region. Publication 56, Swiss Meteorological Institute, Zürich.

[50] Schraff, 1997. Mesoscale data assimilation and prediction of low stratus in the Alpine region. *Meteor. Atmos. Phys.*, **64**, 21-50.

[51] Skamarock and Klemp, 1992. The stability of time-split numerical methods for the hydrostatic and the nonhydrostatic elastic equations. *Mon. Wea. Rev.*, **120**, 2109-2127.

[52] Stanski et al., 1989. Survey of common Verification methods in meteorology. Atmospheric Environmental Service, Canada.

[53] Stephan, Klink and Schraff, 2008. Assimilation of radar-derived rain rates into the convective-scale model COSMO-DE at DWD. *Quart. J. Roy. Meteor. Soc.*, **134**, 1315-1326.

[54] Steppeler, Doms, Schättler, Bitzer, Gassmann, and co-authors. 2003. Meso-gamma scale forecasts using the nonhydrostatic model LM. *Meteor. Atmos. Phys.*, **82**, 75-96.

[55] Sundqvist, 1978. A parameterization scheme for non-convective condensation including prediction of cloud water content. *Quart. J. Roy. Meteor. Soc.*, **104**, 677-690.

[56] Tennekes, Baede and Opsteegh, 1986. Forecastng forecast skill. *Proceedings of the ECMWF Workship on Predictability in the Medium and Extended renge*, Reading, England.

[57] Thomas, Girard, Doms and Schättler, 2000. Semi-implicit scheme for the DWD Lokal-Modell. *Meteor. Atmos. Phys.*, **75**, 105-125.

[58] Tibaldi, Paccagnella, Marsigli, Montani and Nerozzi, 2006. Limited area ensemble forecasting: the COSMO model. Predictability of Weather and Climate. Cambridge University Press, 489-513.

[59] Toth and Kalnay, 1993. Ensemble Forecasting at NMC: The Generation of Perturbations. *Bull. Amer. Met. Soc.*, **74**, 2317-2330.

[60] Yanai, Esbensen and Chu, 1973. Determination of Bulk Properties of Tropical Cloud Clusters from Large-Scale Heat and Moisture Budgets. *J. Atmosph. Sc.*, **30**, 611-627.

[61] Wicker and Skamarock, 2002. Time-splitting methods for elastic models using forward time schemes. *Mon. Wea. Rev.*, **130**, 2088-2097

[62] Wilks, 1995. Statistical methods in the atmospheric sciences. International Geophysics Series, Vol 59. Academic Press.

[63] WMO, 2012. Guidelines on Ensemble Prediction Systems and Forecasting.

Acnowledgements

Un'importante pagina della vita si chiude con la scrittura di questa tesi. Un percorso duro, dedicato alla faticosa rincorsa (che continua!) dei sogni che mi accompagnano fin dall'infanzia. Sento doveroso fermarmi un attimo, dedicando un pensiero a coloro che mi sono stati vicino in questo periodo.

Desidero innanzitutto ringraziare la professoressa Silvana Di Sabatino, che ha accettato di seguirmi nel corso dello stimolante percorso che mi ha portato alla stesura di questa tesi.

Un grazie speciale ai dott. Andrea Montani e Tiziana Paccagnella per avermi accolto in maniera fantastica nel loro gruppo durante il periodo di preparazione della tesi, non facendomi mai mancare supporto e assistenza quando ne ho avuto bisogno, con grande pazienza e disponibilità: da loro ho imparato tantissimo in questi mesi!

Un pensiero va agli amici, da quelli "di una vita"- che ci sono sempre stati e sempre ci saranno ancora - con cui sono cresciuto insieme, a quelli con cui ho condiviso speranze e preoccupazioni in questi anni universitari: con alcuni di loro, compagni negli studi (e non solo!), sarebbe bello ritrovarsi in futuro come colleghi di lavoro nel settore che ci ha sempre affascinato!

Infine un grande grazie va alla mia famiglia, che mi ha sempre sostenuto in questi anni (a tratti anche difficili), agli zii e alle nonne: questo risultato è in primis dedicato a tutti loro.